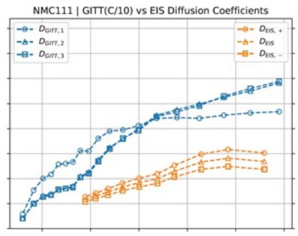

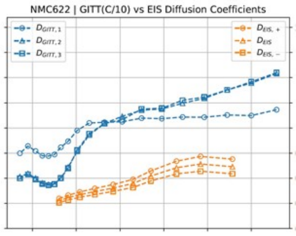

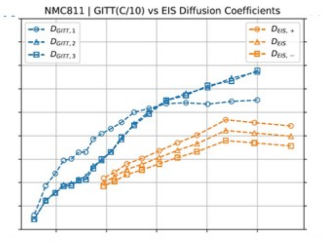

Identification of Material Parameters in Lithium-ion Batteries

A comparative study between NMC111, NMC622 and NMC811 cathodes using electrochemical techniques

Master of Science Thesis

AARUSHI BIJALWAN

PRANAV TALWARE

DEPARTMENT OF ELECTRICAL ENGINEERING

CHALMERS UNIVERSITY OF TECHNOLOGY
Gothenburg, Sweden 2023
www.chalmers.se

MASTER'S THESIS 2023

Identification of Material Parameters in Lithium-ion Batteries

A comparative study between NMC111, NMC622 and NMC811 cathodes using electrochemical techniques

AARUSHI BIJALWAN

PRANAV TALWARE

Department of Electrical Engineering
Division of Electric Power Engineering
CHALMERS UNIVERSITY OF TECHNOLOGY
Gothenburg, Sweden 2023

Identification of Material Parameters in Lithium-ion Batteries
A comparative study between NMC111, NMC622 and NMC811 cathodes using electrochemical techniques
AARUSHI BIJALWAN
PRANAV TALWARE

© AARUSHI BIJALWAN
PRANAV TALWARE, 2023.

Supervisor: Kristian Fernander, Volvo Cars,
Zeyang Geng, Chalmers University of Technology
Examiner: Torbjörn Thiringer, Department of Electrical Engineering

Master’s Thesis 2023: EENX30
Department of Electrical Engineering
Division of Electric Power Engineering
Chalmers University of Technology
SE-412 96 Gothenburg
Telephone +46 31 772 1000

Cover: Diffusion coefficient comparison from GITT and EIS for NMC111 (left), NMC622 (center) and NMC811 (right).

Typeset in LaTeX
Printed by Chalmers Reproservice
Gothenburg, Sweden 2023

Identification of Material Parameters in Lithium-ion Batteries
A comparative study between NMC111, NMC622 and NMC811 cathodes
AARUSHI BIJALWAN
PRANAV TALWARE
Department of Electrical Engineering
Chalmers University of Technology

Abstract

As the world is shifting towards electric vehicles, there is a need for high performing batteries which can be achieved by studying the material parameters in a battery cell in order to understand its behavior. In this thesis work, half cells and 3-electrode cells are assembled with cell chemistries NMC111, NMC622 and NMC811 each as cathodes. Electrochemical techniques are used to estimate material parameters. Galvanostatic Intermittent Titration Technique(GITT) is performed on half cells and three electrode cells. Three methods are used to analyse the GITT results and obtain a range of diffusion coefficients. Electrochemical Impedance Spectroscopy (EIS) is performed on a 3-electrode cell, and the measurement is done between cathode and Li-reference ring. The results of the EIS are analysed using an equivalent circuit model resembling a physical cell. Diffusion coefficients are calculated from both GITT and EIS and a comparative study is presented for each cell chemistry. Some other parameters like the double layer capacitance, exchange current density and cathode electrolyte interface capacitance are also estimated from EIS and a comparative study between different cell chemistries is presented. The diffusion coefficients from GITT are in the order of 10^{-15} $[\mathrm{m}^2/\mathrm{s}]$ whereas from the EIS test, it is in the order of $10^{-12}[\mathrm{m}^2/\mathrm{s}]$.

Keywords: Battery, Cell, Cathode, EL cell, GITT, EIS, Diffusion coefficient, Charge transfer resistance, Double layer capacitance, Cathode-Electrolyte interface capacitance.

Acknowledgements

The thesis work has been carried out at the Division of Electric Power Engineering, Department of Electrical Engineering at Chalmers University of Technology, Sweden and ART Battery, Cell and Module, Volvo Cars, Sweden.

This project would not have been possible without our supervisor Kristian Fernander. Through out the thesis work he has provided us with his valuable inputs, tutelage, patience and moral support. We would also like to extend our deepest gratitude to Zeyang Geng whose crucial feedback nudged us in the right direction.

We would also like to thank our examiner Torbjörn Thiringer who helped us with feedback on the report and efficient conduction of the thesis work.

We would also like to thank other members at Material Center at Volvo Cars for their support.

Finally we would like to thank our families and friends who have always been there for us and without whom this work would not be possible.

Aarushi Bijalwan, Pranav Talware,
Gothenburg, November 2021

Contents

1

Introduction

"The tipping point in passenger EV adoption occurred in the second half of 2020, when EV sales and penetration accelerated in major markets despite the economic crisis caused by the COVID-19 pandemic"[1]. Europe has been at the forefront of this change due to regulatory reasons on OEMs related to stricter emissions and subsidies for consumers.

In 2021, we have seen a great interest in the future ban of internal combustion engines (ICE) vehicle sales was seen. The aim of the European Union and the United States is to have a 50 percent EV share by 2030. Other countries are also following this trend and are planning to ban the sales of ICE vehicles by 2030 or 2035. Companies have started phasing out investment related to ICE technology. They are also setting end dates of ICE vehicle production.

Moreover, there is a shift in consumer mindset. Now more than 45 percent of customers are considering buying an EV instead of an ICE. This has resulted in an increase in pressure on the OEMs to deliver technology which is not only high performing but is also safe and sustainable. It is also predicted that to meet the demand of EVs in the EU, 24 new battery giga-factories will have to be built to meet the local passenger EV battery demand. A 20-fold increase to 965 GWh in the production capacity of batteries in the EU is expected by 2030. It is also expected that in this decade, the mining industry will slow down and supply chain crises will appear periodically which will lead to temporary price hikes in elements like nickel and lithium.

In earlier years, the battery cells were mostly imported from Asia, but now new European countries are also entering the market. OEMs are also forming joint ventures with cell manufacturers to meet their demands and also maximise the development, inhouse [1].

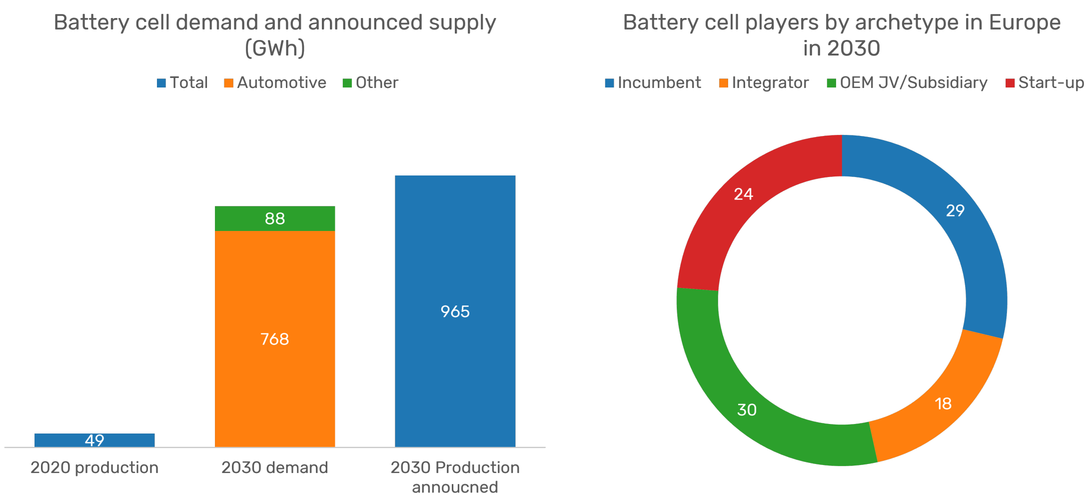

Figure 1.1: McKinsey prediction for about battery cell demand in the coming years

Even though the battery technology has seen many developments from the first introduced lithium-ion battery for consumers by Sony Corp.[2], this boom requires a transformation in battery technology as currently a major limitation for the EVs is its range, which is limited by the traction battery. Lithium-ion batteries are the systems of choice, offering high energy density, a flexible and lightweight design, and longer lifespan than comparable battery technologies[3].

1.1 Problem background

Research in lithium-ion battery models, particularly physics based models, has paved the way to a better understanding of underlying various processes inside the battery. To build better physics based models, we need to know a range of internal parameters of the cell. These parameters are typically considered to be an industrial secret by cell manufacturers. This makes it difficult for academic researchers and hence most of such research is dependent on the generic internal cell parameters. COMSOL might be a good example for this, where we use generic parameters.

To build an actual digital twin of the cell, we need to know the exact values of its internal cell parameters. Determining these is one of the most important and critical processes for physics based models which is also the focus of our thesis work.

1.2 Objectives

The goal of this thesis is to

- Construct half cells and 3-electrode cells for different cell chemistries
- Measure various electrochemical properties of cells by experimentation and identify critical parameters for commercial batteries. The methods we are

focussing on are GITT and EIS.
- A sensitivity analysis will be performed on the estimated parameters to determine its accuracy.

Using a literature study, the critical parameters which affect the commercial batteries the most are shortlisted in table 1.1.

Table 1.1: List of parameters and methods used

Cell parameters	Experimental method
Diffusion coefficient	GITT and EIS
Exchange current density	EIS
Double layer capacitance	EIS
CEI capacitance	EIS

2

Theory

This section summarises the theoretical information on which this thesis is based.

2.1 Lithium-ion battery

Energy storage devices help in storing energy from various sources which can be used later in different sectors. Storing the energy from renewable sources such as wind and sun has become critical as the world is moving towards phasing out fossil fuels[4].

One of the different types of energy storage devices is the electrochemical batteries. There are two types of battery cells, namely primary and secondary batteries. The primary battery cells are the ones which are meant to be disposed of after their use whereas the secondary battery cells can be charged and discharged multiple times. Batteries offer high energy density which is why it is an attractive option when it comes to energy storage devices. This also means that it becomes very critical to choose the electrodes and electrolytes of these cells to improve the energy density and cost of these batteries. Ensuring the safety of the cell and increasing the lifetime are also of high importance to industries and consumers. Lithium-ion batteries convert chemical energy to electrical energy and vice versa. It consists of two electrodes, namely cathode and anode, with a separator soaked in electrolyte to facilitate ion transport while preventing electric short circuit. The ions travel through the electrolyte, however, the electrons travel through the external circuit. This requires that the electrodes must allow an easy flow of these entities which means that the electrodes should be good conductors of ions and electrons[5].

Li-ion batteries have high energy efficiency since Li has some key advantages over other chemistries.

- Li has the lowest reduction potential amongst all the elements which helps these battery cells to have high cell potential[6].
- Li is a very light element with a very small radius amongst the charged ions which helps these batteries to have high power density and high volumetric capacity[6].
- Alternate multivalent cations have high charge capacity per ion. However, this additional charge significantly reduces their mobility[6].

Given these advantages, Li-ion based batteries are a suitable option for application in renewable energy. In order to improve the energy and power density of the battery, electrodes are required with high rate and charge capacity and a high cathode voltage[6].

2.1.1 Electrodes

There are two electrodes in a cell, one is called cathode and the other is called the anode. The cathode is typically a complex compound with different elements and anode is typically graphite which acts as a host to the lithium ions. In order to study pure cathode behaviour, a half cell can be created with lithium metal as anode. The anode is the electrode which stores the lithium ions during charging and releases them during discharging. Sony Corporation discovered the highly reversible carbonaceous material suitable for anodes which has low voltages and were the first ones to commercialise it. Using such a carbon based anode instead of lithium metal prevented the growth of irregular dendritic lithium which reduced the chances of shorting and overheating of these cells[7]. The following points summarise the requirements for choosing a good cathode and anode in rechargeable lithium batteries[5].

1. The electrode material should be a transition metal which can readily reduce or oxidize ion.
2. The host should not change structure when lithium is added.
3. The electrode material reacts reversibly with lithium and has a high free energy with a high capacity and high voltage.
4. The electrode material rapidly reacts with lithium both during slipping in as well as slipping out leading to a high power density.
5. The electrode material should be a good conductor of electricity. This enhances the reaction at all points of the active surface.
6. The electrode material should be stable and due to overcharge or discharge, should not change structure or degrade.
7. The electrode material should be environmentally benign.

2.1.2 Electrolyte

The electrolyte helps in transporting the lithium ions between cathode and anode. A common electrolyte is $\mathrm{LiPF_6}$ solved in a mixture of diethyl carbonate, dimethyl carbonate, and ethylene carbonate in a weight ratio 1:1:1.

Apart from this, the electrolyte also contains some additives which improve stability and prevent dendrite growth and hence prevents the solution from degrading.

2.1.3 Separator

A separator physically separates the cathode and the anode which helps in preventing an electrical contact providing electrical insulation and hence any short circuit which can lead to an explosion. It is a porous membrane which allows flow of ionic charge carriers from the cathode to anode and vice versa during charge and discharge processes. It has pores or voids which increases conductivity and performance[8].

2.1.4 Cell kinetics

Charge

During the charge phase, an electron is pulled from the cathode and sent electrically to the anode. In the meanwhile, a positive lithium ion is released into the electrolyte from the cathode. This ion travels through the solution and reaches the anode where in case of a carbon electrode, it intercalates into its layer where it meets an electron leading to the formation of a neutral species.

Discharge

During the discharge procedure, the reverse of the charge reaction happens. This time, the electron is pulled electrically from the anode and at the cathode, the lithium ion meets an electron to again form a neutral species.

Cathode-Electrolyte Interface (CEI)

This layer passivates the reaction of electrodes with the electrolyte. It is formed on the electrode surfaces during first charge and discharge due to that parts of the electrolyte decomposes on the electrodes. The CEI layer is ionically conducting and allows the lithium ions to pass through it, however, it is electrically non conducting and blocks the flow of electrons from the electrode into the electrolyte. This also prevents the electrolyte from further decomposing on the electrodes[7].

Intercalation

Intercalation happens in a cell during charging and discharging processes and not otherwise. During the charge process, the positively charged lithium ions move from the cathode to the anode via the electrolyte solution. The lithium ions travel and get deposited between the layers of the anode. This phenomenon is called the intercalation process.
The intercalation process is affected by the materials used as anode, cathode and electrolyte. Choosing these materials correctly, can improve the efficiency of these batteries[9].

2.2 Galvanostatic Intermittent Titration Technique (GITT)

GITT is used to analyse diffusion of lithium in electrode materials depending on the amount of lithiation. It helps in determining diffusion coefficient due to (de)intercalation.

Below is an example of a GITT voltage pulse as a result of the current pulse. In the figure $E_1 - E_0$ give the IR drop when the current is switched on, the E_1 to E_2 increase is due to the development of diffusion overvoltage as well as the open circuit voltage. Switching off the current, results in a second IR drop from E_2 to E_3. This is followed by a relaxation time from E_3 to E_4 which is caused due to balancing of lithium-ion concentration[10].

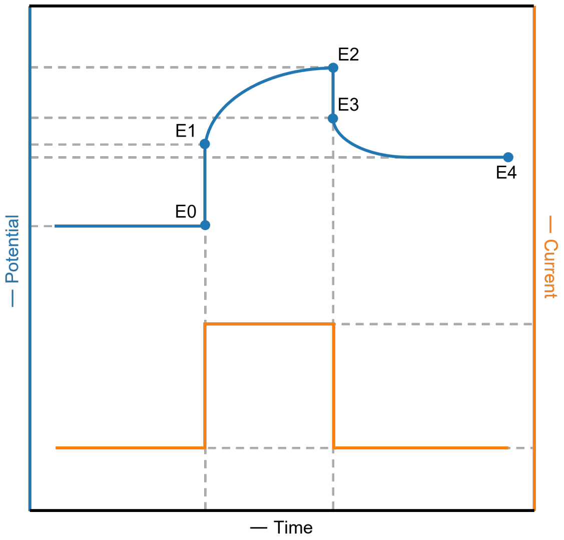

Figure 2.1: Single GITT pulse voltage measurement points as per current pulse

A voltage profile is plotted against time to understand the cell behaviour during the test. Multiple voltage pulses as shown above can be seen in such a plot.

2.2.1 GITT material parameters

Diffusion coefficient

Though diffusion coefficient depends on lithium-ion concentration generally, this dependence can be ignored as the change in this concentration is small during each GITT pulse when describing diffusion. The change in cell potential at a point in time during a GITT pulse can be expressed as,

$$E(t) = \eta_{ohm} + \eta_{CT} + E_{eq}(\chi_s(t)) \tag{2.1}$$

where η_{ohm} is the overvoltage contribution from ohmic resistance, η_{CT} is the overvoltage contribution from charge transfer resistance at SEI, E_{eq} is the open circuit voltage and χ_s is the change is stoichiometry.

For spherical particles, for the limit, $Dt/r_p^2 << 1$

$$\frac{dE}{d\sqrt{t}} = \frac{dE_{eq}(x)}{dx}\frac{d\chi_s}{d\sqrt{t}} = -\frac{2}{\sqrt{\pi}}\frac{j_s}{\sqrt{D}c_{max}}\frac{dE_{eq}(x)}{dx} \tag{2.2}$$

which gives diffusion coefficient formula,

$$D = \frac{4}{\pi}\left(\frac{j_s}{c_{max}}\frac{dE_{eq}}{dx}\frac{d\sqrt{t}}{dE}\right)^2 \tag{2.3}$$

where D is diffusion coefficient, r_p is the particle radius j_s lithium surface flux density and c_{max} is the lithium density (molm^{-3}) of the fully lithiated intercalation host. It is assumed that the lithium concentration is close to equilibrium after the relaxation period, $\frac{dE_{eq}}{dx}$ is approximated to $\frac{E_4 - E_0}{\Delta x}$. For each pulse, stoichiometric change is given by $\Delta x = -\frac{I_p t_p}{F V_{acm} c_{max}}$, where I_p is galvanostatic current, t_p is pulse duration, F is the faraday constant and V_{acm} the volume of the cathode material. The lithium surface flux density into the particle is expressed as $j_s = \frac{I_p}{F A_{acm}}$, where A_{acm} is active surface area of cathode material.

Calculating the surface area A_{acm} of a porous composite electrode is quite difficult. It is often approximated by using the specific surface area $a_s = \frac{3\varepsilon_{acm}}{r_p}$ of a group of spherical particles of equal radius r_p and volume fraction ε_{acm}. Replacing $A_{acm} = a_s * V_{tot}$ and $V_{acm} = \varepsilon_{acm} * V_{tot}$ where V_{tot} is the total electrode volume. The following expression is obtained after simplification,

$$D = \frac{4}{9\pi}\left(\frac{E_4 - E_0}{dE/d\sqrt{t}}\frac{r_p}{t_p}\right)^2 \tag{2.4}$$

2.3 Electrochemical Impedance Spectroscopy(EIS)

EIS is the analysis of the impedance characteristics of a cell over a spectrum of frequencies. The reaction kinetics that happens at the electrode interface is modelled according to the Butler-Volmer equation.

$$j = j_o\left(exp\left(\frac{\alpha_\alpha nF}{RT}\eta\right) - exp\left(\frac{-\alpha_c nF}{RT}\eta\right)\right) \tag{2.5}$$

where j - Electrode current density[A/m2], j_o - Exchange current density[A/m2], α_α - Anodic charge transfer coefficient, α_c - Cathodic charge transfer coefficient, R - Gas constant, 8.314 [J/Kmol], T - Temperature [K], n - number of transferred electrons (per mole reactant), F - Faraday constant [96485 $\mathrm{As/mol}$], η - Overpotential due to charge transfer [V]. Interfacial effects like adsorption or electrochemical double layer are not considered in this equation.
A Nyquist plot is obtained on doing EIS. It is a plot which has real part of the impedance on the x axis and imaginary part of the impedance on the y axis. The values are obtained when a range of frequency is passed through the electrochemical system.

2.3.1 Equivalent circuit model

To study the results obtained by the EIS technique, we need to have the knowledge about the RC modelling of the electrochemical system. It is a simplified way of understanding the processes in the battery by mapping the electrochemical behaviour of the cell by using electrical components such as a resistor or capacitor.

Constant Phase element (CPE)

Constant phase element circuit element is used to describe capacitance as it appears in a real cell, due to issues like surface roughness, reaction rates distribution. It is not a perfect capacitance as it is frequency dependent. The effective capacitance and 'real' resistance increase as the frequency decreases. It can be calculated by using the equation,

$$Z_Q = \frac{1}{Q_0(j\omega)^n} \tag{2.6}$$

where Z_Q is CPE, n is the constant phase$(-90 \times n)^o$ and n is a number between 0 and 1.

For a parallel R-CPE model, it is possible to determine the actual capacitance value behind the CPE using the following relation[11].

$$C = \frac{(RQ)^{\frac{1}{n}}}{R} \tag{2.7}$$

Warburg element

The warburg element according to equivalent circuit model, models the diffusion part of the process. It considers diffusion in one dimension bounded by a large planar electrode on one side. In the Nyquist plot, the Warburg impedance is represented by a straight line with a phase of 45^o [12].

2.3.2 EIS material parameters

Diffusion coefficient

The diffusion coefficient is a key parameter of the battery performance. It is used as an input parameter in the simulation models to understand the behaviour of the cell. For a soluble redox reaction, the following relation is true.

$$\sigma = \frac{RT}{n^2F^2A\sqrt{2}}\left(\frac{1}{D^{1/2}c^{\infty}}\right) \tag{2.8}$$

where D is the diffusion coefficient, c^{∞} is the bulk concentration.

Exchange current density

If small perturbations are considered, the Butler-Volmer equation can be linearized as follows for the charge transfer resistance.

$$R_{ct} = \frac{\partial \eta}{\partial I} = \frac{RT}{nFi_0} \tag{2.9}$$

where η is the overpotential, I is the current and i_0 is the exchange current density. This can be rearranged as,

$$i_0 = \frac{RT}{nAFR_{ct}} \tag{2.10}$$

Double layer capacitance

At the electrode interface, net electric charges are produced as the two interfaces are chemically different and have different conducting domains. There are charged carriers in the electrolyte which adsorb on the electrode, and as a consequence the interface gets charged. This causes a generation of local electric field and a potential difference due to which the interface acts as capacitive which is hence referred as electric double layer capacitance[13].

CEI capacitance

It is a layer formed between the liquid electrolyte and solid cathode electrode. In the equivalent circuit model, this interface can be represented by an RC branch. This interface is characterized by a semi-circle in the Nyquist plot. This layer is formed after the formation cycles.

3

Methods

In this section, we highlight the methods and processes.

3.1 Cell construction

To study cell chemistries in detail, some cells are constructed for each cell chemistry. The cell consists of a cathode and an anode with lithium or graphite as base. These cells are assembled in an argon-filled glove box ($<0.5\text{ppm } H_2O$, $<2\text{ppm } O_2$).

3.1.1 Glove box setup

The common steps for operating the glovebox for both the EL cell and the coin cells are as below.

- The cells are constructed inside a glove box.
- Firstly, the cell materials, EL cell setup and paper towels are kept in a temperature chamber for drying before putting them into the glove box. The materials are dried for around 24 hours whereas the paper towels are kept for longer as they are porous.
- The ante-chamber of the glovebox is brought to atmospheric pressure using the knob which is set to 'Close'. The atmospheric pressure is determined by a pressure gauge. The materials are then kept in the ante-chamber and the door is shut tight.
- The knob is then turned to 'Evacuate' in order to flush the ante-chamber and remove the air that has entered inside the glovebox. This is done in two steps so that a whirl of wind is not created in the ante-chamber and the electrodes do not fly away.
- The knob is then shifted partially towards 'Refill' in order to fill the glovebox with argon gas.
- This process of evacuating the air and then refilling with argon is done thrice to avoid contaminants.
- The knob is then finally turned to 'Close' to avoid any argon waste.

3.1.2 EL cell construction

Some cells are constructed as EL cells. The following steps are followed.

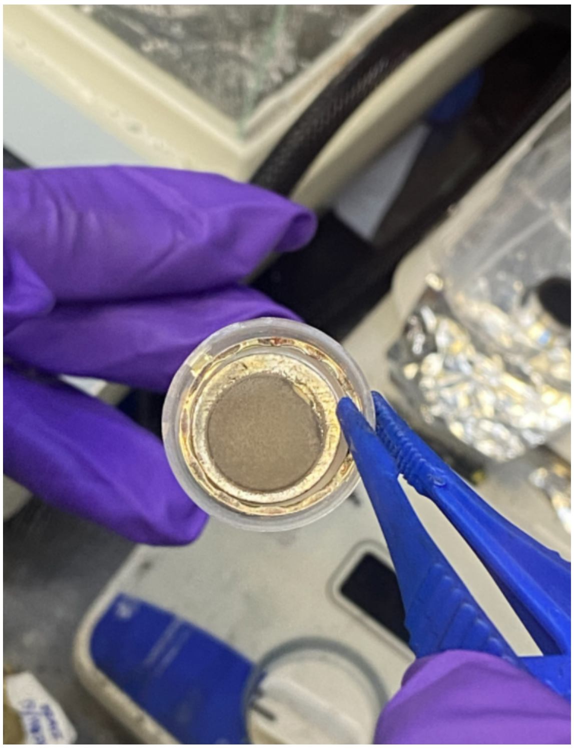

Figure 3.1: PAT core of EL cell showing electrode and reference ring during disassembly

- A plastic separator assembly with separator layer inside and Li reference as a wire around inside it, is taken and the electrode is placed on it using plastic tweezer.
- An aluminium plunger is then placed over the plastic plunger and then pushed on it to tightly fit both together.
- The assembly is then inverted and pushed inside the PAT cell.
- A tip is taken and is fit on the pipette. Using this pipette, 100μL electrolyte is added above the separator. The electrolyte used is $1\mathrm{M}\ \mathrm{LiPF_6}$ solved in a mixture of diethyl carbonate, dimethyl carbonate, and ethylene carbonate in a weight ratio 1:1:1.
- Thin lithium metal or a graphite based anode which would act as counter electrode is then placed over it using the lithium or normal tweezers respectively to avoid contamination.
- The copper plunger is placed over it and the cover of the PAT cell is then tightened over the assembly.

3.1.3 Coin cell construction

Some cells are constructed as coin cells. The following steps are followed.

- The negative side or the smaller container with dotted pattern is placed on the workplace.
- The lithium or graphite based electrode is placed inside the container.
- A separator is placed over the lithium electrode.

- Electrolyte is dropped over the separator using a pipette.
- The electrode is placed over the electrolyte.
- The spacer and the spring are placed over the electrode simultaneously and the big cover is then placed over the rest of the assembly.
- The cell assembly is then stored in a small bag which is then taken out of the glovebox.
- The coin cell assembly is the placed in a crimping tool and using the mechanical force, the coin cell is crimped and sealed permanently.
- The cells are then cleaned with acetone to rinse off any electrolyte present on the surface.

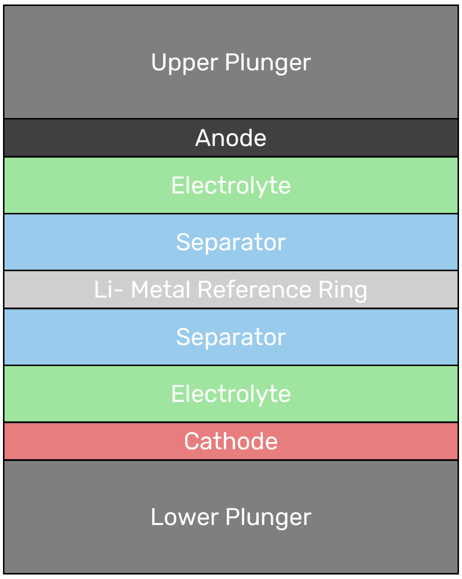

Figure 3.2: EL-Cell Illustration

3.1.4 Built cell chemistries

Multiple cell chemistries are built for this thesis.

In the first test, the plunger is reused from an aged cell. This is done to evaluate the reusability of the plunger.

Table 3.1: Built cell chemistries

Cathode	Anode	Reference ring	Test	Plunger
NCA	Li metal	No	Formation cycle	Reused plunger
NMC111	Li metal	No	GITT (Rate:C/10)	Fresh plunger
NMC622	Li metal	No	GITT (Rate:C/10)	Fresh plunger
NMC811	Li metal	No	GITT (Rate:C/10)	Fresh plunger
NMC111	Li metal	Yes	GITT (Rate:C/20)	Fresh plunger
NMC622	Li metal	Yes	GITT (Rate:C/20)	Fresh plunger
NMC811	Li metal	Yes	GITT (Rate:C/20)	Fresh plunger
NMC111	GSi	Yes	EIS (Cathode vs Reference)	Fresh plunger
NMC622	GSi	Yes	EIS (Cathode vs Reference)	Fresh plunger
NMC811	GSi	Yes	EIS (Cathode vs Reference)	Fresh plunger

3.2 Formation cycles

To stabilize the cells before testing it, formation cycles are run on it. The diameter of cathode is $d_{cathode} = 14\mathrm{mm}$. The capacities are summarized as follows,

Table 3.2: Capacities for different chemistries

Chemistry	Area Capacity(q_{area})	Capacity(Q)
NMC111	3.5 $\mathrm{mAh/cm^2} \pm$ 2%	5.3878mAh
NMC622	3.5 $\mathrm{mAh/cm^2} \pm$ 2%	5.3878mAh
NMC811	3.4 $\mathrm{mAh/cm^2} \pm$ 2%	5.2339mAh
NCA	1.0 $\mathrm{mAh/cm^2} \pm$ 2%	1.54mAh

The recommended formation cycle from the company CUSTOMCELLS for the given electrodes is

2 × C/10

2 × C/5

Charge: CC+CV up to 1/10 of the C-rate current

Discharge: CC up to cut-off voltage

Pause: 30min resting phase after each cycle

The voltage safety limits margin are considered to be $10\mathrm{mV}$ for this cell.

Table 3.3: Voltage limits

Parameter	Voltage(V)
Cell datasheet - Maximum Voltage	4.3
Cell datasheet - Minimum Voltage	3.0
Safety limit - Maximum Voltage	4.31
Safety limit - Minimum Voltage	2.99

3.3 Galvanostatic Intermittent Titration Technique (GITT)

The GITT sequence, fed to the Neware software is as follows.

1. Charge for 30 minutes
2. Rest for 4 hours
3. If voltage < maximum charge voltage, then go to first step again
4. If voltage > maximum charge voltage, then go to next step
5. Discharge for 30 minutes
6. Rest for 4 hours
7. If voltage > cut off discharge voltage, then go to fifth step again
8. If voltage < cut off discharge voltage, then end the test

Current value for charge and discharge is given. Two GITT tests are conducted, one at $C/10$ rate and the other with $C/20$ rate.

The maximum charge voltage and the Cut off discharge voltage is taken from the CUSTOMCELLS data sheet for each cell chemistry.

In the Neware software, a safety limit is given. For the upper voltage level, an additional $10\mathrm{mV}$ to the data sheet value of the Maximum charge voltage is declared as the upper safety limit. For the lower voltage level, the safety limit is considered $50\mathrm{mV}$ less than the datasheet Cut off discharge voltage.

The sampling during the test is done at a voltage change of $2\mathrm{mV}$.

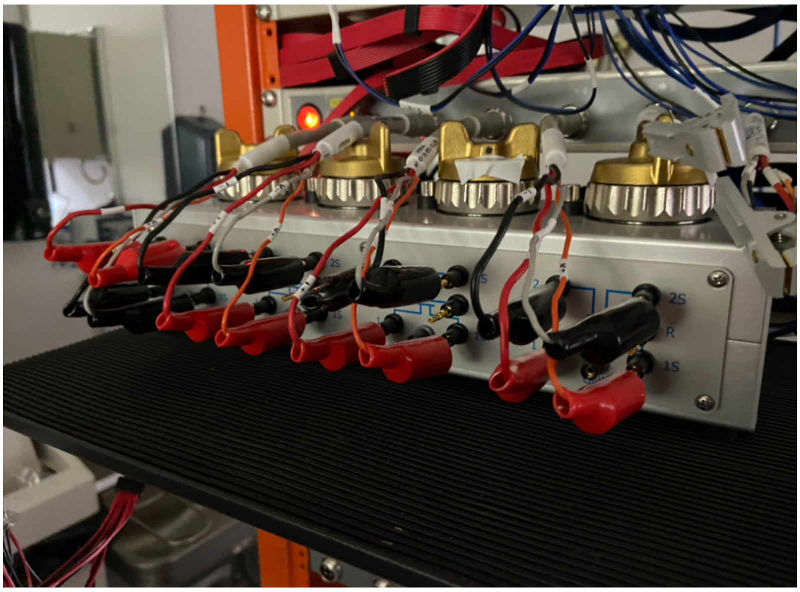

Figure 3.3: GITT test set-up

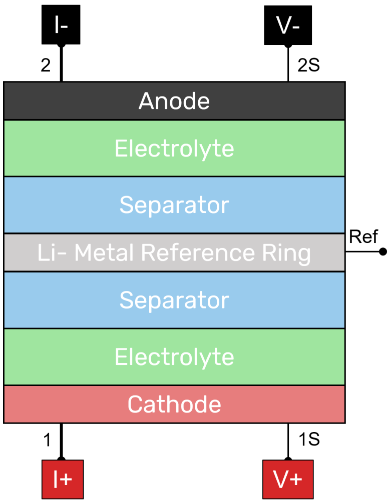

Figure 3.4: Illustration of GITT measurement points

3.4 Electrochemical Impedance Spectroscopy (EIS)

The equipment used to perform the EIS testing is the Gamry REF3000-35150. The Gamry is connected to a computer using a USB. Another cable attached to the Gamry had 6 probes.

1. Working electrode probe (Green)
2. Counter electrode probe (Red)
3. Working sense probe (Blue)
4. Counter sense probe (Orange)
5. Reference electrode probe (White)
6. Floating ground probe (Black)

The EL cell on which the EIS testing is performed are placed in the PAT-Stand-4 docking station.

The tests are done between cathode and the reference ring. The following summarizes the test conditions for each test.

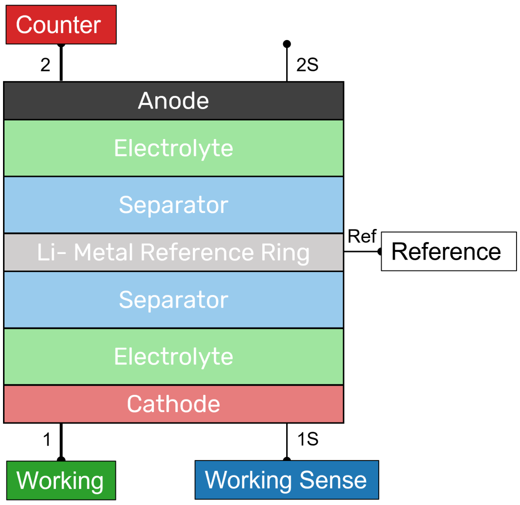

Figure 3.5: Illustration of EIS measurement points

Table 3.4: Test conditions for cells

Parameter	Value
Initial Frequency	1 MHz
Final Frequency	0.01 Hz
Points/decade	10
AC current	9.5e-5 Arms
Area	1 cm^2

The EIS is done at different voltage levels. Firstly, the cell is fully charged and then the EIS test is performed. Then the cell is discharged for half hour and the EIS is performed again. In total, the EIS is performed at 10 different voltage levels for each test. Below is the test setup for performing EIS.

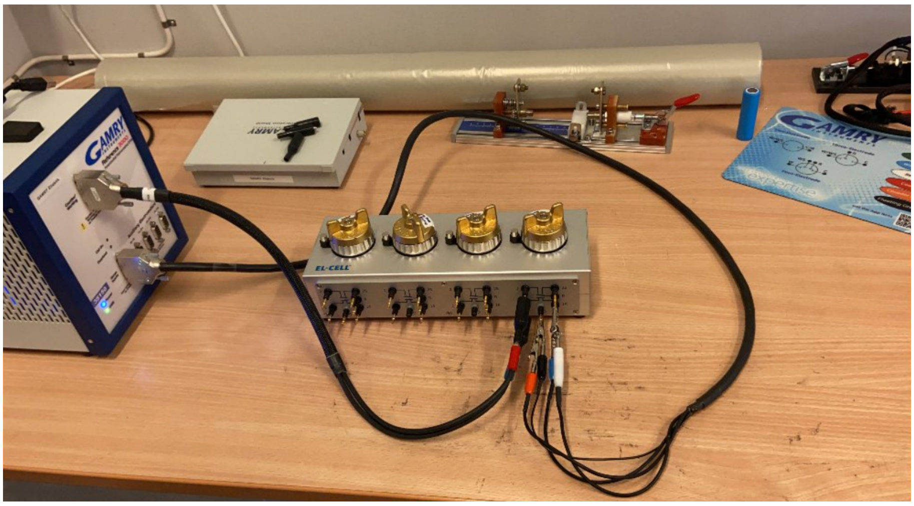

Figure 3.6: EIS test set-up

For the testing, NMCXXX is considered as the working electrode while the GSi is considered as the counter electrode. However, the counter sense measurement is done at the reference. In this test, the following connections are made:

1. Working probe is connected to the working electrode of EL cell
2. Counter probe is connected to the counter electrode of EL cell
3. Working sense is connected to the 1S of the EL cell (written on the docking station)
4. Counter sense is connected to the GND of the EL cell (written on the docking station)
5. Reference is connected to the R of the EL cell (written on the docking station)
6. Floating ground is connected to the GND of the EL cell (written on the docking station)

After making the connections a test script is constructed using the GAMRY Framework software. A sequence is created as follows:

1. OCP test before charging - 60s
2. Charging the cell to 4.2 V
3. OCP test after charging - 3600s
4. Perform the below in Loop - 10 times
    (a) OCP test before EIS - 60s
    (b) Perform EIS
    (c) OCP test after EIS - 60s
    (d) OCP test before Discharging - 60s
    (e) Discharging for 30 minutes
    (f) OCP after discharging - 3600s

In this way, the EIS is performed at different SoC levels. A cell is fully charged to 4.2V, at which the EIS is performed. After that, discharge for half hour is performed. The cell is allowed to rest for an hour after which the EIS is again performed. The cell is discharged again for half hour and the after resting, EIS is performed again at this new lower SoC level. This is repeated in loops 10 times. Hence, the test is conducted at 10 SoC levels.

4

Analysis and Results

In this section, we highlight the analysis and results.

4.1 Galvanostatic Intermittent Titration Technique (GITT)

4.1.1 GITT analysis

The GITT analysis is done following the work of A. Nickol[4] which follows the seminal work of Weppner and Huggins[5]. The lithium spherical particle of radius r_p undergoing oxidation is considered. The voltage behaviour observed for the GITT algorithm is that there is a sudden rise in voltage on switching on of the current known as the IR drop. After which a gradual increase in the voltage is observed which is the diffusion overvoltage. When the current is switched off, there is a sudden drop in voltage which is the second IR drop after which the voltage gradually drops as it relaxes till it reaches a stable voltage as the lithium ions become balanced.

The potential at any point during a GITT test can be derived as per (1) to (10) in [4]. A brief background is also mentioned in the Theory section of this thesis work. The analysis in this thesis has been done using (10), (11) and (12) in [4]. These three equations are summarized as methods below for this thesis work:
Method 1:

$$D1 = \frac{4}{9\pi}\left(\frac{r_p}{t_p}\frac{E4 - E0}{dE/d\sqrt{t}}\right)^2 \tag{4.1}$$

Method 2:

$$D2 = \frac{4}{9\pi}\left(\frac{E4 - E0}{E3 - E0}\right)^2 \frac{(r_p)^2}{t_p} \tag{4.2}$$

Method 3:

$$D3 = \frac{4}{9\pi}\left(\frac{E4 - E0}{E2 - E1}\right)^2 \frac{(r_p)^2}{t_p} \tag{4.3}$$

For method 1, if the GITT pulse exhibits the $\sqrt{t}$ time dependence, it can be written as method 3. Assuming that first IR drop $E_1 - E_0$ is identical to the second IR drop $E_2 - E_3$, the denominator of method 3 can be rewritten as that in method 2.

The value of spherical radius of the particles is considered from previous literature

[4]. The constant parameter values selected for these equations are summarized as follows.

Table 4.1: Constant parameter values for GITT calculation

Parameter	Value
r_p	$5{\times}10^{-6}\mathrm{m}$
t_p	$1800\mathrm{s}$

The values of the rest of the parameters change with each pulse in the GITT test. For each pulse, the value of the diffusion coefficient is calculated.

4.1.2 NMC111 parameters

The average values of diffusion coefficients for $\mathrm{NMC111}$ calculated via the three methods are summarized in Table 4.2.

Table 4.2: The average of diffusion coefficients from each method for the NMC111 Cathode

Method	C/10 rate $[\mathrm{m}^2/\mathrm{s}]$	C/20 rate $[\mathrm{m}^2/\mathrm{s}]$
1	$0\,83 \times 10^{-15}$	$0\,67 \times 10^{-15}$
2	$0\,75 \times 10^{-15}$	$0\,64 \times 10^{-15}$
3	$0\,76 \times 10^{-15}$	$0\,62 \times 10^{-15}$

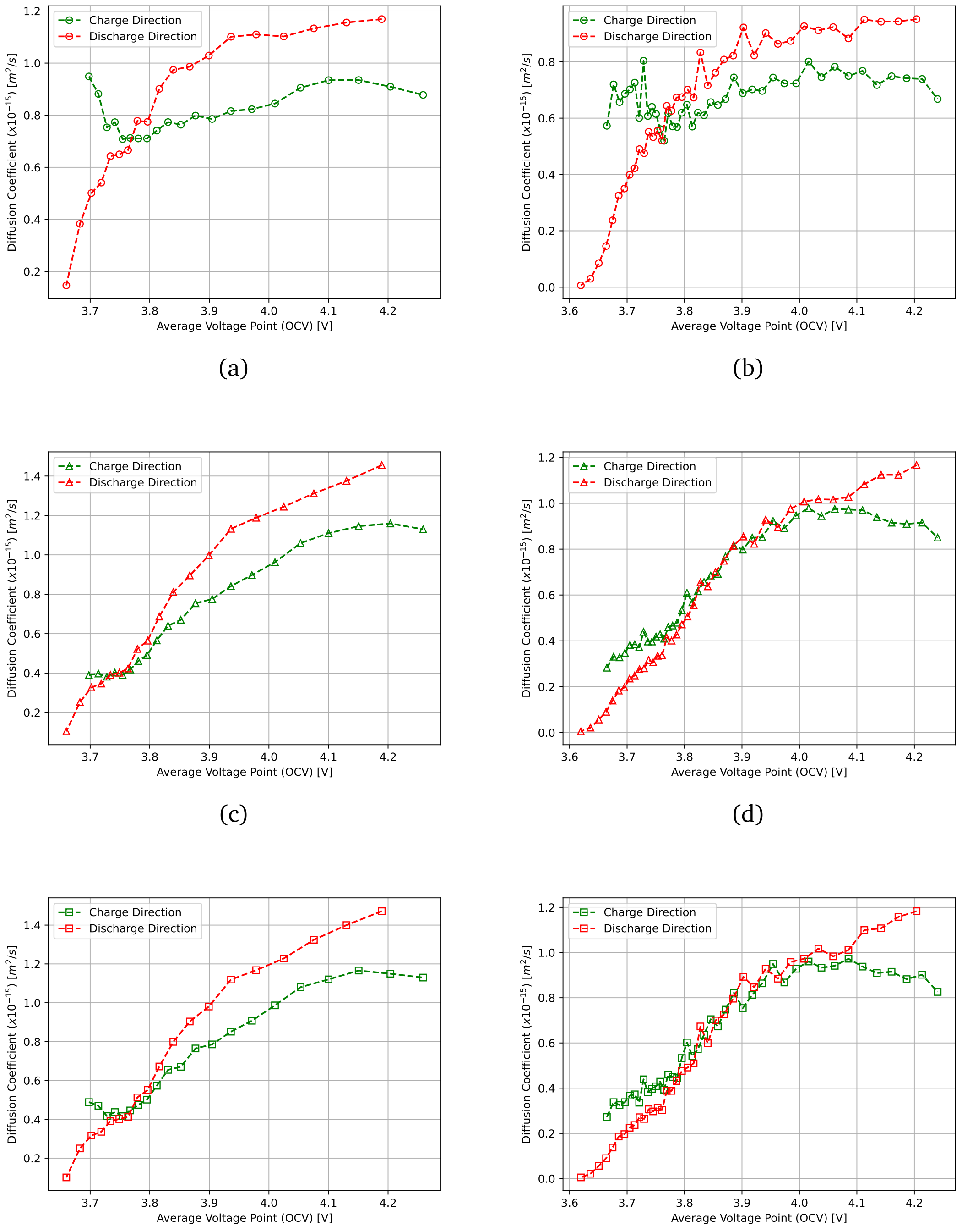

(a) (b)

(c) (d)

(e) (f)

Figure 4.1: NMC111 diffusion coefficients comparison in charge (green curve) and discharge (red curve) direction. Diffusion coefficients using (a) method 1 at C/10, (b) method 1 at C/20, (c) method 2 at C/10, (d) method 2 at C/20, (e) method 3 at C/10, (f) method 3 at C/20, plotted against the average of the E0 and E4 OCV points

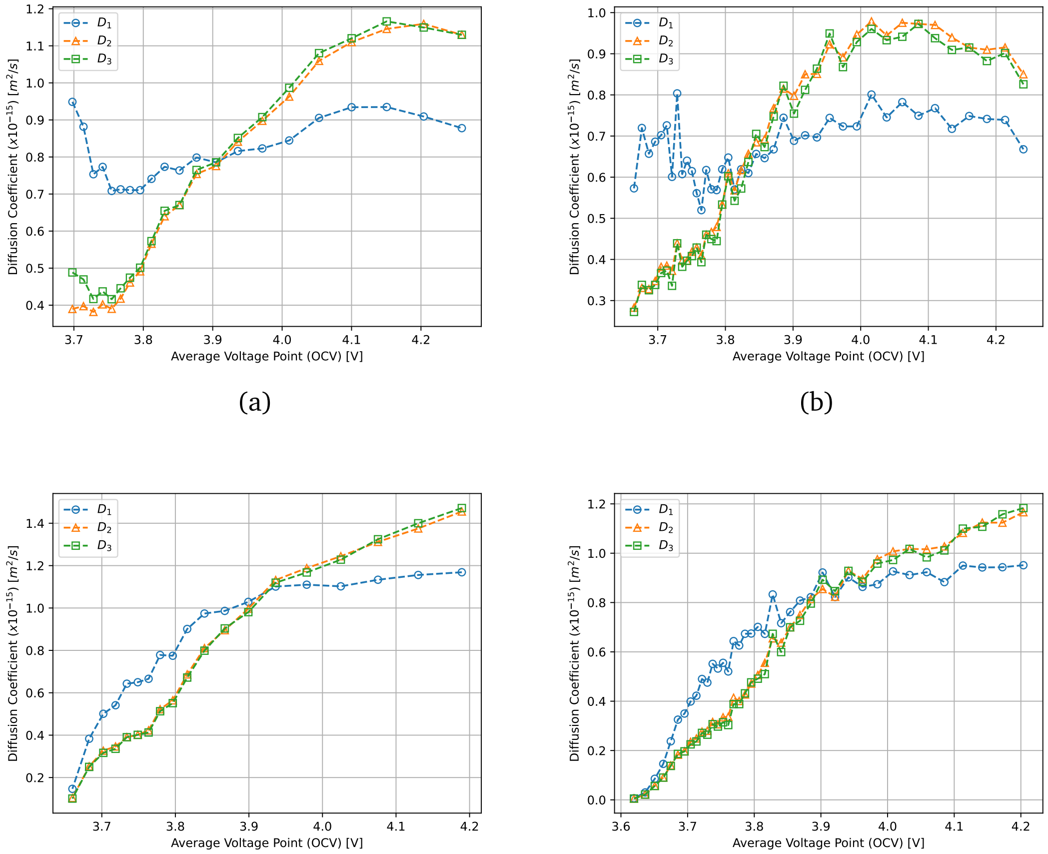

(a) (b) (c) (d)

Figure 4.2: NMC111 diffusion coefficients comparison from the three different methods. Diffusion coefficients in (a) charge direction at C/10, (b) charge direction at C/20, (c) discharge direction at C/10, (d) discharge direction at C/20, plotted against the average of the E0 and E4 OCV points

4.1.3 NMC622 parameters

The average values of diffusion coefficients for NMC622 calculated via the three methods are summarized in Table 4.3. below table.

Table 4.3: The average of diffusion coefficients for NMC622 Cathode

Method	C/10 rate $[\mathrm{m}^2/\mathrm{s}]$	C/20 rate $[\mathrm{m}^2/\mathrm{s}]$
1	0.87805×10^{-15}	0.66954×10^{-15}
2	0.79158×10^{-15}	0.74372×10^{-15}
3	0.80625×10^{-15}	0.74746×10^{-15}

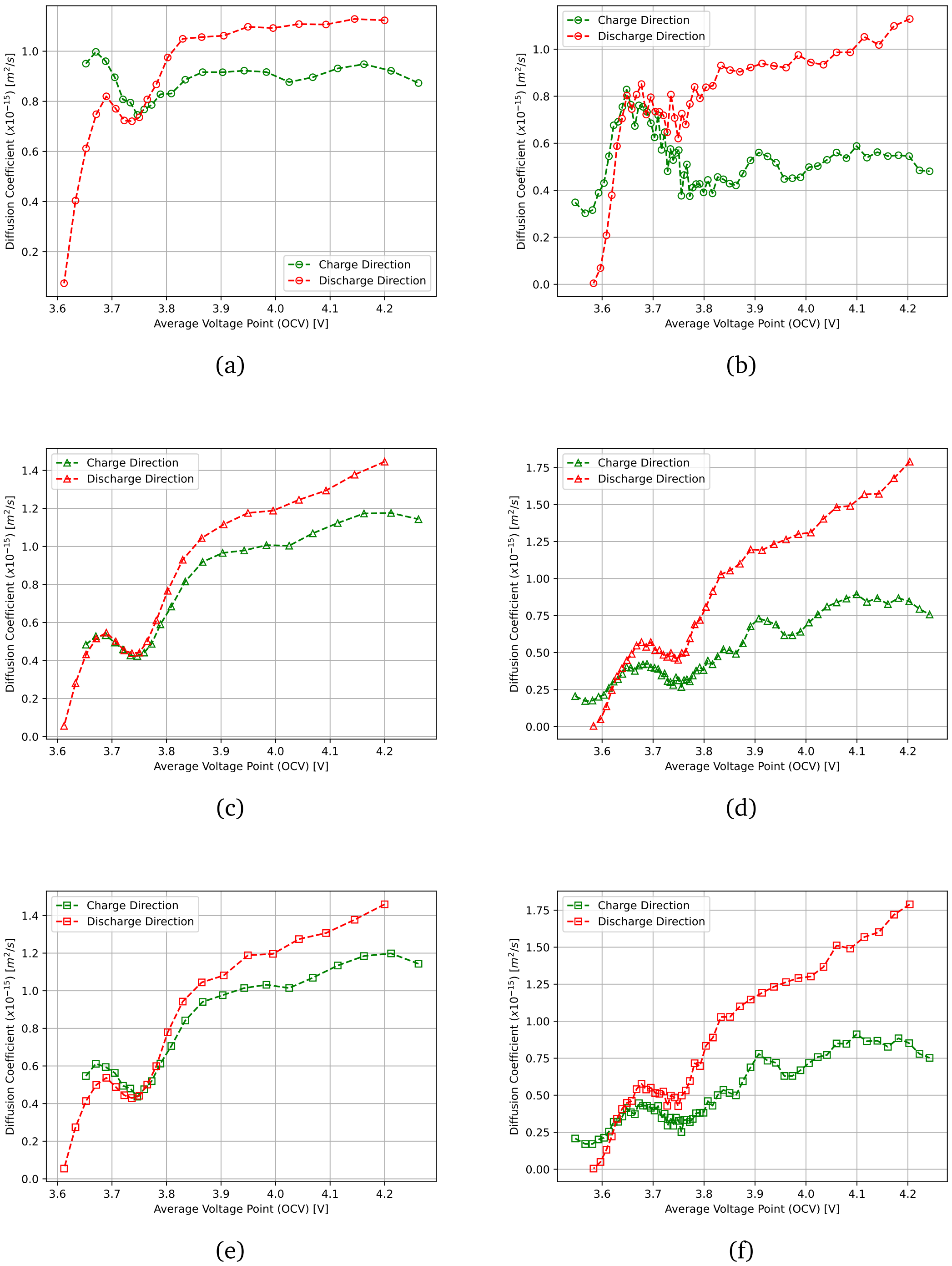

(a) (b)

(c) (d)

(e) (f)

Figure 4.3: NMC622 diffusion coefficients comparison in charge (green curve) and discharge (red curve) direction. Diffusion coefficients using (a) method 1 at C/10, (b) method 1 at C/20, (c) method 2 at C/10, (d) method 2 at C/20, (e) method 3 at C/10, (f) method 3 at C/20, plotted against the average of the E0 and E4 OCV points

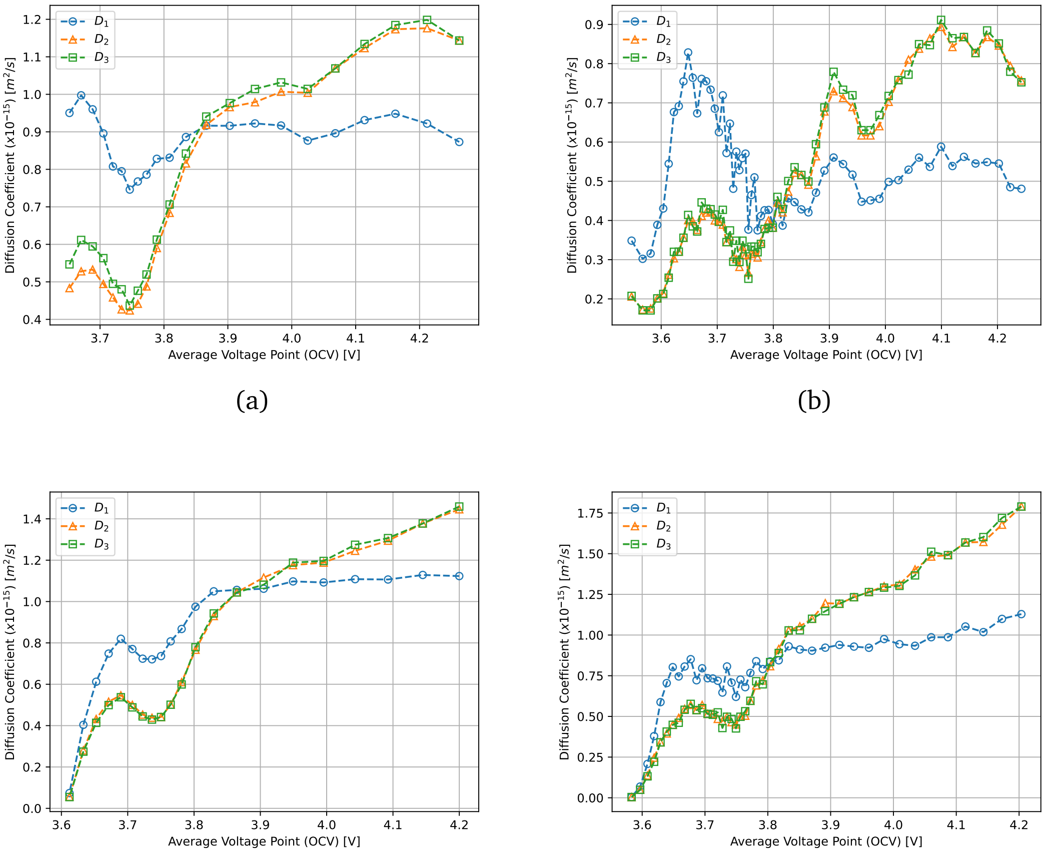

(a) (b) (c) (d)

Figure 4.4: NMC622 diffusion coefficients comparison from three different methods. Diffusion coefficients in (a) charge direction at C/10, (b) charge direction at C/20, (c) discharge direction at C/10, (d) discharge direction at C/20, plotted against average of E0 and E4 OCV points

4.1.4 NMC811 parameters

The average values of diffusion coefficients for NMC811 calculated via the three methods are summarized in Table 4.4. below table.

Table 4.4: The average of diffusion coefficients for NMC811 Cathode

Method	C/10 rate $[\mathrm{m}^2/\mathrm{s}]$	C/20 rate $[\mathrm{m}^2/\mathrm{s}]$
1	0.77285×10^{-15}	0.49848×10^{-15}
2	0.68236×10^{-15}	0.56809×10^{-15}
3	0.69032×10^{-15}	0.56666×10^{-15}

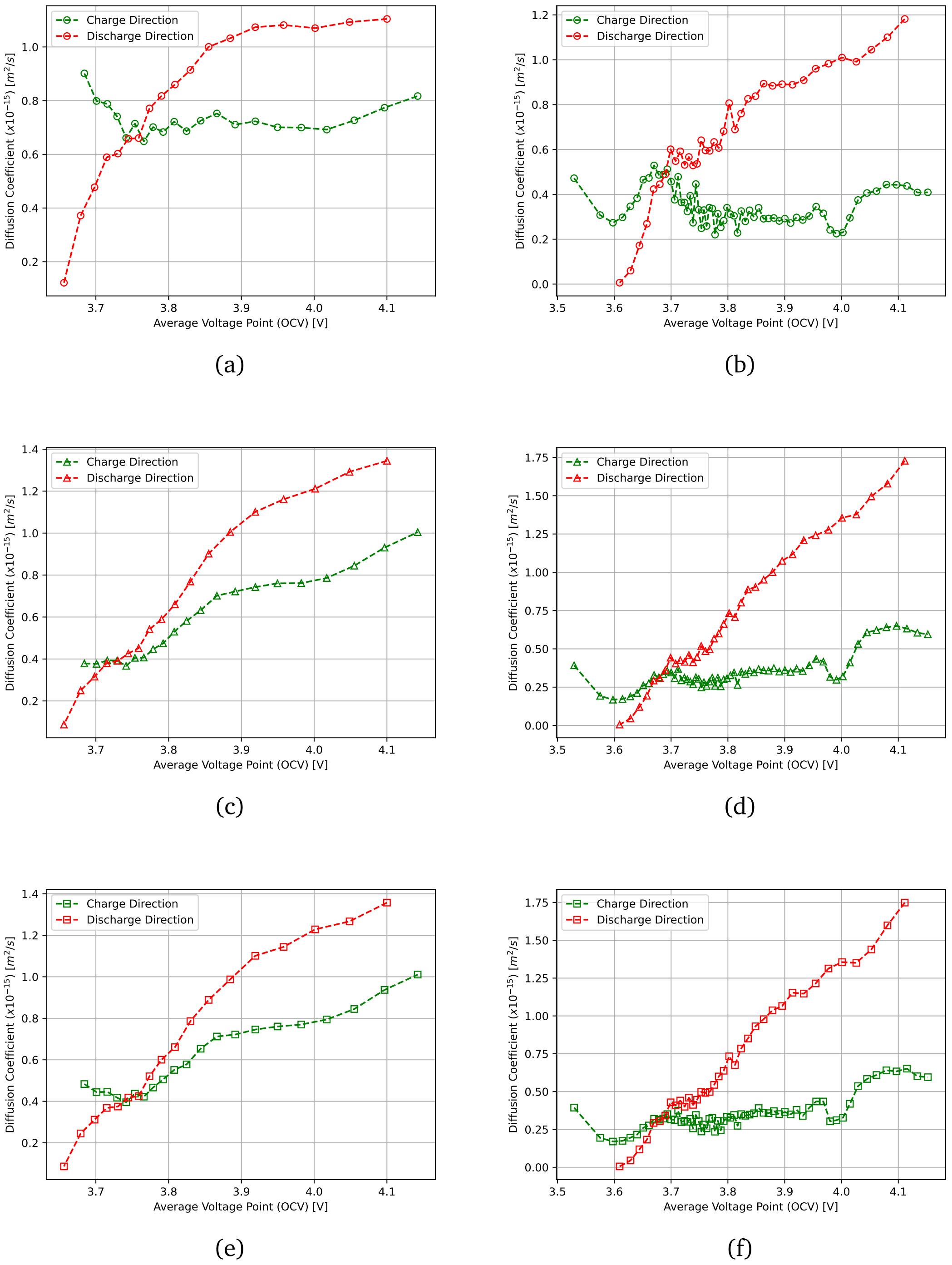

(a) (b)

(c) (d)

(e) (f)

Figure 4.5: NMC811 diffusion coefficients comparison in charge (green curve) and discharge (red curve) direction. Diffusion coefficients using (a) method 1 at C/10, (b) method 1 at C/20, (c) method 2 at C/10, (d) method 2 at C/20, (e) method 3 at C/10, (f) method 3 at C/20, plotted against average of E0 and E4 OCV points

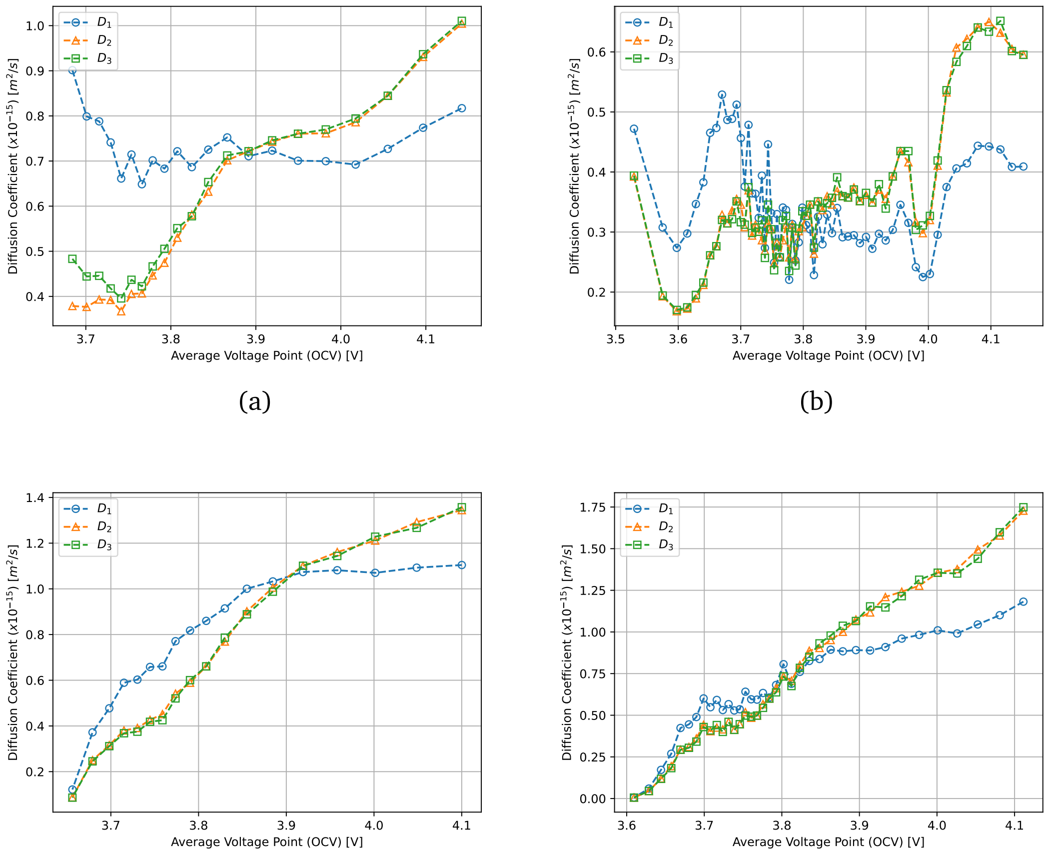

(a) (b)

(c) (d)

Figure 4.6: NMC811 diffusion coefficients comparison from three different methods. Diffusion coefficients in (a) charge direction at C/10, (b) charge direction at C/20, (c) discharge direction at C/10, (d) discharge direction at C/20, plotted against the average of the E0 and E4 OCV points

4.1.5 NMC111, NMC622 and NMC811 comparison

Diffusion Coefficient

A common observation is that the diffusion coefficient has a strong voltage dependence.

At very low voltages during charging, there are higher estimations of diffusion coefficients which might be because of cell instability. After this, the diffusion coefficient value increases with increasing voltage. This increase is sharper at lower SOC but becomes more constant at higher SOC. This is due to that at these points, Li mobility is stimulated by the creation of Li vacancies which increases the number of carriers as well as the substantial increase in Li layer spacing which decreases the activation barrier for Li hops [16].

The discharge curves, show a near reversible behaviour of the charge curves. It also has more consistent drop in diffusion coefficient compared to during charging.

On using method 1 for calculation, the graphs look different when compared to method 2 and method 3 which are quite similar. This is because method 1 has a root time dependence.

While charging, in all cases, NMC811 has the lowest values of diffusion coefficients. For discharging, for C/10 rate, the diffusion coefficient values are almost equal but for C/20 rate, the NMC111 consistently show slightly lower values. For all the below cases, generally NMC622 has highest diffusion coefficient values at lower voltages compared to the other two cathodes.

Diffusion coefficient from Method 1

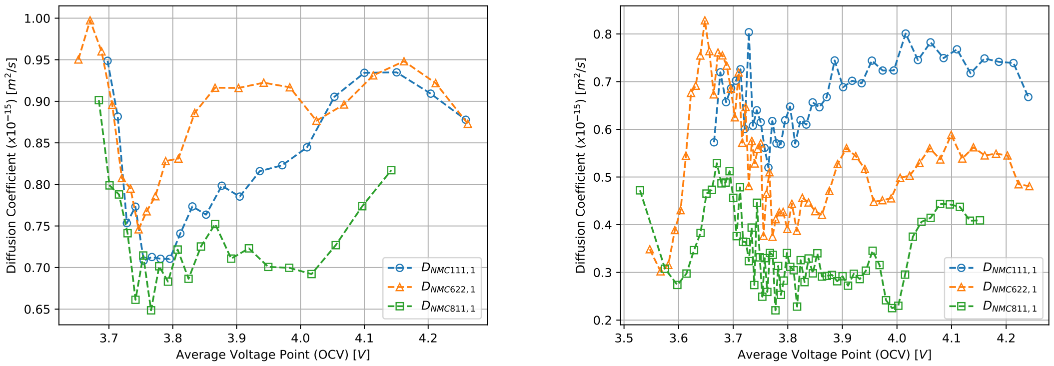

(a)

(b)

Figure 4.7: NMC111, NMC622 and NMC811 diffusion coefficient comparison for (a) C/10 and (b) C/20 charge rate using method 1

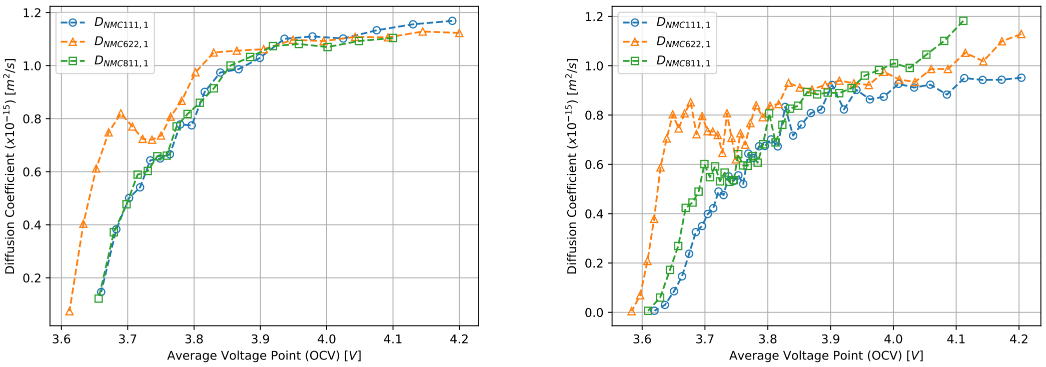

(a) (b)

Figure 4.8: NMC111, NMC622 and NMC811 diffusion coefficient comparison for C/10 discharge rate using method 1

Diffusion coefficient from Method 2

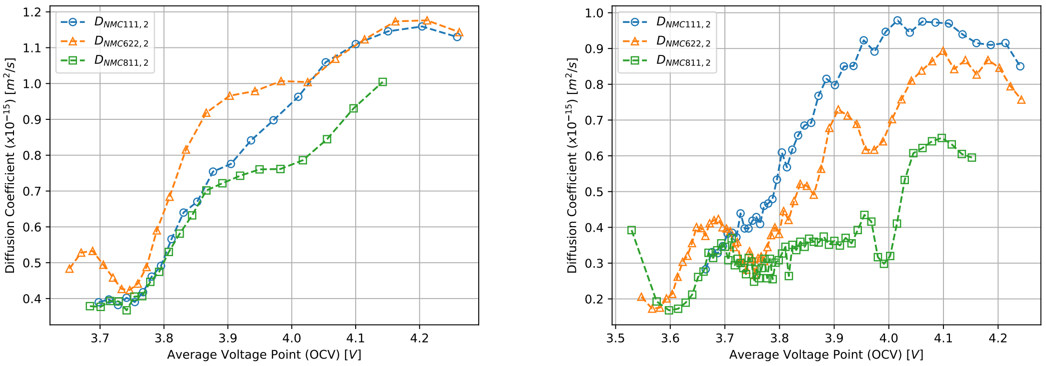

(a) (b)

Figure 4.9: NMC111, NMC622 and NMC811 diffusion coefficient comparison for (a) C/10 and (b) C/20 charge rate using method 2

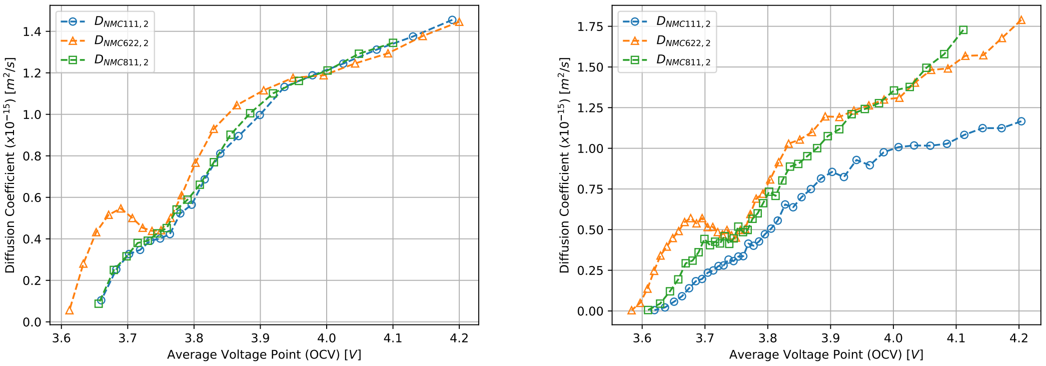

(a) (b)

Figure 4.10: NMC111, NMC622 and NMC811 diffusion coefficient comparison for (a) C/10 and (b) C/20 discharge rate using method 2

Diffusion coefficient from Method 3

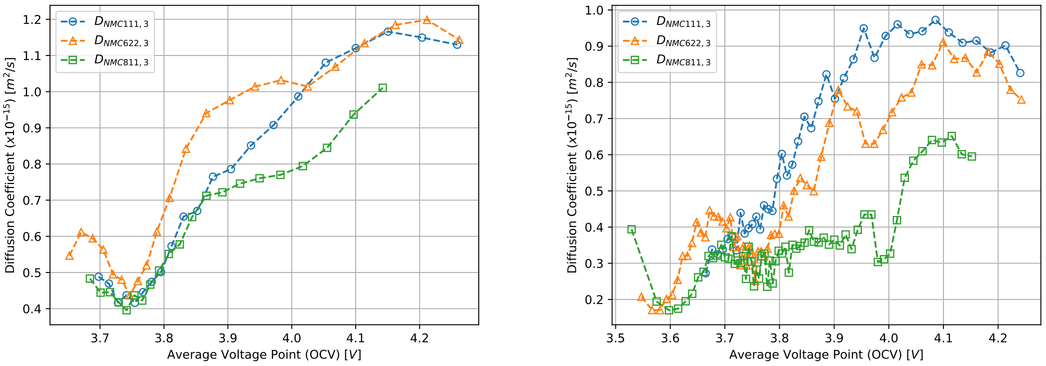

(a) (b)

Figure 4.11: NMC111, NMC622 and NMC811 diffusion coefficient comparison for (a) C/10 and (b) C/20 charge rate using method 3

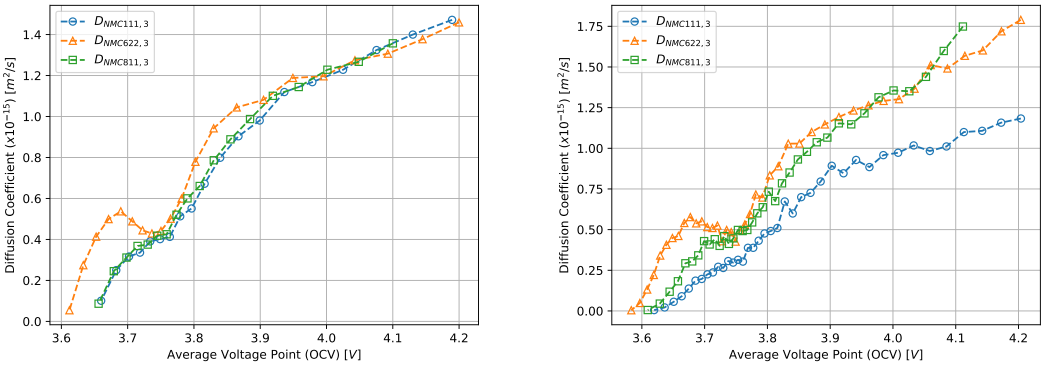

(a) (b)

Figure 4.12: NMC111, NMC622 and NMC811 diffusion coefficient comparison for (a) C/10 and (b) C/20 discharge rate using method 3

4.2 Electrochemical Impedance Spectroscopy (EIS)

4.2.1 EIS analysis

By conducting EIS at different voltages, Nyquist plots are obtained. These plots are analysed by fitting experimental data using an electrochemical model.

EIS curve fitting

In the Nyquist plot we see two semicircles followed by a straight line. One semicircle represents the cathode electrolyte interface (CEI) resistance and capacitance while the other semicircle represents the double layer capacitance and charge transfer resistance of the electrodes. At the end of the semicircles at low frequencies, is a line of a constant slope which represents the diffusion taking place in the active materials of the electrodes[14].

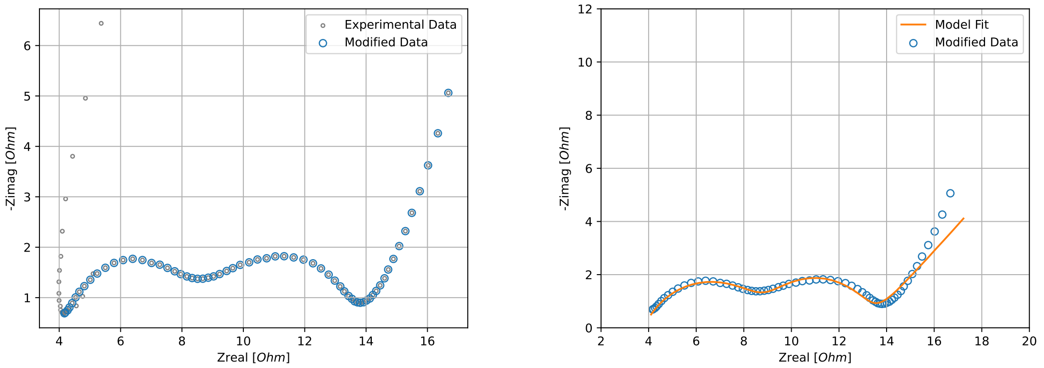

(a)

(b)

Figure 4.13: Nyquist plots for the NMC111 cathode half-cell. (a) Experimental and modified data points. Experimental data is shown with grey circle markers, while modified data is shown in blue circle markers. (b) Model fit and modified points.

The plots are curve fitted using the following steps.

- **Step 1, Data cleaning:** While analyzing the nyquist plots for all chemistries, a capacitive behaviour is observed at higher frequencies. Approximately, the first 16 initial points due to this behaviour, are removed from every test for the purpose of data cleaning so that the analysed data starts from 20kHz.
- **Step 2, Locking $R0$:** The start of the semicircle is a non-zero value as per the real axis, which corresponds to the sum of the ohmic resistances of the active material, electrolyte, separator and the current collectors. The starting point of the curve which is the $R0$ value is fixed by locking it in the GAMRY software. This is a very important task as the curve fit is highly sensitive to this value and even a slight deviation in 1-2 decimal places can give a significant change in the curve fit.
- **Step 3, Fitting $R1$ and $R2$:** The locking of $R0$ gives some fit values for $R1$ and $R2$. It is important to ensure that the fit values of these resistances are very close to the original data values. This inspection is done visually. If the deviations are too high, then the $R0$ value is re-fit and re-locked to get better fits for $R1$ and $R2$.

This following observations were made using the above approach which can also be seen in Appendix 2.

- The local minima where $R1$ ends and $R2$ starts is accurately fit in most cases.
- The local minima where the $R2$ ends and the diffusion line begins is not very accurately fit with the original data. It shows a slight deviation.
- Even though the diffusion curve fit seems off in all cases, the error margins in the fit given by the software is very low for the warburg element and in general for all parameters. If an attempt is made to fit the diffusive tail by locking the Warburg element, the error margins increase a lot for other parameters like charge transfer resistances. Locking a combination of resistances also gives high error margins for the Warburg element.

- Amongst all the different attempts made in fitting the curve, locking $R0$ to a good value, gives more accurate results with very low error margins and better values of goodness of fit.

Electrochemical model

For the EIS analysis, electrochemical models are studied and then a model is created which resembles the physical reactions happening inside the cell. For choosing an electrochemical model, three major points are followed in the order:

- **Physical interpretation**: The elements of the model should be physical
- **Simplified**: The model should be simplified, i.e. repetitive elements should be avoided as it causes an overfit.
- **Minimum error and maximum goodness of fit**: The goodness of fit in the software should be good.

Keeping these in mind, the below equivalent circuit model is considered for the analysis.

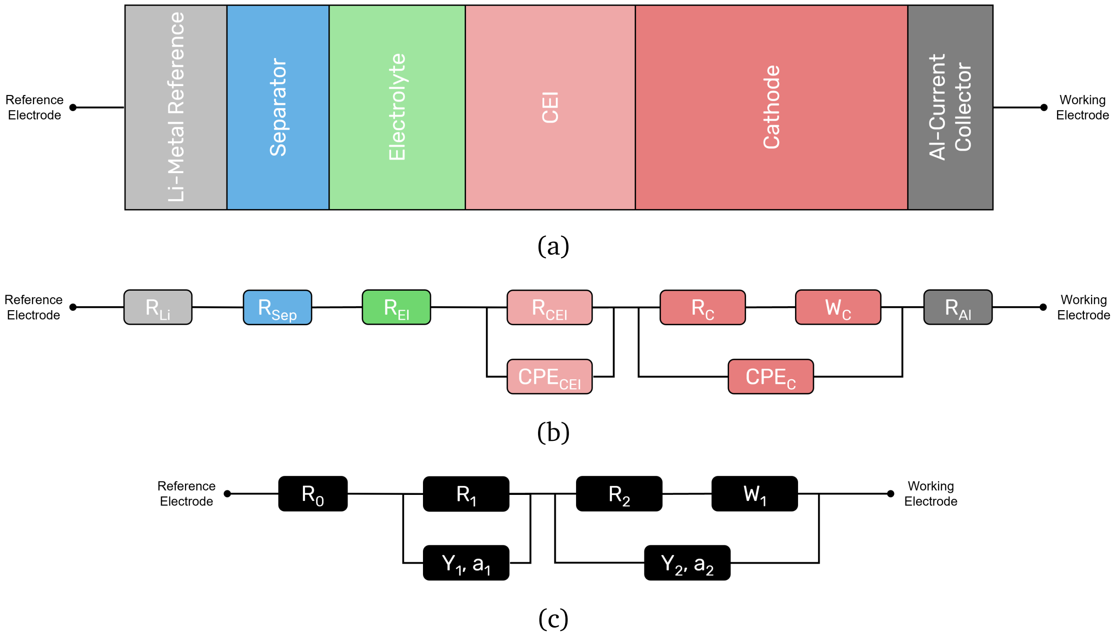

Figure 4.14: (a) Illustration of half cell physics (b) Equivalent circuit model of the physical half cell (c) Simplified equivalent circuit model used for EIS fitting

where $R0$ is the sum of resistances from the electrolyte, reference ring, separator and current collectors, $R1$ is the CEI resistance, $Y1$ and $a1$ are used for the CPE calculation of CEI, $R2$ is the Charge transfer resistance, $Y2$ and $a2$ are used for CPE calculation of the cathode and $W1$ is Warburg element of diffusion.

The following values are considered for the constant parameters for calculations.

Table 4.5: Constant parameter values for EIS calculations

Parameter	Value
R	8.314 $(\mathrm{JmolK})^{-}1$
T	290 K
A	1.539×10^{-4} m^2
c	1000 $\mathrm{mol/m}^3$
F	96485 $\mathrm{A\,s\,mol}^{-}1$
n	1

where R is the universal gas constant, T is the absolute temperature A is the working surface area of the cathode electrode, c is the molar density of a lithium ion in an electrode due to electrolyte, F is the faraday constant, n is the electronic transport ratio during a redox reaction.

Diffusion coefficient

The diffusion coefficient in $[\mathrm{m}^2/\mathrm{s}]$ is calculated using the following relation,

$$D = \left(\frac{RT}{n^2F^2A\sqrt{2}\sigma}\right)^2 \tag{4.4}$$

where $\sigma = \frac{1}{W}$ is the slope on the diffusion state of EIS measurement and W is the warburg element which we obtain from the fit.
The error margin due to uncertainty in the fitting is taken from the software and the parameter is considered as follows,

$$W_{\pm} = W \pm error\ margin(W) \tag{4.5}$$

For each of these cases D_+ and D_- are calculated. The values of these error margins are mentioned in the Appendix 2.

Exchange current Density

The exchange current density is calculated in $[\mathrm{A/m}^2]$ as per the following formula,

$$i_0 = \frac{RT}{nA_{acm}FR_{ct}} \tag{4.6}$$

where R_{ct} is the charge transfer resistance which is equal to $R2$ from the fit, A_{acm} is the actual surface area of the electrode including the effect of porosity and is calculated according to,

$$A_{acm} = \frac{3\varepsilon}{r_p}V_{tot} \tag{4.7}$$

In the above equation, ε is the porosity, r_p is the particle radius and V_{tot} is the total volume of the electrode. The r_p value is considered the same as for the GITT analysis. The thickness of the electrode used to calculate the total volume of the electrode is taken from the CUSTOMCELL datasheet and is actually the thickness of collector. The porosity is obtained by contacting them via e-mail. The values are summarized as follows.

Table 4.6: CUSTOMCELL material values

Chemistry	Porosity	Electrode thickness
NMC111	35%	$20\mu m$
NMC622	40%	$20\mu m$
NMC811	42%	$20\mu m$

The error margin due to uncertainty in the fitting is taken from the software and the parameter is considered as follows.

$$R2_{\pm} = R2 \pm error\ margin(R2) \tag{4.8}$$

For each of these cases $i0_+$ and $i0_-$ are calculated. The values of these error margins are mentioned in the Appendix 2.

Double layer capacitance

$Y2$, $a2$ and R_{ct}(which is equal to $R2$), are the parameters related to the CPE calculation obtained from the EIS fit of one of the semicircles on the Nyquist plot. The double layer capacitance is calculated using the expression,

$$C_{dl} = \frac{(R_{ct}Y2)^{\frac{1}{a2}}}{R_{ct}} \tag{4.9}$$

The error margin due to uncertainty in the fitting is taken from the software and the parameters are considered as follows.

$$R2_{\pm} = R2 \pm error\ margin(R2) \tag{4.10}$$

$$Y2_{\pm} = Y2 \pm error\ margin(Y2) \tag{4.11}$$

$$a2_{\pm} = a2 \pm error\ margin(a2) \tag{4.12}$$

For these two cases Cdl_+ is calculated using each parameter with the error margin added to their value and Cdl_- is calculated using each parameter with the error margin subtracted from their value. The values of these error margins are mentioned in the Appendix 2.

CEI capacitance

$Y1$, $a1$ and $R1$ are the parameters related to the CPE calculation of one of the semicircles on the Nyquist plot. The CEI capacitance is calculated as per the following formula.

$$C_{cei} = \frac{(R1Y1)^{\frac{1}{a1}}}{R1} \tag{4.13}$$

The error margin due to the uncertainty in fitting is taken from the software and the parameters are considered as follows.

$$R1_{\pm} = R1 \pm error\ margin(R1) \tag{4.14}$$

$$Y1_{\pm} = Y1 \pm error\ margin(Y1) \tag{4.15}$$

$$a1_{\pm} = a1 \pm error\ margin(a1) \tag{4.16}$$

For these cases $Ccei_{+}$ is calculated using each parameter with error margin added to their value and $Ccei_{-}$ is calculated using each parameter with error margin subtracted from their value. The values of these error margins are mentioned in the Appendix 2.

4.2.2 NMC111 parameters

Diffusion coefficient

The diffusion coefficient range is depicted below. The range can be seen vertically at any given point. The higher line shows the value of the diffusion coefficient when the error margin is added to the equation and the lower line shows the value of the diffusion coefficient when the error margin is subtracted in the equation. It can also be observed that there is a consistent decrease in error margin gap as the cell is discharged to lower voltages.

The diffusion constant phase element exponent, $a2$, is more than 0.7 for all values except for the fourth and eight and hence the approximation of the Warburg element for these can be considered good. Hence, the diffusion coefficient values determined from it can be said to be precise. [17]

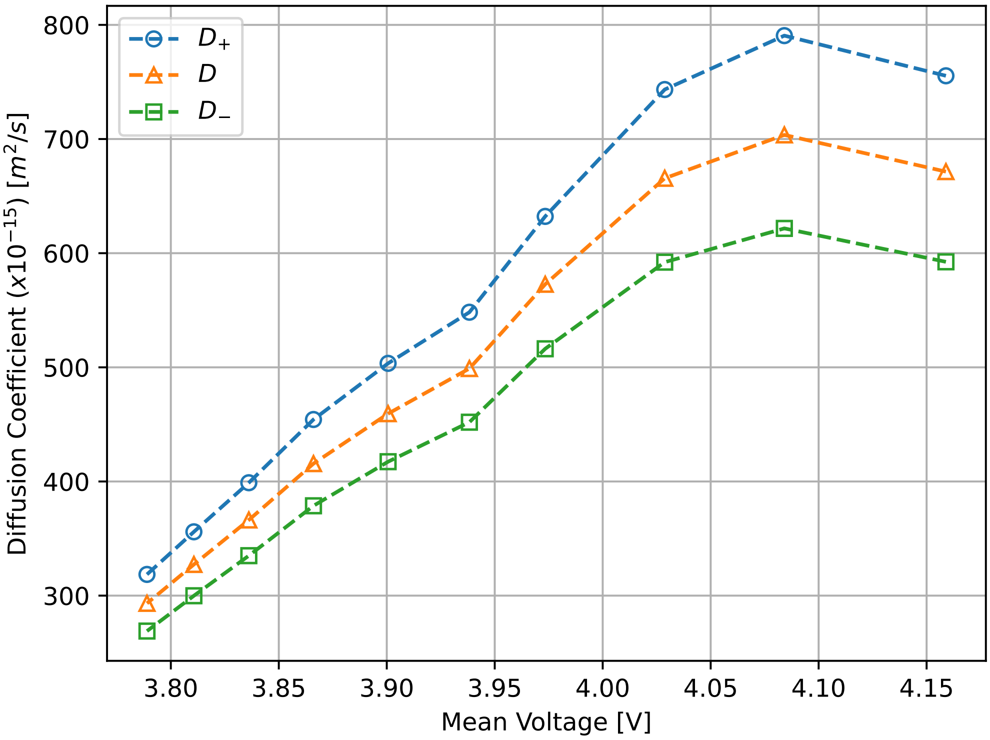

Figure 4.15: Diffusion coefficient range for NMC111

Table 4.7: NMC111 half-cell D_+, D and D_- cathode diffusion coefficient range values

Sr No	V_{mean} [V]	D_+ [m^2/s]	D [m^2/s]	D_- [m^2/s]
1	4.159	7.55×10^{-13}	6.71×10^{-13}	5.92×10^{-13}
2	4.084	7.90×10^{-13}	7.03×10^{-13}	6.21×10^{-13}
3	4.029	7.43×10^{-13}	6.65×10^{-13}	5.92×10^{-13}
4	3.973	6.32×10^{-13}	5.72×10^{-13}	5.16×10^{-13}
5	3.938	5.48×10^{-13}	4.98×10^{-13}	4.51×10^{-13}
6	3.901	5.03×10^{-13}	4.59×10^{-13}	4.17×10^{-13}
7	3.866	4.54×10^{-13}	4.15×10^{-13}	3.78×10^{-13}
8	3.836	3.98×10^{-13}	3.66×10^{-13}	3.35×10^{-13}
9	3.811	3.55×10^{-13}	3.27×10^{-13}	2.99×10^{-13}
10	3.789	3.18×10^{-13}	2.93×10^{-13}	2.68×10^{-13}

Exchange current density

The exchange current density increases as voltage drops initially as per table, after which it is constant and then it starts to decrease. It has an inverse relation to the charge transfer resistance.

The error margin range can be vertically observed at every point. The error margin gap is nearly consistent at any point. It is unclear why the fourth point as per table gives a large deviation. It could be due to underlying reaction or EIS fitting issues.

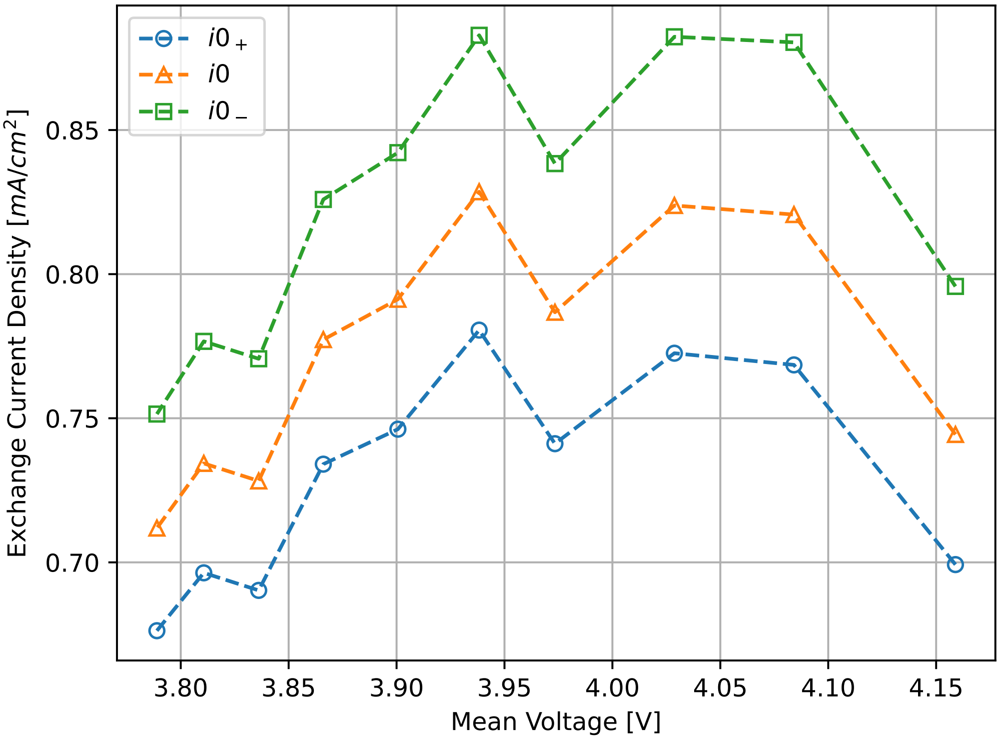

Figure 4.16: Exchange current density range for NMC111

Table 4.8: NMC111 half-cell $i0_+$, $i0$ and $i0_-$ cathode exchange current density range values

Sr No	V_{mean} [V]	$i0_+$ [mA/cm^2]	$i0$ [mA/cm^2]	$i0_-$ [mA/cm^2]
1	4.159	0.69	0.74	0.79
2	4.084	0.76	0.82	0.88
3	4.029	0.77	0.82	0.88
4	3.973	0.74	0.78	0.83
5	3.938	0.78	0.82	0.88
6	3.901	0.74	0.79	0.84
7	3.866	0.73	0.77	0.82
8	3.836	0.69	0.72	0.77
9	3.811	0.69	0.73	0.77
10	3.789	0.67	0.711	0.75

Double layer capacitance

The double layer capacitance of NMC111 cathode has a constant behaviour and does not change drastically with voltage.

The range gap is not equal for the double layer because of the way the Cdl_+ and Cdl_- are calculated. For the former, the error margins of each parameter used to calculate Cdl_+ are added to their respective values. For the later, same procedure is followed except that the Error margins are subtracted from their respective values. Hence the graph does not show the extreme values of the double layer capacitance and only shows how it would look if all parameters used to calculate it are at the highest or lowest levels in their respective range.

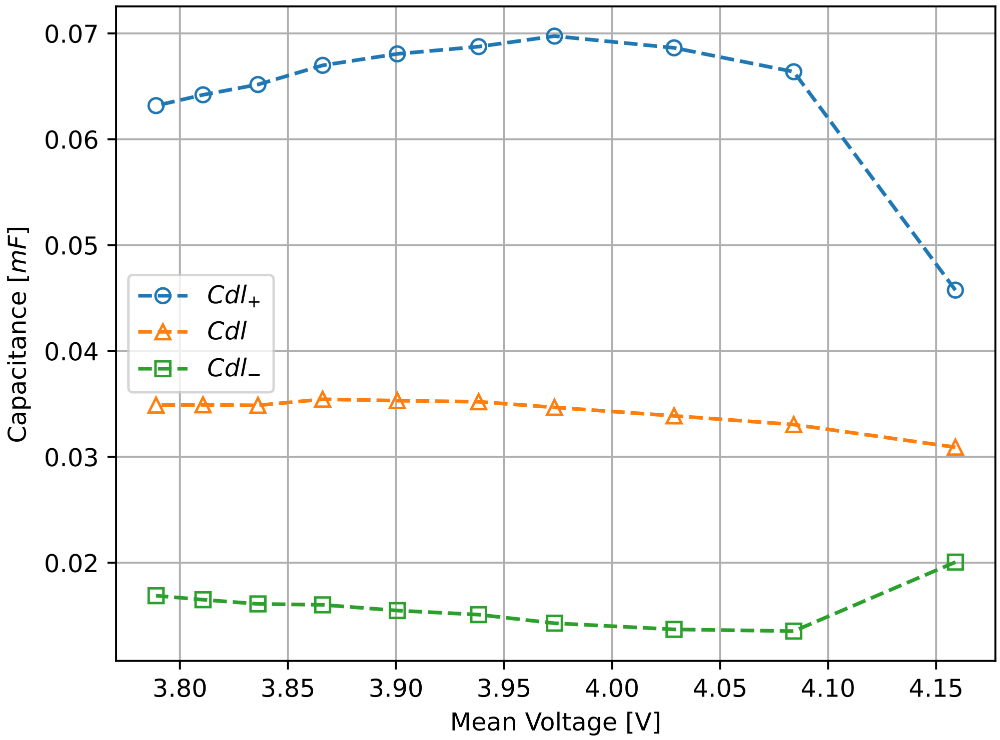

Figure 4.17: Double layer capacitance range for NMC111

Table 4.9: NMC111 Cdl_+, Cdl and Cdl_- cathode double layer capacitance range values

NMC111 Half Cell				
$SrNo$	V_{mean} [V]	Cdl_+ [F]	Cdl [F]	Cdl_- [F]
1	4.159	4.57×10^{-5}	3.09×10^{-5}	2.00×10^{-5}
2	4.084	6.63×10^{-5}	3.30×10^{-5}	1.35×10^{-5}
3	4.029	6.86×10^{-5}	3.38×10^{-5}	1.37×10^{-5}
4	3.973	6.97×10^{-5}	3.46×10^{-5}	1.42×10^{-5}
5	3.938	6.87×10^{-5}	3.52×10^{-5}	1.51×10^{-5}
6	3.901	6.80×10^{-5}	3.53×10^{-5}	1.54×10^{-5}
7	3.866	6.69×10^{-5}	3.54×10^{-5}	1.60×10^{-5}
8	3.836	6.51×10^{-5}	3.48×10^{-5}	1.61×10^{-5}
9	3.811	6.41×10^{-5}	3.49×10^{-5}	1.65×10^{-5}
10	3.789	6.31×10^{-5}	3.48×10^{-5}	1.68×10^{-5}

CEI capacitance

The CEI capacitance is also more or less a constant value and is not highly potential dependent.

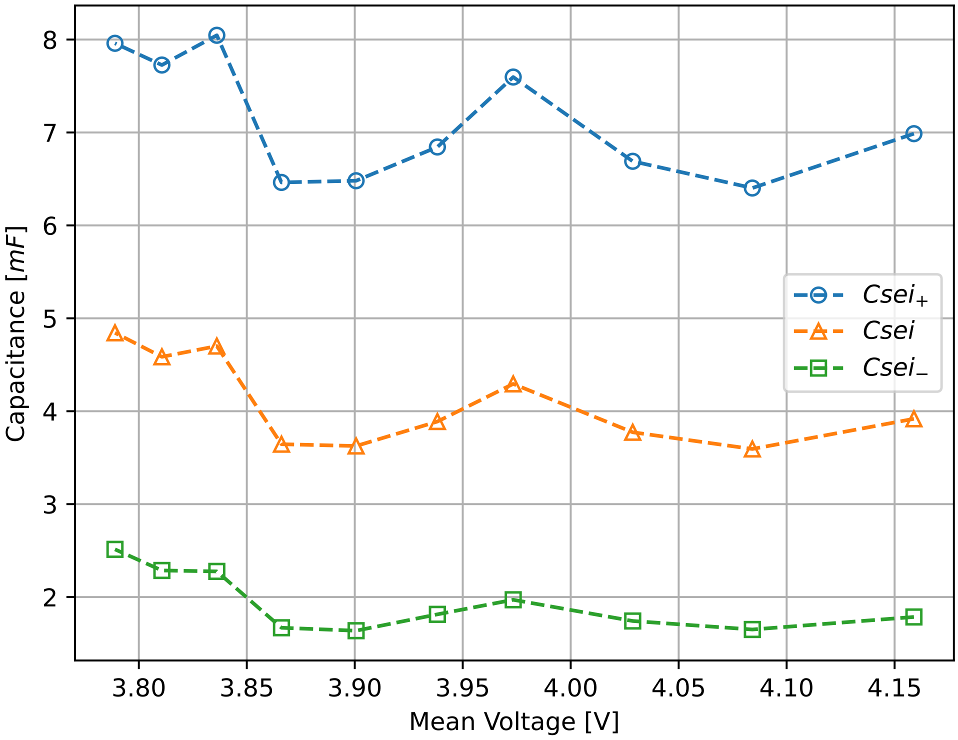

Figure 4.18: CEI capacitance range for NMC111

Table 4.10: NMC622 half-cell $Ccei_+$, $Ccei$ and $Ccei_-$ cathode double layer capacitance range values

Sr No	V_{mean} [V]	$Ccei_+$ [F]	$Ccei$ [F]	$Ccei_-$ [F]
1	4.159	6.98×10^{-3}	3.91×10^{-3}	1.78×10^{-3}
2	4.084	6.40×10^{-3}	3.59×10^{-3}	1.65×10^{-3}
3	4.029	6.68×10^{-3}	3.77×10^{-3}	1.74×10^{-3}
4	3.973	7.59×10^{-3}	4.29×10^{-3}	1.97×10^{-3}
5	3.938	6.84×10^{-3}	3.88×10^{-3}	1.81×10^{-3}
6	3.901	6.48×10^{-3}	3.62×10^{-3}	1.63×10^{-3}
7	3.866	6.46×10^{-3}	3.64×10^{-3}	1.66×10^{-3}
8	3.836	8.04×10^{-3}	4.70×10^{-3}	2.27×10^{-3}
9	3.811	7.72×10^{-3}	4.58×10^{-3}	2.28×10^{-3}
10	3.789	7.95×10^{-3}	4.84×10^{-3}	2.51×10^{-3}

4.2.3 NMC622 parameters

Diffusion coefficient

The diffusion coefficients behaviour for $\mathrm{NMC622}$ are observed as stated for $\mathrm{NMC111}$.

All values of the diffusion constant phase element exponent, $a2$, are more than 0.7 for all values and hence approximation of the Warburg element for these can be considered good. Hence, diffusion coefficient values determined from it can be said to be precise. [17]

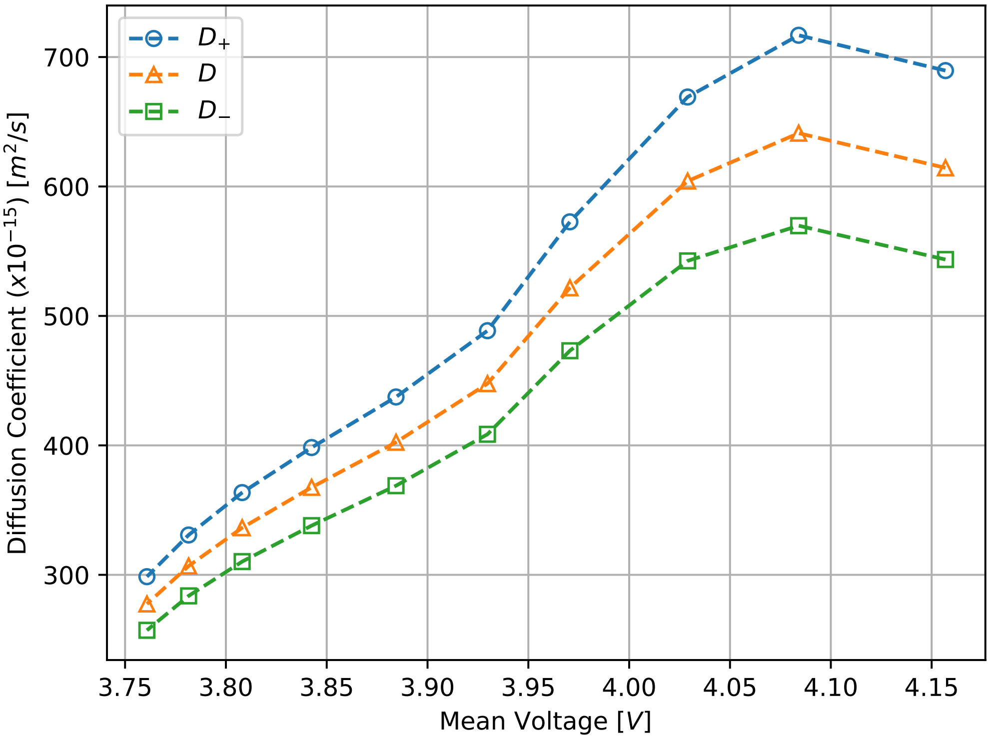

Figure 4.19: Diffusion coefficient range for NMC622

Table 4.11: NMC622 half-cell D_+, D and D_- cathode diffusion coefficient range values

Sr No	V_{mean} [V]	D_+ [$\mathrm{m^2/s}$]	D [$\mathrm{m^2/s}$]	D_- [$\mathrm{m^2/s}$]
1	4.157	6.89×10^{-13}	6.14×10^{-13}	5.43×10^{-13}
2	4.084	7.16×10^{-13}	6.41×10^{-13}	5.69×10^{-13}
3	4.029	6.69×10^{-13}	6.04×10^{-13}	5.42×10^{-13}
4	3.971	5.72×10^{-13}	5.21×10^{-13}	4.73×10^{-13}
5	3.930	4.88×10^{-13}	4.47×10^{-13}	4.08×10^{-13}
6	3.884	4.37×10^{-13}	4.02×10^{-13}	3.68×10^{-13}
7	3.843	3.98×10^{-13}	3.67×10^{-13}	3.38×10^{-13}
8	3.808	3.63×10^{-13}	3.36×10^{-13}	3.10×10^{-13}
9	3.782	3.30×10^{-13}	3.06×10^{-13}	2.83×10^{-13}
10	3.761	2.98×10^{-13}	2.77×10^{-13}	2.57×10^{-13}

Exchange current density

The exchange current density behaviour for NMC622 are observed as stated for NMC111.

For NMC622, the deviation point is the third value as per the Table 4.12.

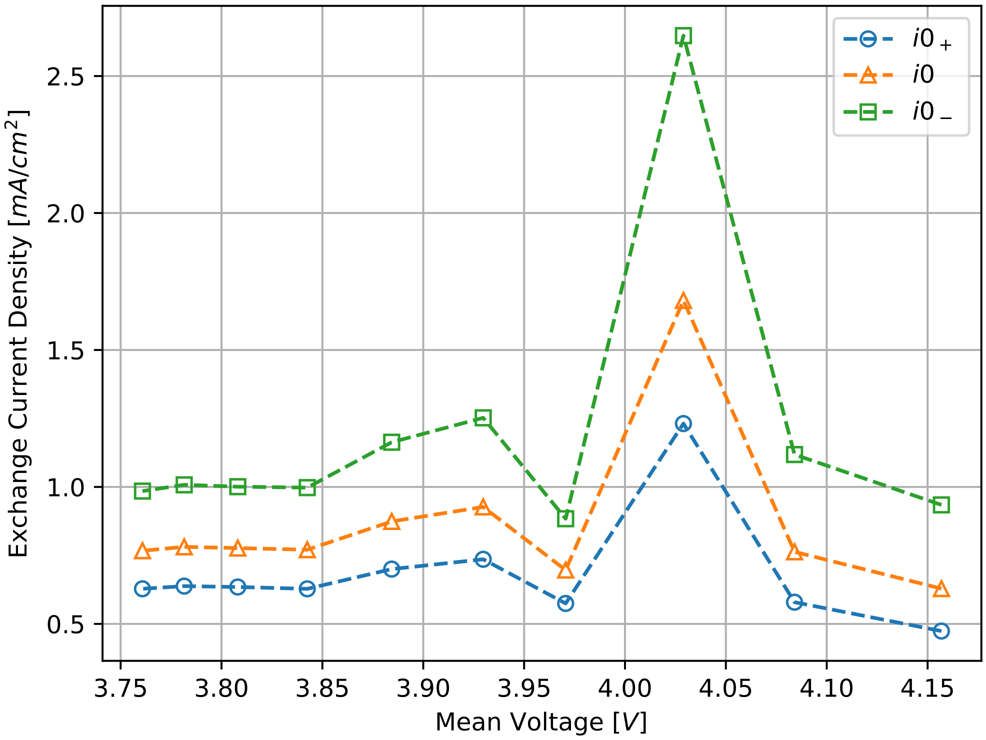

Figure 4.20: Exchange current density range for NMC622

Table 4.12: NMC622 half-cell $i0_+$, $i0$ and $i0_-$ cathode exchange current density range values

Sr No	V_{mean} [V]	$i0_+$ [mA/cm^2]	$i0$ [mA/cm^2]	$i0_-$ [mA/cm^2]
1	4.157	0.47	0.62	0.93
2	4.084	0.57	0.76	1.11
3	4.029	1.23	1.68	2.64
4	3.971	0.57	0.69	0.88
5	3.930	0.73	0.92	1.25
6	3.884	0.70	0.87	1.16
7	3.843	0.62	0.77	0.99
8	3.808	0.63	0.77	1.00
9	3.782	0.63	0.78	1.00
10	3.761	0.62	0.76	0.98

Double layer capacitance

The double layer capacitance behaviour for NMC622 is observed as stated for NMC111.

It is unclear why the third point in the Table 4.13 gives a large deviation. It could be due to underlying reaction or EIS fitting issues

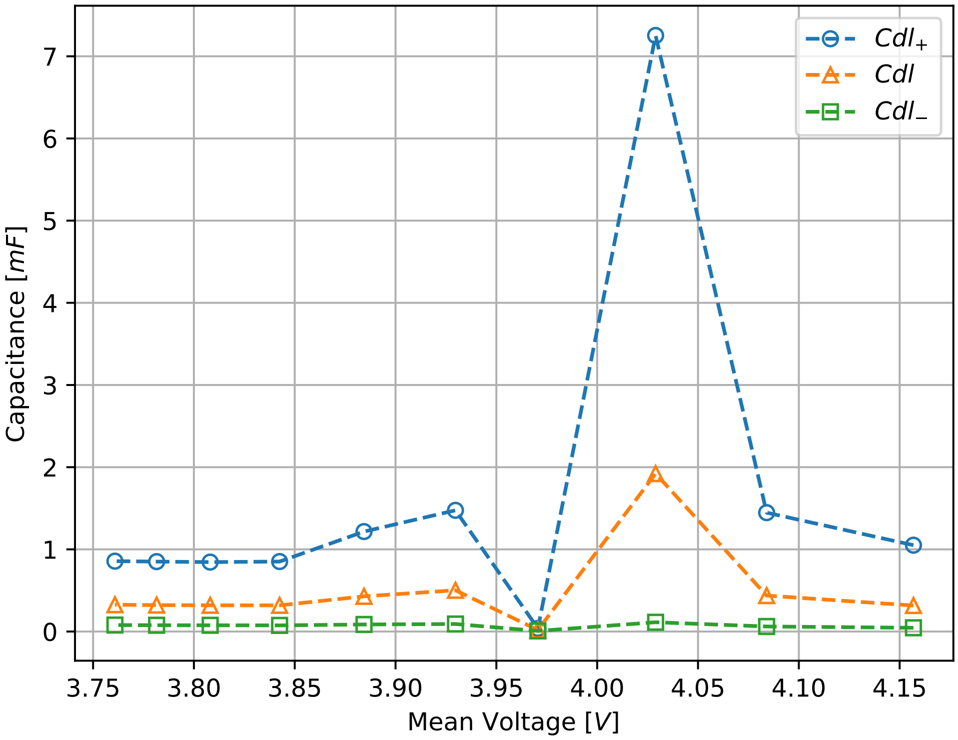

Figure 4.21: Double layer capacitance range for NMC622

Table 4.13: NMC622 half-cell Cdl_+, Cdl and Cdl_- cathode double layer capacitance range values

$SrNo$	V_{mean} [V]	Cdl_+ [F]	Cdl [F]	Cdl_- [F]
1	4.157	1.05×10^{-3}	0.31×10^{-3}	4.56×10^{-5}
2	4.084	1.44×10^{-3}	0.43×10^{-3}	6.13×10^{-5}
3	4.029	7.25×10^{-3}	1.92×10^{-3}	0.11×10^{-3}
4	3.971	3.79×10^{-5}	1.87×10^{-5}	7.33×10^{-6}
5	3.930	1.47×10^{-3}	0.50×10^{-3}	9.15×10^{-5}
6	3.884	1.21×10^{-3}	0.42×10^{-3}	8.59×10^{-5}
7	3.843	0.85×10^{-3}	0.31×10^{-3}	7.47×10^{-5}
8	3.808	0.84×10^{-3}	0.31×10^{-3}	7.61×10^{-5}
9	3.782	0.85×10^{-3}	0.32×10^{-3}	7.67×10^{-5}
10	3.761	0.85×10^{-3}	0.32×10^{-3}	7.89×10^{-5}

CEI capacitance

The CEI capacitance behaviour for NMC622 are observed as stated for NMC111.

It is unclear why the fourth point as per table gives a large deviation. It could be due to the underlying reaction or EIS fitting issues

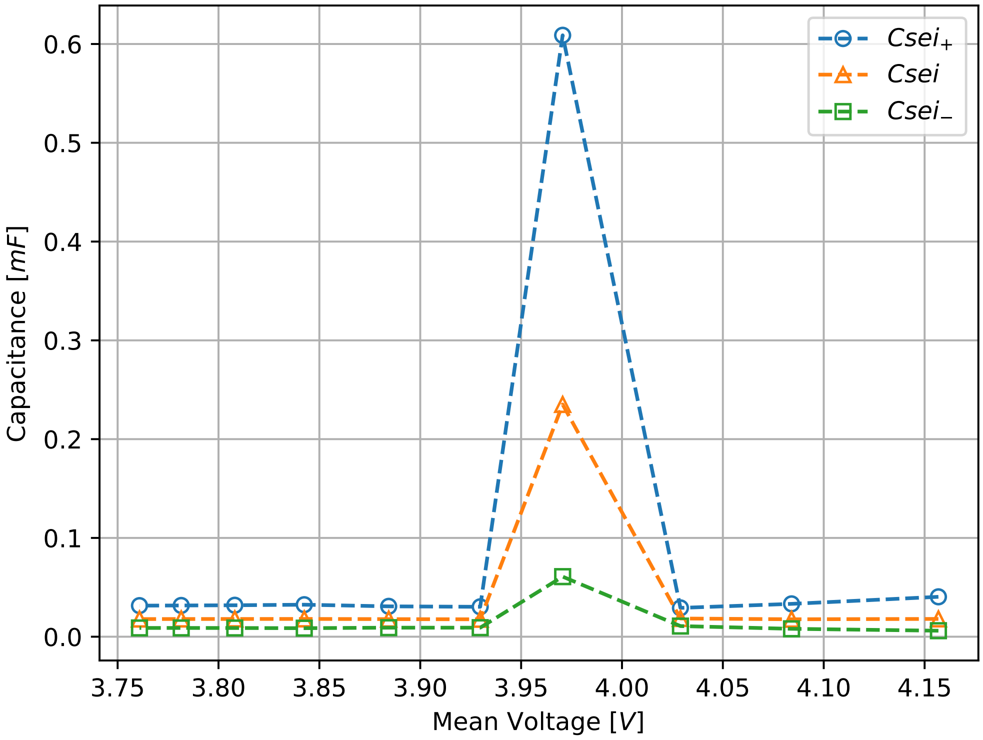

Figure 4.22: CEI capacitance range for NMC622

Table 4.14: NMC622 half-cell $Ccei_{+}$, $Ccei$ and $Ccei_{-}$ cathode double layer capacitance range values

Sr No	V_{mean} [V]	$Ccei_{+}$ [F]	$Ccei$ [F]	$Ccei_{-}$ [F]
1	4.157	4.03×10^{-5}	1.80×10^{-5}	6.08×10^{-6}
2	4.084	3.32×10^{-5}	1.76×10^{-5}	8.00×10^{-6}
3	4.029	2.91×10^{-5}	1.84×10^{-5}	1.07×10^{-5}
4	3.971	0.60×10^{-3}	0.23×10^{-3}	6.08×10^{-5}
5	3.930	3.02×10^{-5}	1.76×10^{-5}	9.14×10^{-6}
6	3.884	3.07×10^{-5}	1.78×10^{-5}	9.14×10^{-6}
7	3.843	3.24×10^{-5}	1.80×10^{-5}	8.64×10^{-6}
8	3.808	3.18×10^{-5}	1.79×10^{-5}	8.81×10^{-6}
9	3.782	3.16×10^{-5}	1.79×10^{-5}	8.86×10^{-6}
10	3.761	3.14×10^{-5}	1.78×10^{-5}	8.86×10^{-6}

4.2.4 NMC811 parameters

Diffusion coefficient

The diffusion coefficients behaviour for NMC811 are observed as stated for NMC622.

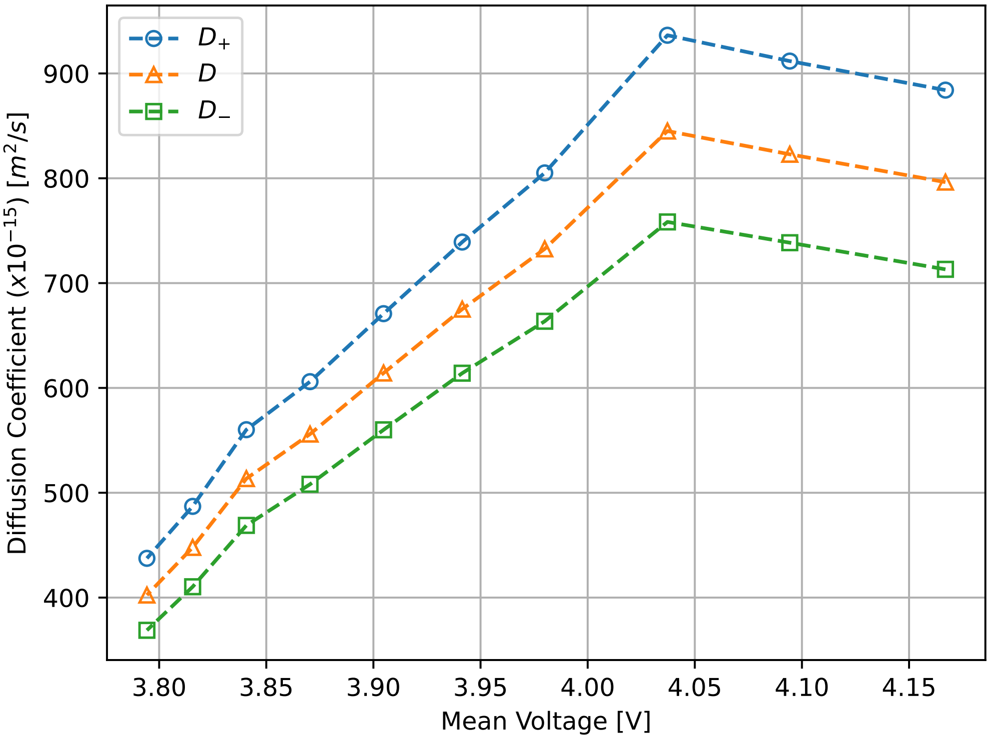

Figure 4.23: Diffusion coefficient range for NMC811

Table 4.15: NMC811 half-cell D_+, D and D_- cathode diffusion coefficient range values

Sr No	V_{mean} [V]	D_+ [$\mathrm{m^2/s}$]	D [$\mathrm{m^2/s}$]	D_- [$\mathrm{m^2/s}$]
1	4.167	8.84×10^{-13}	7.96×10^{-13}	7.13×10^{-13}
2	4.094	9.11×10^{-13}	8.22×10^{-13}	7.38×10^{-13}
3	4.037	9.36×10^{-13}	8.45×10^{-13}	7.58×10^{-13}
4	3.980	8.05×10^{-13}	7.32×10^{-13}	6.63×10^{-13}
5	3.941	7.39×10^{-13}	6.75×10^{-13}	6.14×10^{-13}
6	3.905	6.70×10^{-13}	6.14×10^{-13}	5.60×10^{-13}
7	3.870	6.05×10^{-13}	5.55×10^{-13}	5.08×10^{-13}
8	3.841	5.60×10^{-13}	5.13×10^{-13}	4.68×10^{-13}
9	3.816	4.87×10^{-13}	4.47×10^{-13}	4.10×10^{-13}
10	3.794	4.37×10^{-13}	4.02×10^{-13}	3.68×10^{-13}

Exchange current density

The exchange current density behaviour for NMC811 is observed as stated for NMC111.

The error margin gap is not consistent. It is lower at lower voltages and higher at higher voltages.

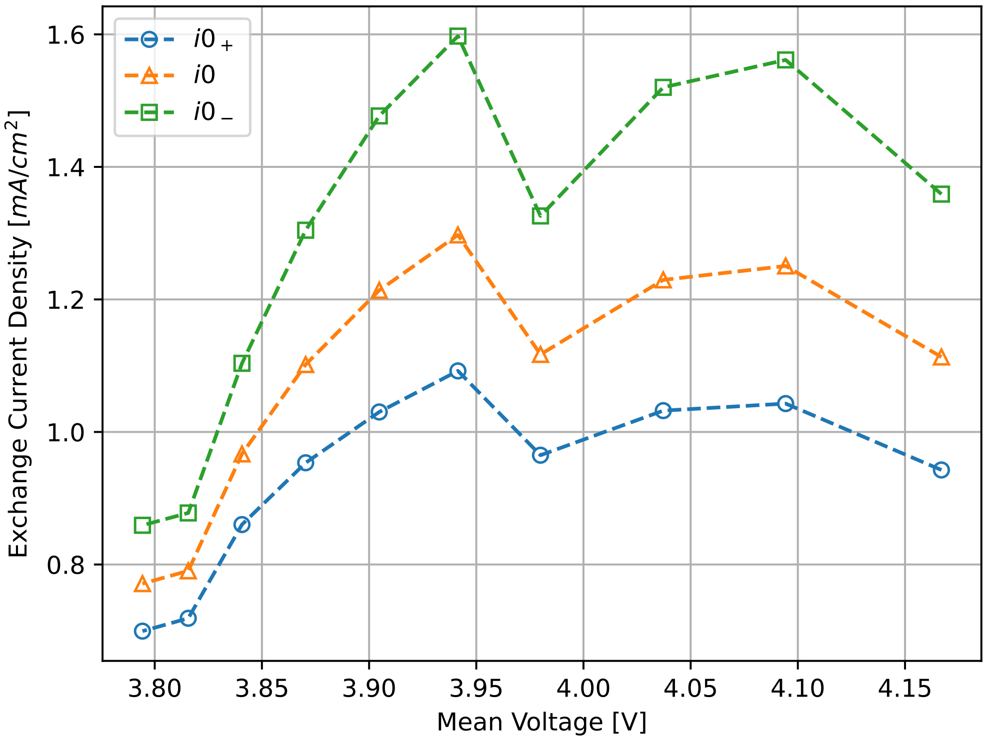

Figure 4.24: Exchange current density range for NMC811

Table 4.16: NMC811 half-cell $i0_+$, $i0$ and $i0_-$ cathode exchange current density range values

Sr No	V_{mean} [V]	$i0_+$ [mA/cm^2]	$i0$ [mA/cm^2]	$i0_-$ [mA/cm^2]
1	4.167	0.94	1.11	1.35
2	4.094	1.04	1.25	1.56
3	4.037	1.03	1.22	1.52
4	3.980	0.96	1.11	1.32
5	3.941	1.09	1.29	1.59
6	3.905	1.03	1.21	1.47
7	3.870	0.95	1.10	1.30
8	3.841	0.86	0.96	1.10
9	3.816	0.71	0.79	0.87
10	3.794	0.69	0.77	0.85

Double layer capacitance

The double layer capacitance behaviour for NMC811 is observed as stated for NMC622.

The deviating points for this chemistry are the fourth, eighth, ninth and tenth values in the Table 4.17.

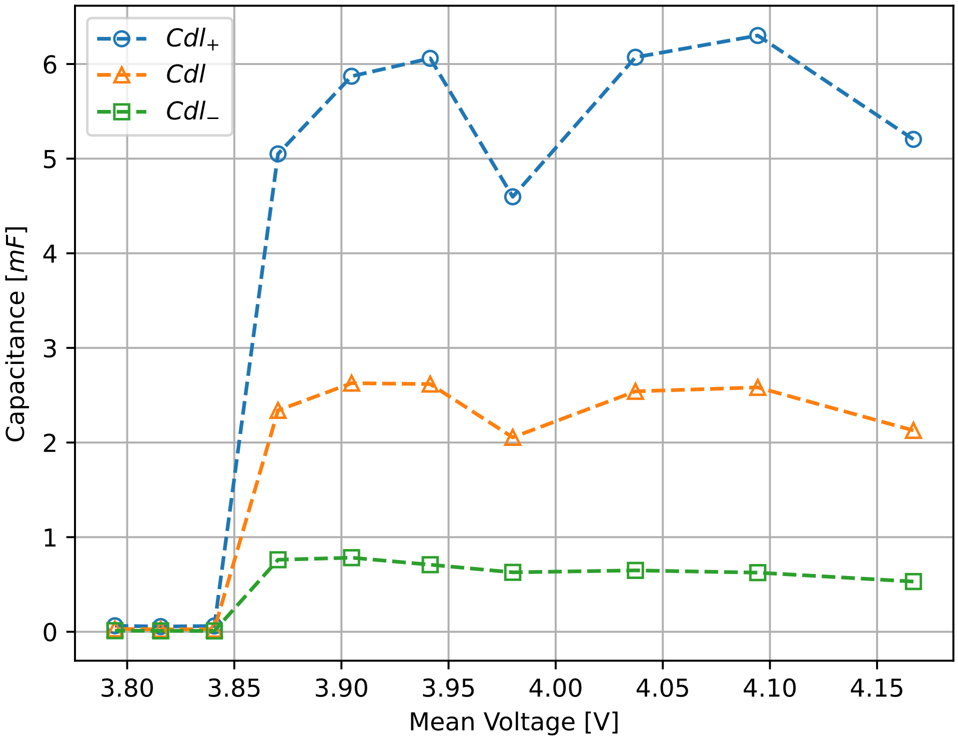

Figure 4.25: Double layer capacitance range for NMC811

Table 4.17: NMC811 half-cell Cdl_+, Cdl and Cdl_- cathode double layer capacitance range values

Sr No	V_{mean} [V]	Cdl_+ [F]	Cdl [F]	Cdl_- [F]
1	4.167	5.20×10^{-3}	2.12×10^{-3}	0.53×10^{-3}
2	4.094	6.30×10^{-3}	2.58×10^{-3}	0.625×10^{-3}
3	4.037	6.07×10^{-3}	2.54×10^{-3}	0.64×10^{-3}
4	3.980	4.59×10^{-3}	2.05×10^{-3}	0.62×10^{-3}
5	3.941	6.06×10^{-3}	2.61×10^{-3}	0.70×10^{-3}
6	3.905	5.87×10^{-3}	2.62×10^{-3}	0.78×10^{-3}
7	3.870	5.05×10^{-3}	2.33×10^{-3}	0.76×10^{-3}
8	3.841	6.15×10^{-5}	2.71×10^{-5}	8.88×10^{-6}
9	3.816	5.51×10^{-5}	2.61×10^{-5}	9.90×10^{-6}
10	3.794	6.36×10^{-5}	3.02×10^{-5}	1.14×10^{-5}

CEI capacitance

The CEI capacitance behaviour for NMC811 is observed as stated for NMC622.

The deviating points for this chemistry are the eighth, ninth and tenth values as per table.

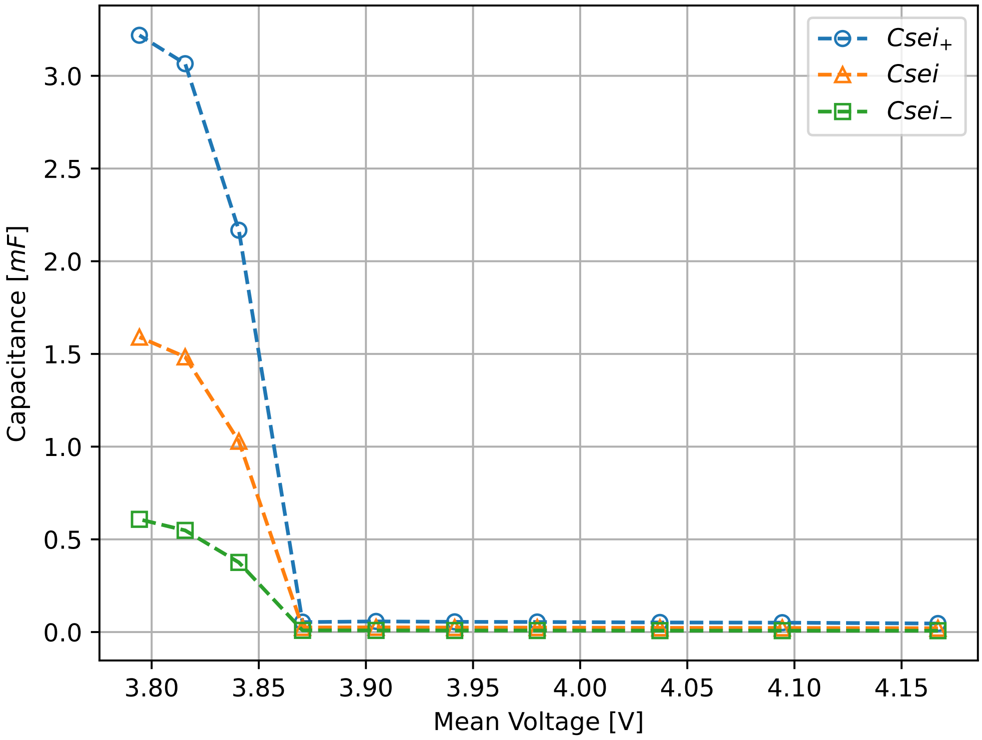

Figure 4.26: CEI capacitance range for NMC811

Table 4.18: NMC111 half-cell $Ccei_+$, $Ccei$ and $Ccei_-$ cathode double layer capacitance range values

Sr No	V_{mean} [V]	$Ccei_+$ [F]	$Ccei$ [F]	$Ccei_-$ [F]
1	4.167	4.59×10^{-5}	2.05×10^{-5}	7.23×10^{-6}
2	4.094	5.06×10^{-5}	2.21×10^{-5}	7.56×10^{-6}
3	4.037	5.17×10^{-5}	2.25×10^{-5}	7.66×10^{-6}
4	3.980	5.42×10^{-5}	2.40×10^{-5}	8.26×10^{-6}
5	3.941	5.50×10^{-5}	2.42×10^{-5}	8.40×10^{-6}
6	3.905	5.73×10^{-5}	2.53×10^{-5}	8.77×10^{-6}
7	3.870	5.35×10^{-5}	2.46×10^{-5}	9.10×10^{-6}
8	3.841	2.16×10^{-3}	1.02×10^{-3}	0.37×10^{-3}
9	3.816	3.06×10^{-3}	1.48×10^{-3}	0.54×10^{-3}
10	3.794	3.21×10^{-3}	1.59×10^{-3}	0.60×10^{-3}

4.2.5 NMC111, NMC622 and NMC811 comparison

Diffusion coefficient

It is interesting to see the comparison of the three diffusion coefficients of the respective chemistries. The three cathodes follow a very similar pattern with strong dependence of the diffusion coefficient on the voltage.

At very high voltages, the diffusion coefficient is more constant and lower. However, after a point, the voltage drop is sharp as the SOC decreases. This point comes at a slightly lower voltage for NMC811 when compared to the other cathodes. This behaviour is due to that the Li mobility changes [16]. The decrease of diffusion coefficient at higher potential is due to structural stresses in the NMC lattice [17].

At very low SOC levels, the diffusion coefficient for NMC622 becomes larger than the NMC111.

There is also a slight change in slope for NMC622 and NMC111 at around 3.95V and for NMC811 at around 3.85V. This could be due to underlying reactions.

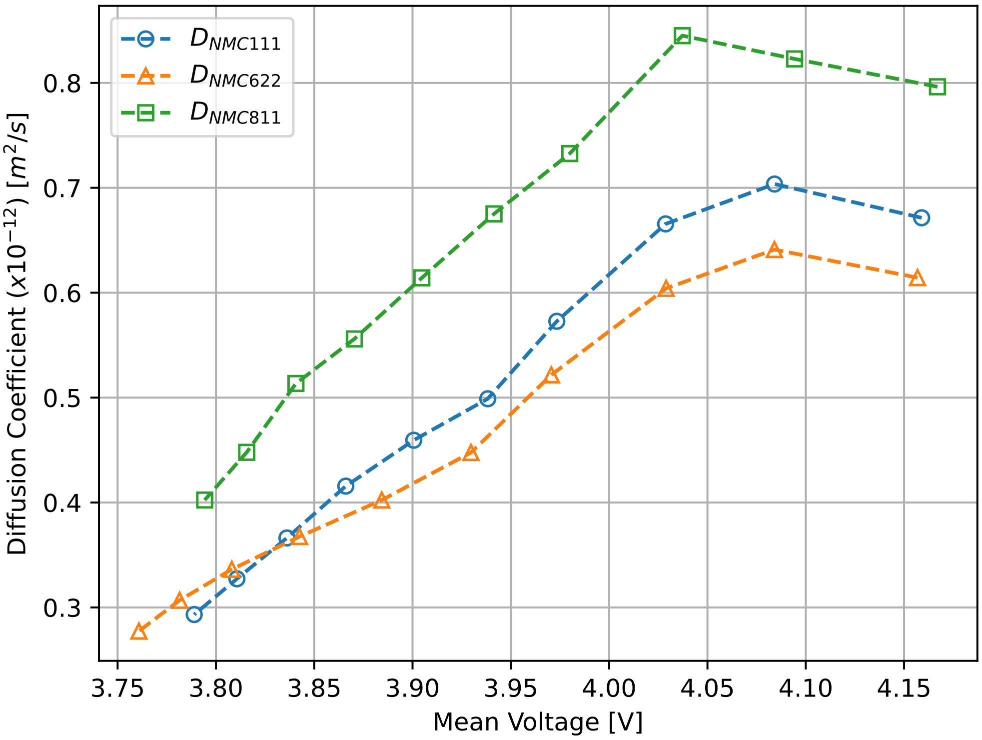

Figure 4.27: Diffusion coefficient comparison between NMC111, NMC622 and NMC811 cathodes

Charge transfer resistance

In general, the charge transfer resistance is strongly dependent on potential and forms a ’U’ shape which is in line with previous literature [17].

The charge transfer resistance from right to left, decreases with voltage till a point around 4.1V. After this till 3.9V the value is nearly constant. Finally, below 3.9V, an increase in charge transfer resistance is observed.

The charge transfer resistance values are maximum for NMC111 and minimum for NMC811.

It can be observed that deviations occur mostly in the mid voltage range.

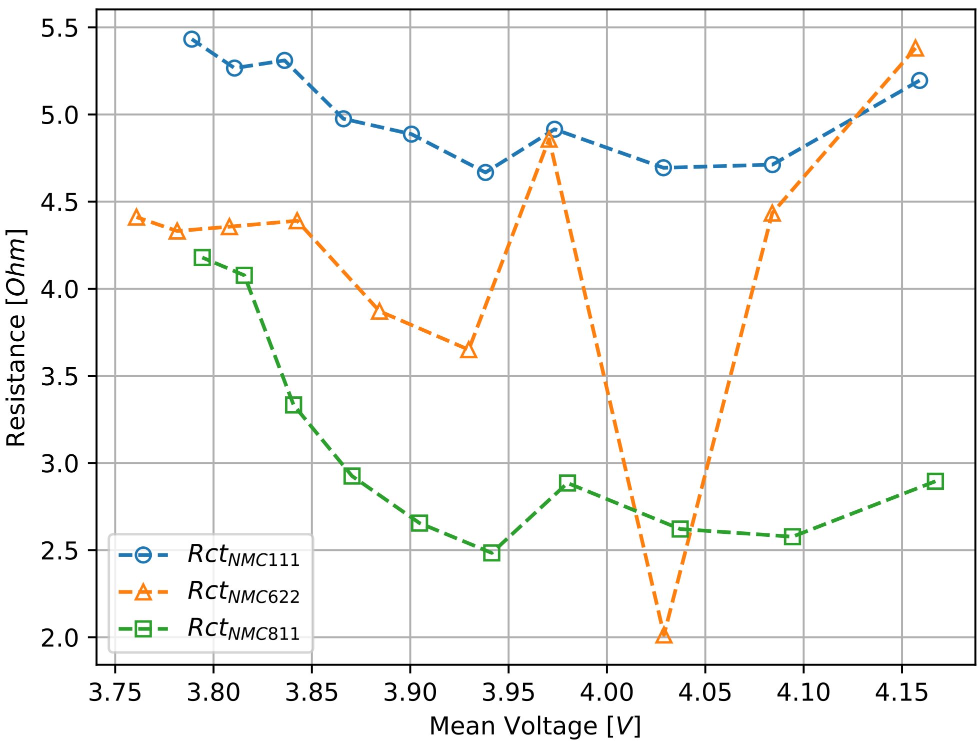

Figure 4.28: Charge transfer resistance comparison between NMC111, NMC622 and NMC811 cathodes

Exchange current density

The NMC811 cathode has the highest exchange current density whereas the NMC111 has mostly the lowest. The patterns followed by the graphs seem to be an inverted U with high values at middle voltages and lower values at extreme SOC levels. This is due to an inverse relation to charge transfer resistance.

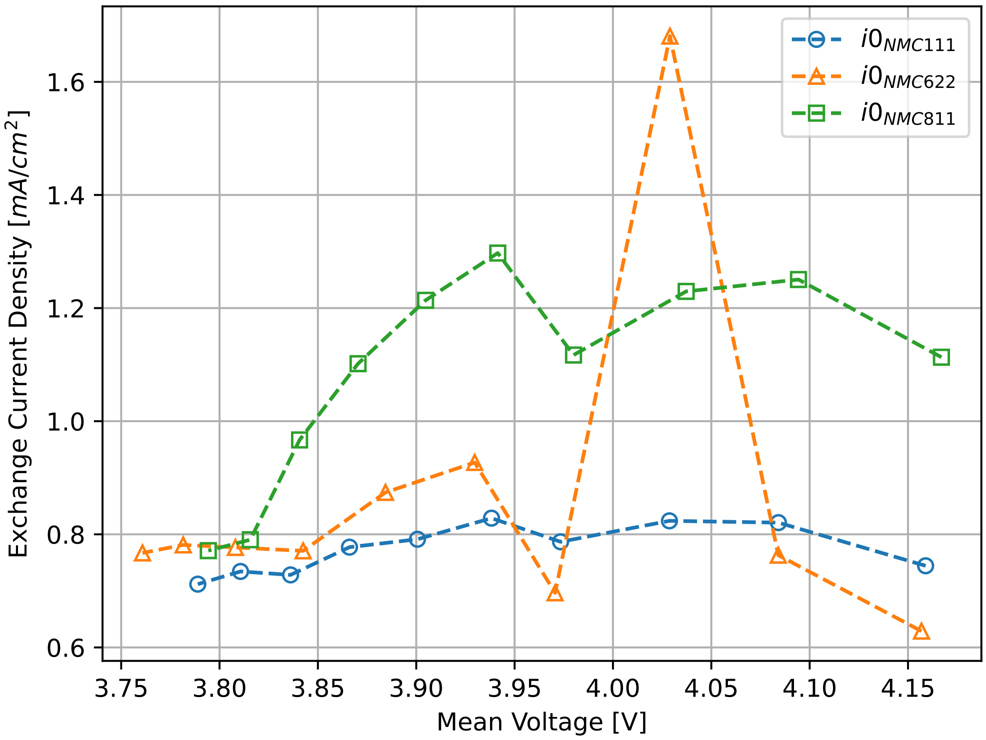

Figure 4.29: Exchange current density comparison between NMC111, NMC622 and NMC811 cathodes

Double layer capacitance

The double layer capacitance of NMC811 is highest after around 3.85V. The double layer capacitance of NMC111 is lowest over all voltages.

The double layer of NMC622 and NMC111 do not drastically change and show a more constant behaviour which means that there is no embrittlement of particles or formation of small particles on the electrode surface. The double layer for NMC811 is constant but at very low SOC level, it has very low value. This could be either due to EIS fitting issues or change in the double layer area [17].

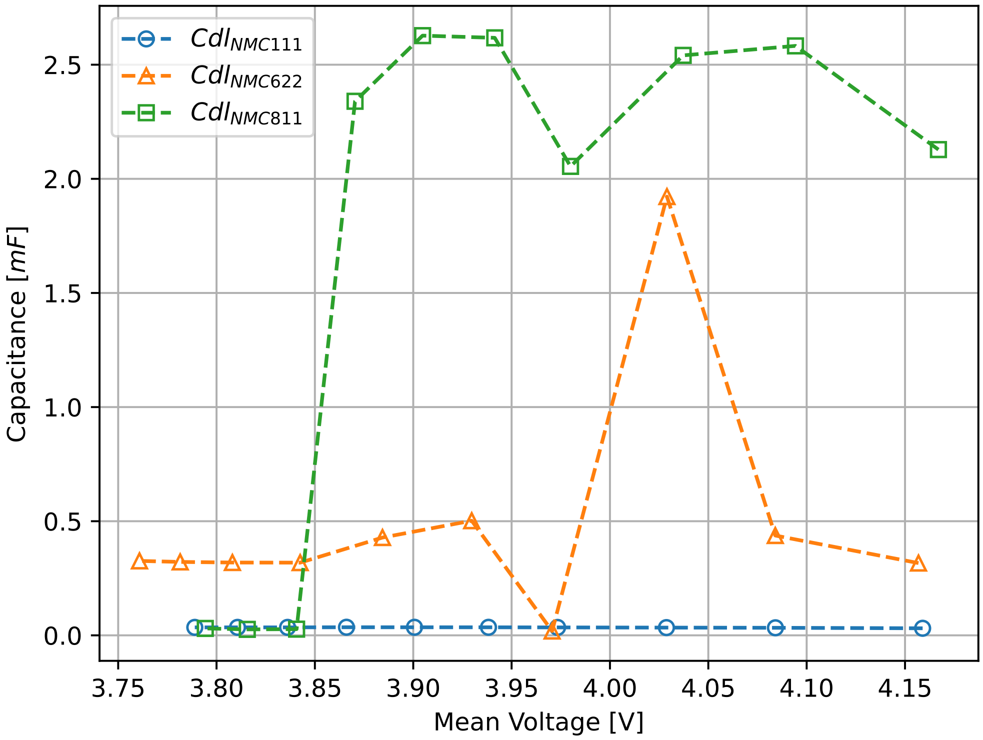

Figure 4.30: Double layer capacitance comparison between NMC111, NMC622 and NMC811 cathodes

CEI capacitance

The CEI capacitance is highest for the $\mathrm{NMC111}$ cathode and minimum for the $\mathrm{NMC622}$ cathode.

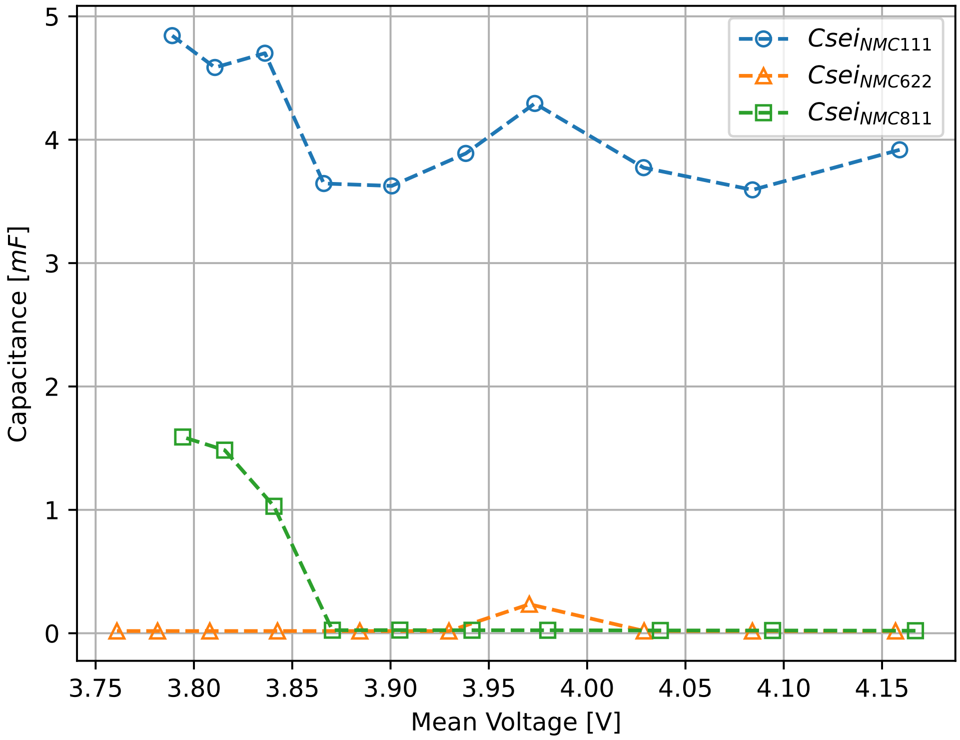

Figure 4.31: CEI capacitance comparison between NMC111, NMC622 and NMC811 cathodes

Ohmic Resistance

The resistance $R0$ is the sum of resistances due to electrolyte, reference ring, separator and current collectors. Overall, this resistance seems constant for the three chemistries and does not have a strong dependence on voltage.

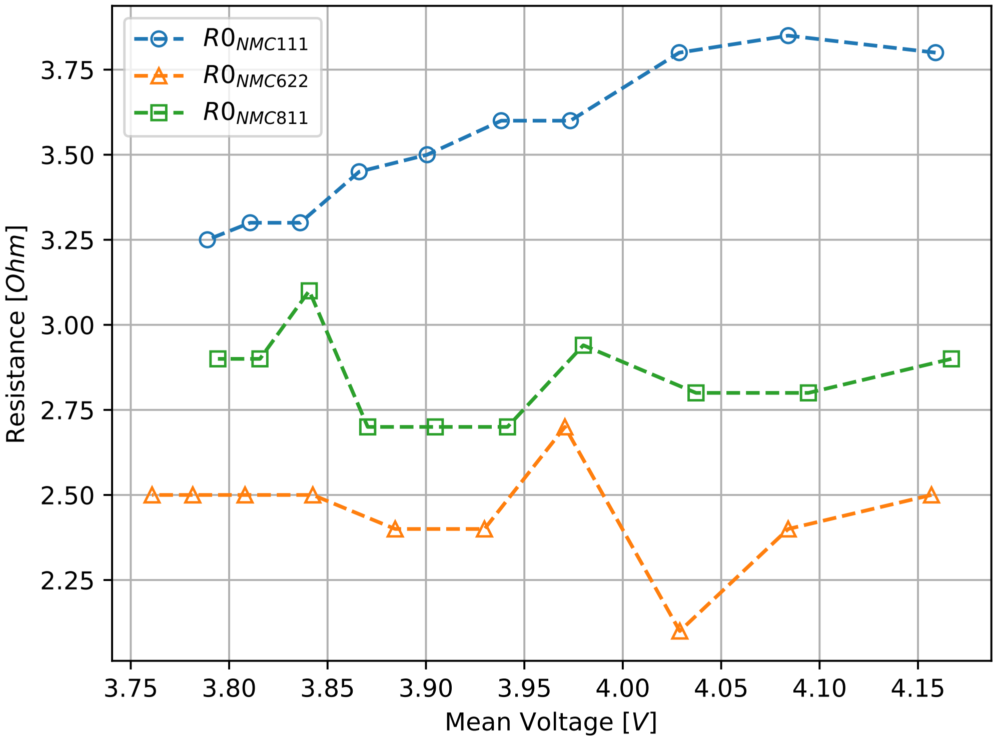

Figure 4.32: R0 comparison between NMC111, NMC622 and NMC811 cathodes

CEI Resistance

The resistance R_{cei} is almost constant over voltages with no strong voltage dependence.

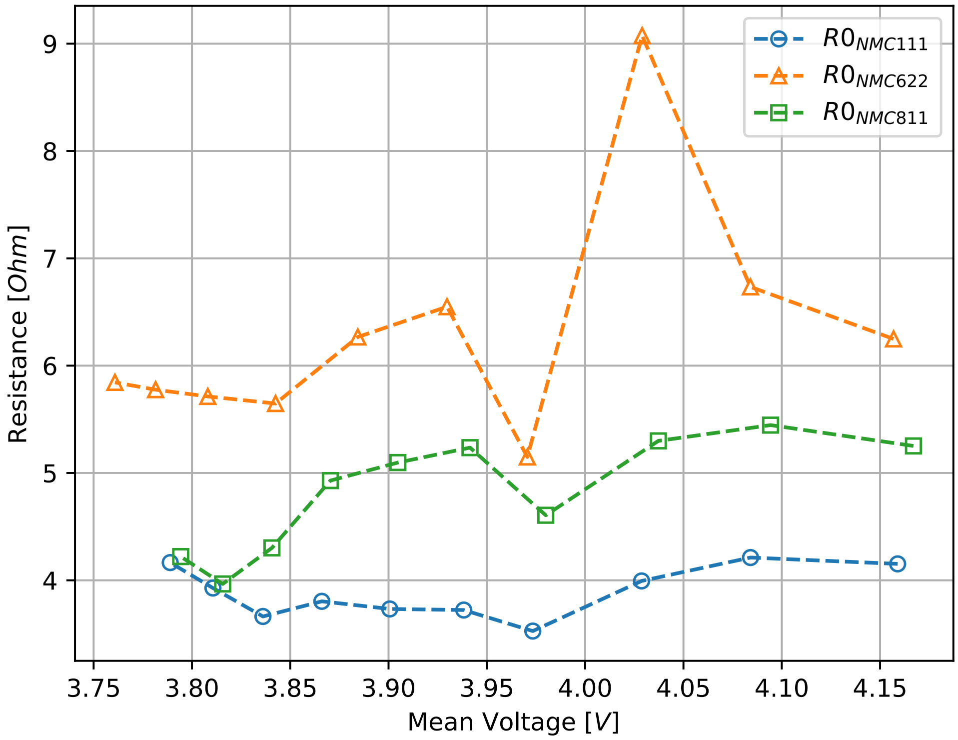

Figure 4.33: CEI resistance comparison between NMC111, NMC622 and NMC811 cathodes

4.3 Comparison between diffusion coefficient from GITT and EIS

In this section, we compare the diffusion coefficients obtained from GITT and EIS. An important point to highlight is that GITT testing is performed on a two electrode half cell while EIS is performed on a 3-eletrode cell between cathode and lithium reference ring. The comparison is only for discharge direction with C/10 as discharge rate.

An interesting observation from the comparison is that the diffusion coefficients obtained from EIS are 2-3 order of magnitude higher than those obtained from GITT. Another point is that the SOC dependence of GITT results is more than that of EIS results [15].

4.3.1 NMC111

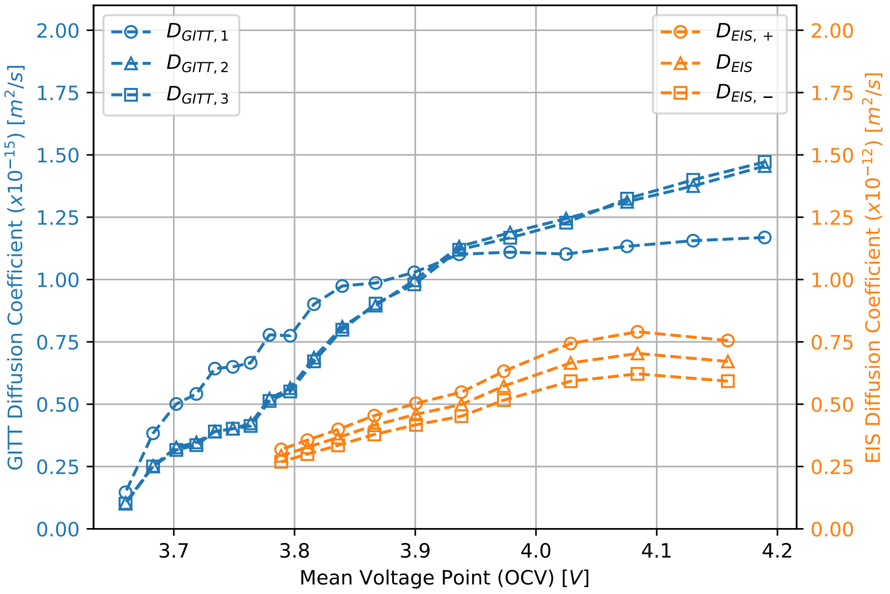

Figure 4.34: NMC111 GITT vs EIS diffusion coefficient comparison

4.3.2 NMC622

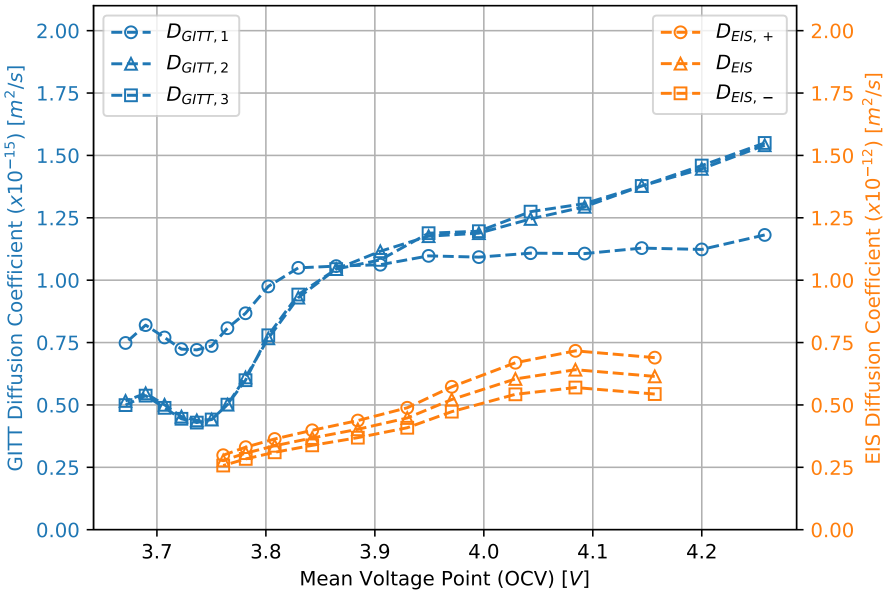

Figure 4.35: NMC622 GITT vs EIS diffusion coefficient comparison

4.3.3 NMC811

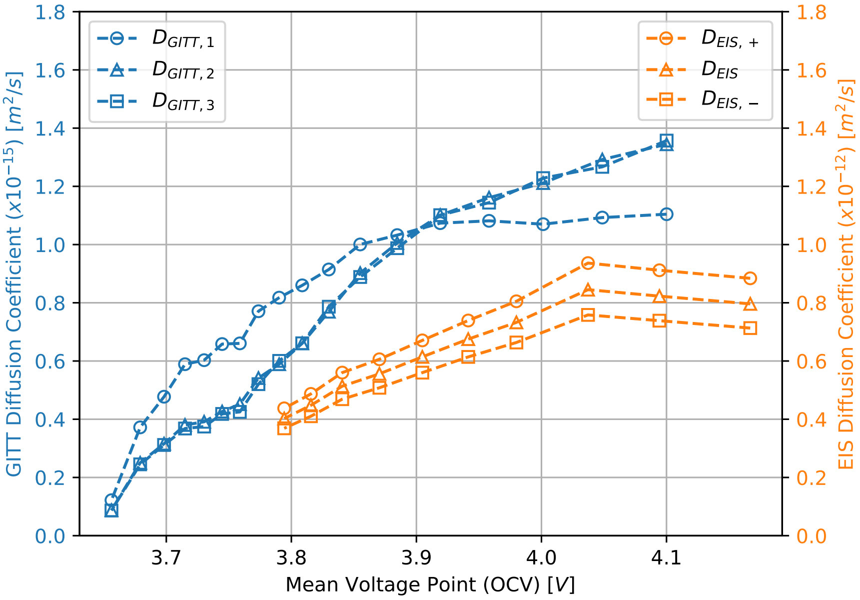

Figure 4.36: NMC811 GITT vs EIS diffusion coefficient comparison

Table 4.19: Comparing GITT and EIS diffusion coefficients from different literature

Source	Chemistry	GITT $[m^2/s]$		EIS $[m^2/s]$		Other
		min	max	min	max	
This study	NMC111	1×10^{-16}	1.5×10^{-15}	2.6×10^{-13}	7.9×10^{-13}	-
Maria et al. [21]	NMC111	7.8×10^{-19}	1.6×10^{-18}	1.6×10^{-18}	9.6×10^{-18}	-
Hao et al.	NMC111	10^{-14}		-	-	-
Wu et al.	NMC111	10^{-16}	10^{-14}	-	-	-
Gu et al.	NMC111	-	-	-	-	5×10^{-18}
Li et al.	NMC111	-	-	-	-	3×10^{-14}
Hyung et al. [25]	NMC111	-	-	-	-	10^{-16} to 10^{-14}
Ruhul et al. [18]	NMC111	10^{-16}	10^{-14}	10^{-20}	10^{-12}	-
Bai et al. [19]	NMC523	3.1×10^{-20}	7.2×10^{-14}	1.9×10^{-18}	8.1×10^{-14}	-
This study	NMC622	5×10^{-17}	1.5×10^{-15}	2.5×10^{-13}	7.1×10^{-13}	-
Hyung et al. [25]	NMC622	-	-	-	-	10^{-15} to 10^{-13}
Gao et al. [22]	NMC622	10^{-15}	10^{-12}	10^{-15}	10^{-12}	-
This study	NMC811	8.6×10^{-17}	1.4×10^{-15}	3.6×10^{-13}	9.1×10^{-13}	-
Thomas et al. [23]	NMC811	10^{-15}	10^{-12}	10^{-15}	10^{-12}	-
Ting et al. [24]	NMC811	-	-	1×10^{-15}	6×10^{-15}	
Hyung et al. [25]	NMC811	-	-	-	-	10^{-14} to 10^{-12}
Chen et al. [20]	NMCA	10^{-20}	10^{-12}	-	-	-

4.4 Sustainable and ethical aspects

Currently the internal parameters of the cell are considered company secrets and hence such information is not shared by the cell manufactures which hinders the academic research as they are dependent on more general values of such parameters. This thesis work will help researchers in understanding certain critical cell parameters and hence the cell behaviour. Better insights in the design will help the Original Equipment Manufacturers (OEMs) as well, to optimize the whole vehicle system to the best use of the battery. An efficient use of the battery and optimized vehicle characteristics will aid in taking one step closer to the carbon-neutral goal that more and more companies today, are aiming for, and which is needed for a sustainable future.

A drawback of EVs today is the range of the vehicle and the charging speed which leads to that there is still some hesitance from some customers to go all in for EVs. Research about the cell characteristics can help overcome these hurdles making customers more attracted towards EVs and a switch from conventional to EVs will be seen sooner and faster helping in reduction of fossil based fuels and making the future more sustainable.

There is however an ethical challenge while manufacturing batteries which comes from the sourcing of materials. Many of the critical materials used in manufacturing a cell are extracted by mining which has negative environmental effects. Non-sustainable techniques are also used in the supply chain. Elements like cobalt are mined form countries like Democratic Republic of Congo (DRC) where child labour is often used in unethical mining. It is the duty of the OEMs to ensure that the suppliers show transparency in their supply chain and comply with the sustainable and ethical standards. Also the companies should be transparent with their customers informing them about their materials and manufacturing processes. The research in this field has taken a big leap in the last couple of years but still has a long way to go. It is crucial that the foundation of this work matches the ethical and sustainable standards so that it takes us towards a better future.

This thesis compares experimentally estimated parameter values with the current state of the art values in literature. The research papers have been cited which complies with IEEE code of ethics.

5

Conclusion

5.1 Experimental work

Forming coin cells as half cells is extremely difficult. Out of the four chemistries that are built using coin cells during this thesis, none of them gave stable voltages which can be analysed. Since the data is highly irregular, it can be concluded that the best option to construct and analyse half cells is by using the EL cell technology. EL cells give very reliable results for half cells and are very easy to build.

An initial NCA half cell is built using a used plunger in the EL cell after cleaning. The formation cycle could not be completed on these cells as the voltages became very irregular and unstable. This is mainly because there are unknown reactions happening in the plunger due to residues left on the old plungers. Hence, new plungers should be used for testing to get stable results.

5.2 Data analysis

From both GITT and EIS tests it can be observed that there is an overall pattern of strong dependence of diffusion coefficient on voltage level. The diffusion coefficient increases with increasing voltage till a point after which it drops. This behaviour is because of Li mobility. The Li mobility is stimulated by the creation of Li vacancies which increases the number of carriers as well as the substantial increase in Li layer spacing which decreases the activation barrier for Li hops. However, at very high voltages due to structural stresses on the NMC lattice, there is Li vacancy ordering which makes extraction of Li-ions harder. Hence the Li mobility decreases due to which the diffusion coefficient drops [16].

The overall order of magnitude of the diffusion coefficient from EIS results is 2-3 times more than that obtained from GITT results which is in line with previous literature. Also, the SOC dependence of the GITT results is more than that of the EIS results [15].

During EIS fitting, it is not possible to fit just the diffusive tail and ignore the semicircles as that leads to very high error margins or absurd values of the Warburg element. It is also observed that for many cases the error margin is bigger than the values which is a sign of an incorrect fit. So, it is important to fit the semicircles along with the diffusive tail. Fitting semicircles correctly as best as we can and then trying to fit the diffusive tail as best as we can by adjusting $R0$ value gives reliable and consistent results.

6

Future work

Tests on the same chemistry should be repeated a couple of times for checking the repeatability before moving to another chemistry.

The effect of changing particle radius should be studied. Tests should be repeated after cycling to check the effect of aging.

The error margins calculated by the GAMRY software is using the Maximum Likelihood Estimation statistical method. Studying these error margins is not included in the scope of this thesis work. However, it should be looked into to understand how good the EIS fit is and the deviation from correct results.

PyBaMM simulations could be done, and results could be compared with experimental results for verification purpose. A sensitivity analysis could also be done to understand the effect of changing parameters.

Bibliography

[1] Julian Conzade, Andreas Cornet, Patrick Hertzke, Russell Hensley, Ruth Heuss, Timo Möller, Patrick Schaufuss, Stephanie Schenk, Andreas Tschiesner, Karsten von Laufenberg (2021) 'Mainstream EVs will transform the automotive industry and help decarbonize the planet', *McKinsey & Company*, September 7, Available at: https://www.mckinsey.com/industries/automotive-and-assembly/our-insights/why-the-automotive-future-is-electric

[2] Nathaniel Bullard (2019), 'How a Battery Can Lead a Quiet Revolution', *Bloomberg*, October 11, Available at: https://www.bloomberg.com/opinion/articles/2019-10-11/nobel-prize-lithium-ion-battery-creators-led-a-revolution

[3] J.-M. Tarascon and M. Armand, "Issues and challenges facing rechargeable lithium batteries," Nature, vol. 414, pp. 359-367, 2001.

[4] S. Koohi-Fayegh, M.A. Rosen (2020), "A review of energy storage types, applications and recent developments", Jouranl of Energy Storage vol 27, Article 101047

[5] M. Stanley Whittingham (2004), "Lithium Batteries and Cathode Materials", Chem. Rev, 104, 4271-4301

[6] N. Nitta, F. Wu, J.T. Lee, G. Yushin (2015), "Li-ion battery materials: present and future", Materials Today 18 (5), 252–264.

[7] Wang, A., Kadam, S., Li, H. et al. Review on modeling of the anode solid electrolyte interphase (SEI) for lithium-ion batteries. npj Comput Mater 4, 15 (2018). https://doi.org/10.1038/s41524-018-0064-0

[8] Gary M. Gladysz, Krishan K. Chawla (2015), "Voids in Materials", Retrieved from https://www.sciencedirect.com/book/9780444563675/voids-in-materials

[9] Bobby (2014), Available at: https://www.upsbatterycenter.com/blog/intercalation-work-batteries/

[10] A. Nickol et al 2020 J. Electrochem. Soc. 167 090546

[11] Matt Lacey, Battery science and electrochemistry, Available at: http://lacey.se/science/eis/constant-phase-element/

[12] Matt Lacey, Battery science and electrochemistry, Available at: http://lacey.se/science/eis/diffusion-impedance/

[13] Jessica Lück and Arnulf Latz (2019), "The electrochemical double layer and its impedance behavior in lithium-ion batteries", Phys. Chem. Chem. Phys.,21, 14753-14765

[14] Brian Agudelo, Walter Zamboni, Eric Monmasson, Giovanni Spagnuolo. Identification of battery circuit model from EIS data. JCGE - Congrès des Jeunes Chercheurs en Génie Electrique, Jun 2019, Saint Pierre d'Oléron, France. ffhal-02915697f

[15] Ping Yu et al (1999), "Determination of the Lithium Ion Diffusion Coefficient in Graphite", J. Electrochem. Soc. 146 8, Available at: https://iopscience.iop.org/article/10.1149/1.1391556/pdf

[16] Katharina Märker, Philip J. Reeves, Chao Xu, Kent J. Griffith, and Clare P. Grey (2019), "Evolution of Structure and Lithium Dynamics in LiNi0.8Mn0.1Co0.1O2 (NMC811) Cathodes during Electrochemical Cycling", Chemistry of Materials 2019 31 (7), 2545-2554 DOI: 10.1021/acs.chemmater.9b00140

[17] Valérie Charbonneau, Andrzej Lasia, Gessie Brisard (2020), "Impedance studies of Li+ diffusion in nickel manganese cobalt oxide (NMC) during charge/discharge cycles", Journal of Electroanalytical Chemistry Volume 875 113944, DOI: https://doi.org/10.1016/j.jelechem.2020.113944

[18] Ruhul Amin and Yet-Ming Chiang (2016), "Characterization of Electronic and Ionic Transport in Li1-xNi0.33Mn0.33Co0.33O2 (NMC333) and Li1-xNi0.50Mn0.20Co0.30O2 (NMC523) as a Function of Li Content", Journal of The Electrochemical Society, Volume 163, Number 8, DOI: https://doi.org/10.1149/2.0131608jes

[19] Yansong Bai, Xianyou Wang, Xiaoyan Zhang, Hongbo Shu, Xiukang Yang, Benan Hu, Qiliang Wei, Hao Wu, Yunfeng Song (2013), "The kinetics of Li-ion deintercalation in the Li-rich layered Li1.12[Ni0.5Co0.2Mn0.3]0.89O2 studied by electrochemical impedance spectroscopy and galvanostatic intermittent titration technique", Electrochimica Acta, Volume 109, Pages 355-364, ISSN 0013-4686, DOI: https://doi.org/10.1016/j.electacta.2013.06.134

[20] Chang-Hui Chen et al 2020, "Development of Experimental Techniques for Parameterization of Multiscale Lithium-ion Battery Models", J. Electrochem. Soc. 167 080534, DOI: https://doi.org/10.1149/1945-7111/ab9050

[21] Maria Varini, Jing Ying Ko, Matilda Klett, Henrik Ekström, Göran Lindbergh (2020), "Electrochemical techniques for characterizing LiNixMnyCo1xyO2 battery electrodes", Electrochimica Acta, Volume 359, 136887, ISSN 0013-4686,DOI: https://doi.org/10.1016/j.electacta.2020.136887

[22] Han Gao, Qiang Wu, Yixin Hu, Jim P. Zheng, Khalil Amine, and Zonghai Chen (2018), "Revealing the Rate-Limiting Li-Ion Diffusion Pathway in Ultrathick Electrodes for Li-Ion Batteries", J. Phys. Chem. Lett. 2018, 9, 17, 5100–5104, DOI: https://doi.org/10.1021/acs.jpclett.8b02229

[23] Thomas E. Ashton, Peter J. Baker, Carlos Sotelo-Vazquez, Charles J. M. Footer, Kenji. M. Kojima, Takeshi Matsukawa, Takashi Kamiyama and Jawwad A. Darr (2021), "Stoichiometrically driven disorder and local diffusion in NMC cathodes†", J. Mater. Chem. A, 2021, 9, 10477-10486, DOI: https://doi.org/10.1039/D1TA01639C

[24] Ting Wang, Keliang Ren, Wei Xiao, Wenhao Dong, Huali Qiao, Anran Duan, Hongyu Pan, Yang Yang, and Hailong Wang (2020), "Tuning the Li/Ni Disorder of the NMC811 Cathode by Thermally Driven

Competition between Lattice Ordering and Structure Decomposition",The Journal of Physical Chemistry C 2020 124 (10), 5600-5607, DOI: https://doi.org/10.1021/acs.jpcc.0c00720

[25] Hyung-Joo Noh, Sungjune Youn, Chong Seung Yoon, Yang-Kook Sun(2013), "Comparison of the structural and electrochemical properties of layered Li[NixCoyMnz]O2 (x = 1/3, 0.5, 0.6, 0.7, 0.8 and 0.85) cathode material for lithium-ion batteries", Journal of Power Sources, Volume 233, Pages 121-130, ISSN 0378-7753, DOI: https://doi.org/10.1016/j.jpowsour.2013.01.063.

A

Appendix 1: Galvanostatic Intermittent Titration Technique (GITT)

A.1 NMC111 vs Li GITT data

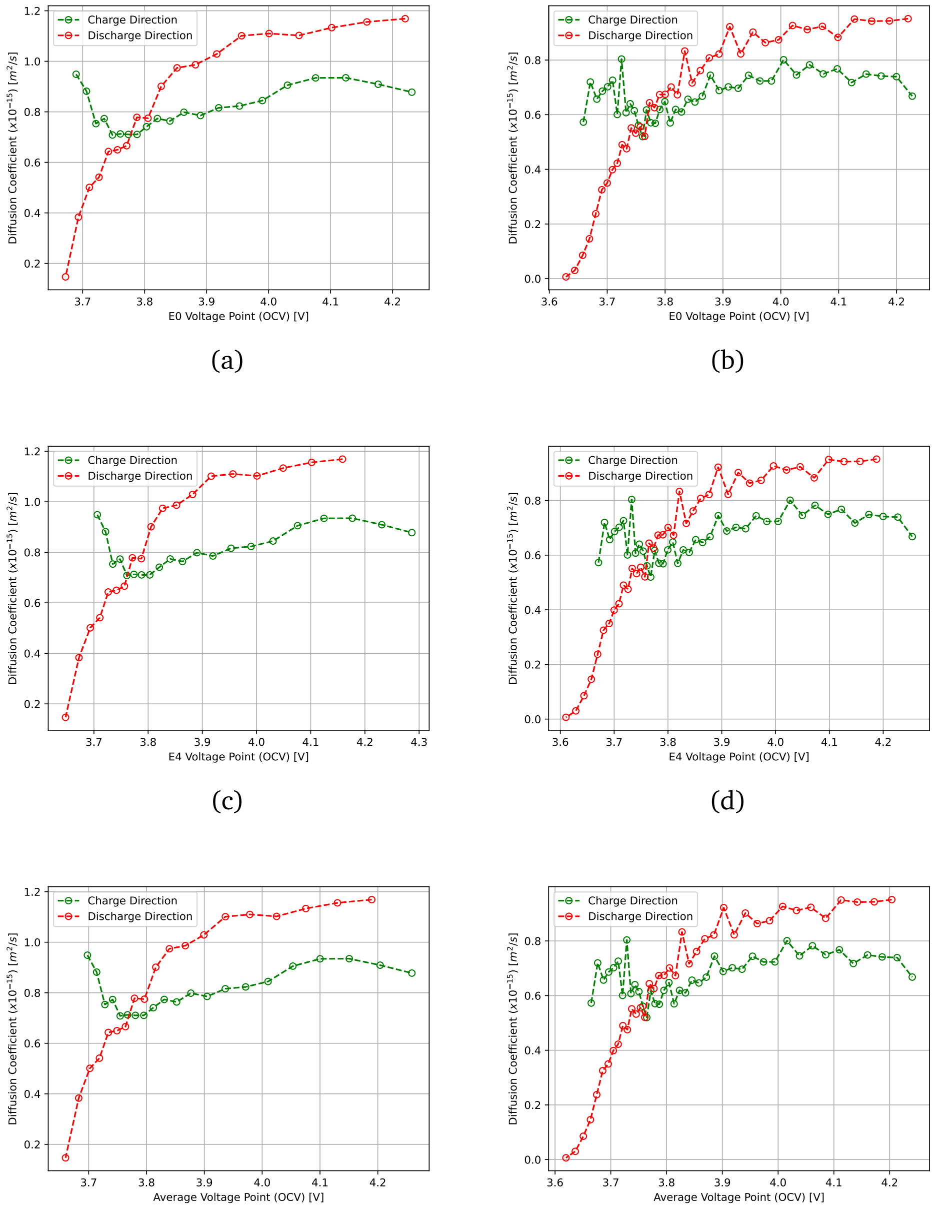

(a) (b)

(c) (d)

(e) (f)

Figure A.1: NMC111 diffusion coefficients using equation 1 in charge (green curve) and discharge (red curve) direction. Diffusion coefficients plotted against (a) E0 voltage points at C/10, (b) E0 voltage points at C/20, (c) E4 voltage points at C/10, (d) E4 voltage points at C/20, (e) Average of E0 and E4 voltage points at C/10, (f) Average of E0 and E4 voltage points at C/20

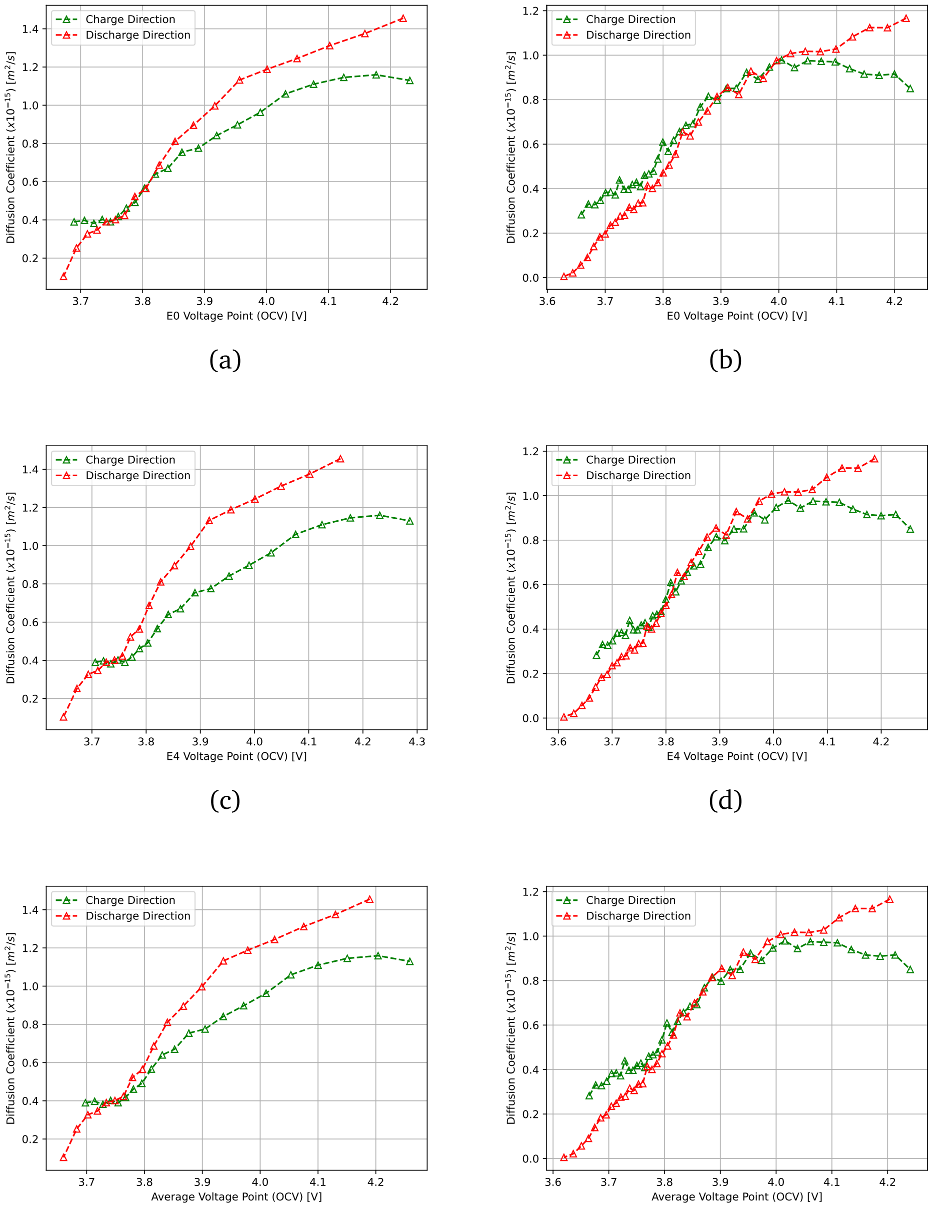

(a) (b)

(c) (d)

(e) (f)

Figure A.2: NMC111 diffusion coefficients using equation 2 in charge (green curve) and discharge (red curve) direction. Diffusion coefficients plotted against (a) E0 voltage points at C/10, (b) E0 voltage points at C/20, (c) E4 voltage points at C/10, (d) E4 voltage points at C/20, (e) Average of E0 and E4 voltage points at C/10, (f) Average of E0 and E4 voltage points at C/20

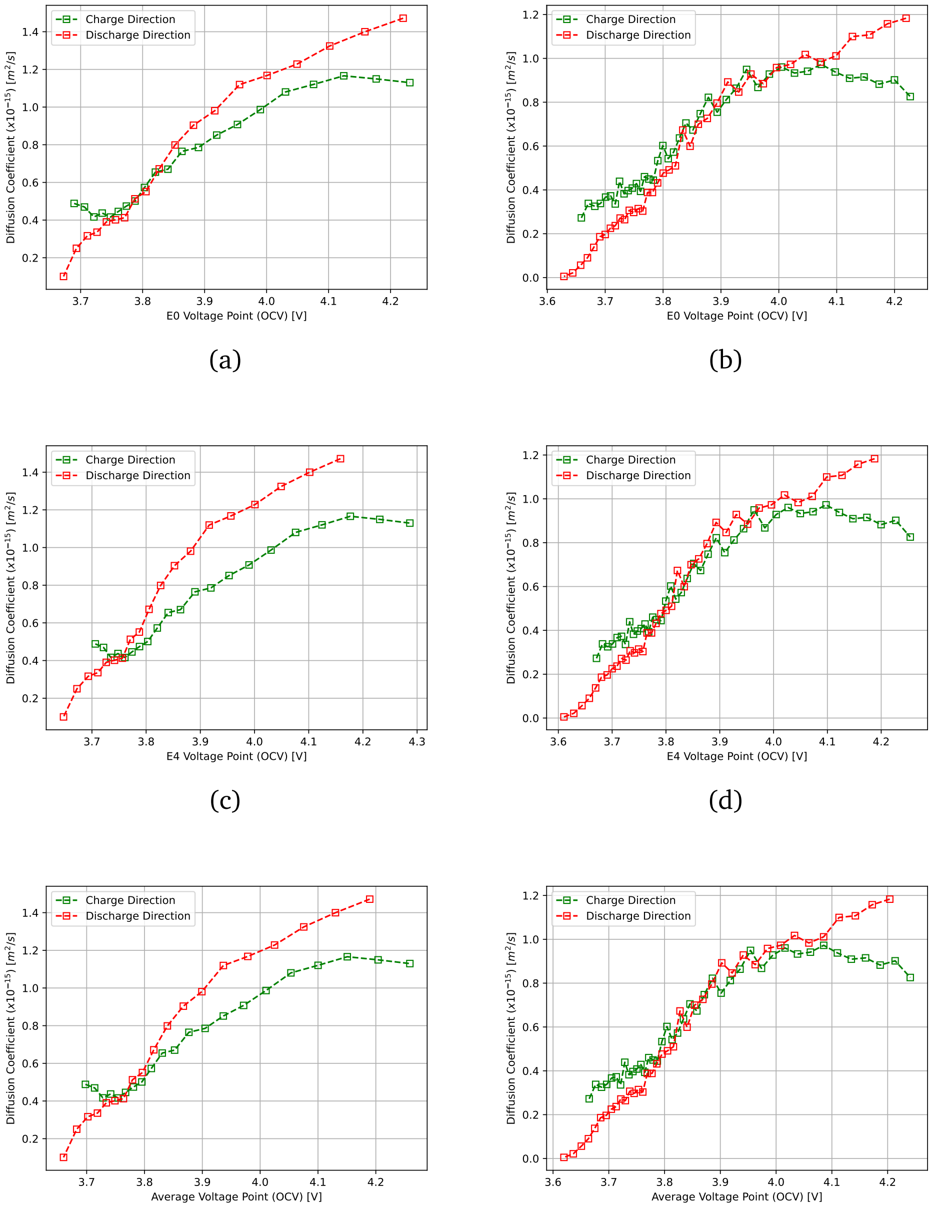

(a) (b)

(c) (d)

(e) (f)

Figure A.3: NMC111 diffusion coefficients using equation 3 in charge (green curve) and discharge (red curve) direction. Diffusion coefficients plotted against (a) E0 voltage points at C/10, (b) E0 voltage points at C/20, (c) E4 voltage points at C/10, (d) E4 voltage points at C/20, (e) Average of E0 and E4 voltage points at C/10, (f) Average of E0 and E4 voltage points at C/20

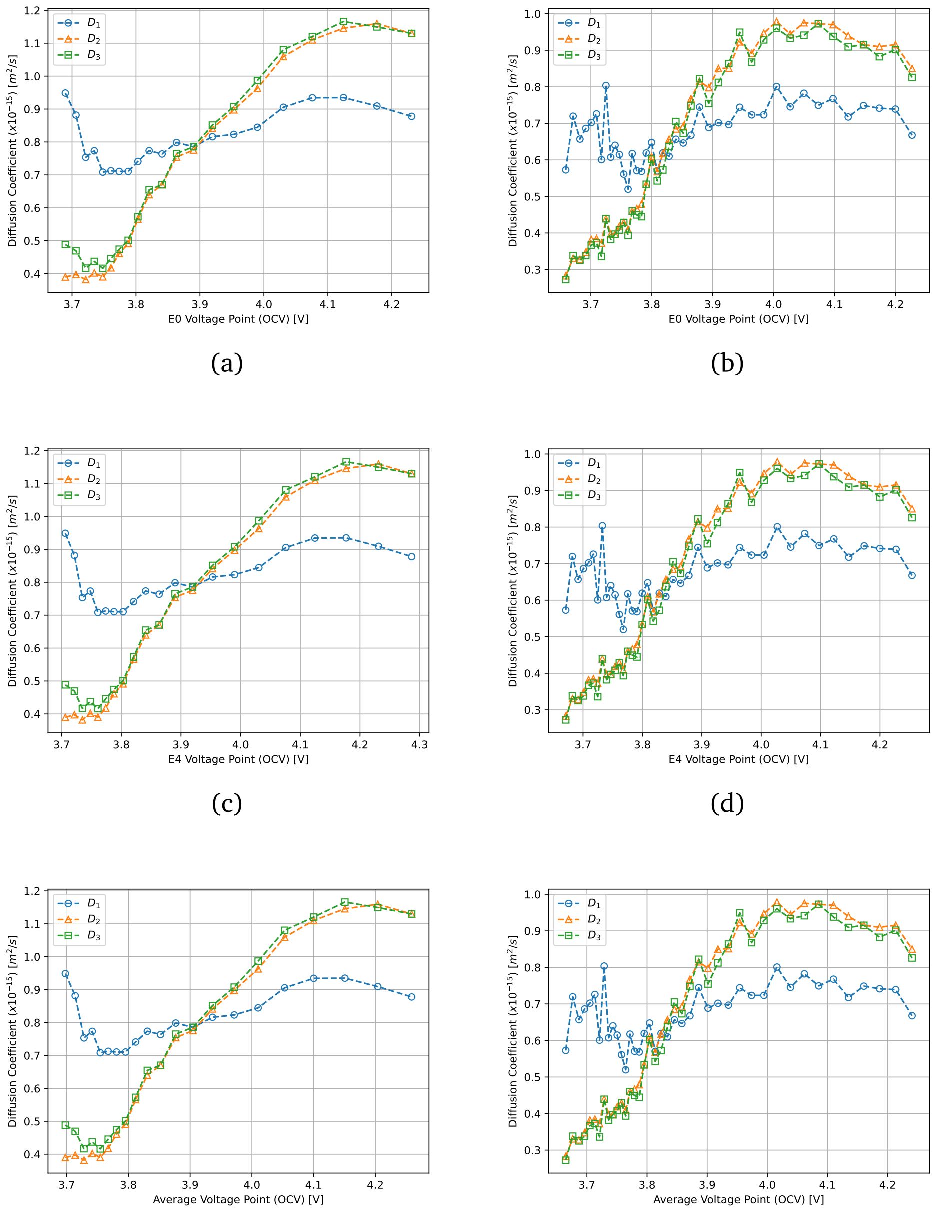

(a) (b)

(c) (d)

(e) (f)

Figure A.4: NMC111 diffusion coefficient comparison between three different equations in charge direction. Diffusion coefficients from equation 1, 2 and 3 are shown in blue (circle marker), orange (triangle marker) and green (square marker) colour curve respectively. Diffusion coefficients plotted against (a) E0 voltage points at C/10, (b) E0 voltage points at C/20, (c) E4 voltage points at C/10, (d) E4 voltage points at C/20, (e) Average of E0 and E4 voltage points at C/10, (f) Average of E0 and E4 voltage points at C/20

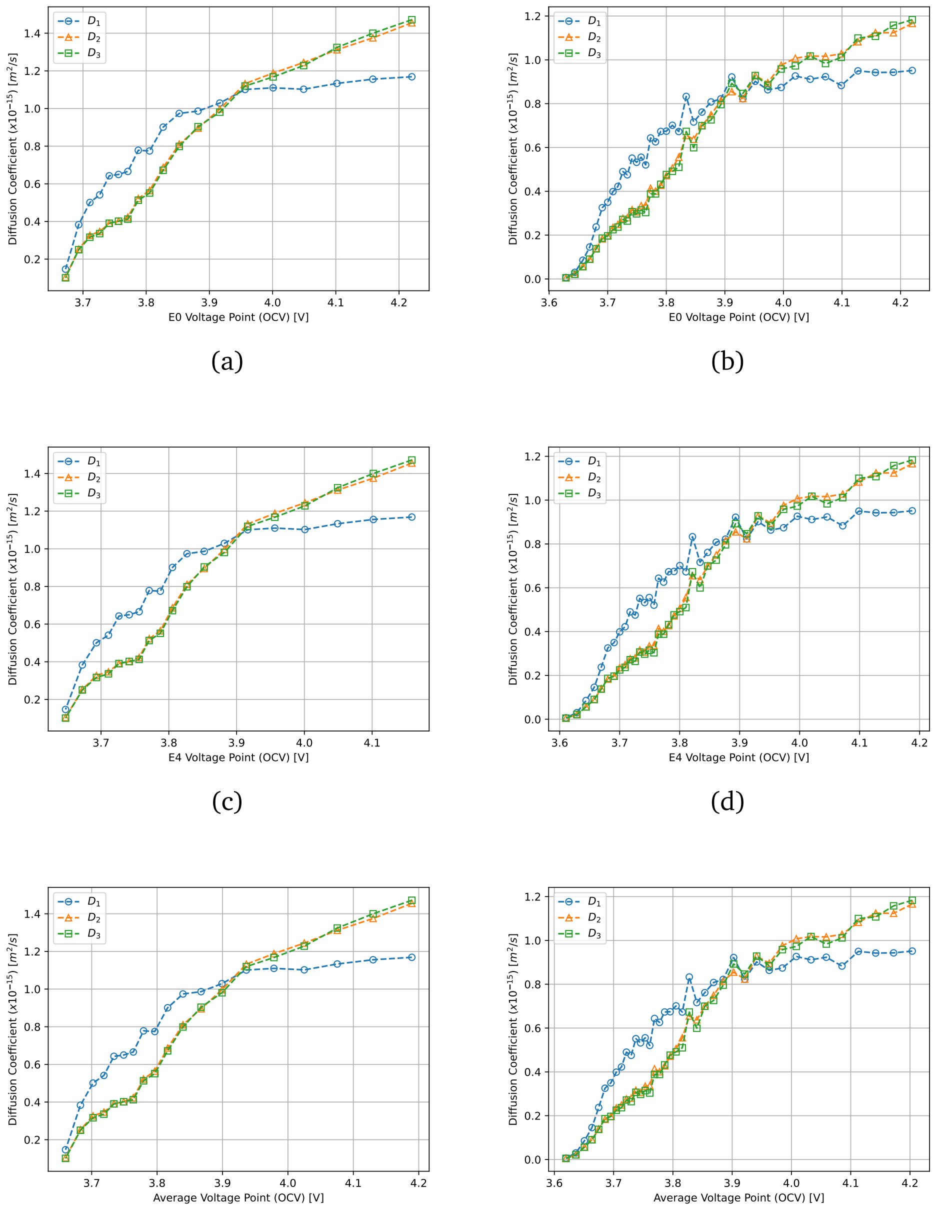

(a) (b)

(c) (d)

(e) (f)

Figure A.5: NMC111 diffusion coefficient comparison between three different equations in discharge direction. Diffusion coefficients from equation 1, 2 and 3 are shown in blue (circle marker), orange (triangle marker) and green (square marker) colour curve respectively. Diffusion coefficients plotted against (a) E0 voltage points at C/10, (b) E0 voltage points at C/20, (c) E4 voltage points at C/10, (d) E4 voltage points at C/20, (e) Average of E0 and E4 voltage points at C/10, (f) Average of E0 and E4 voltage points at C/20

A.2 NMC622 vs Li GITT data

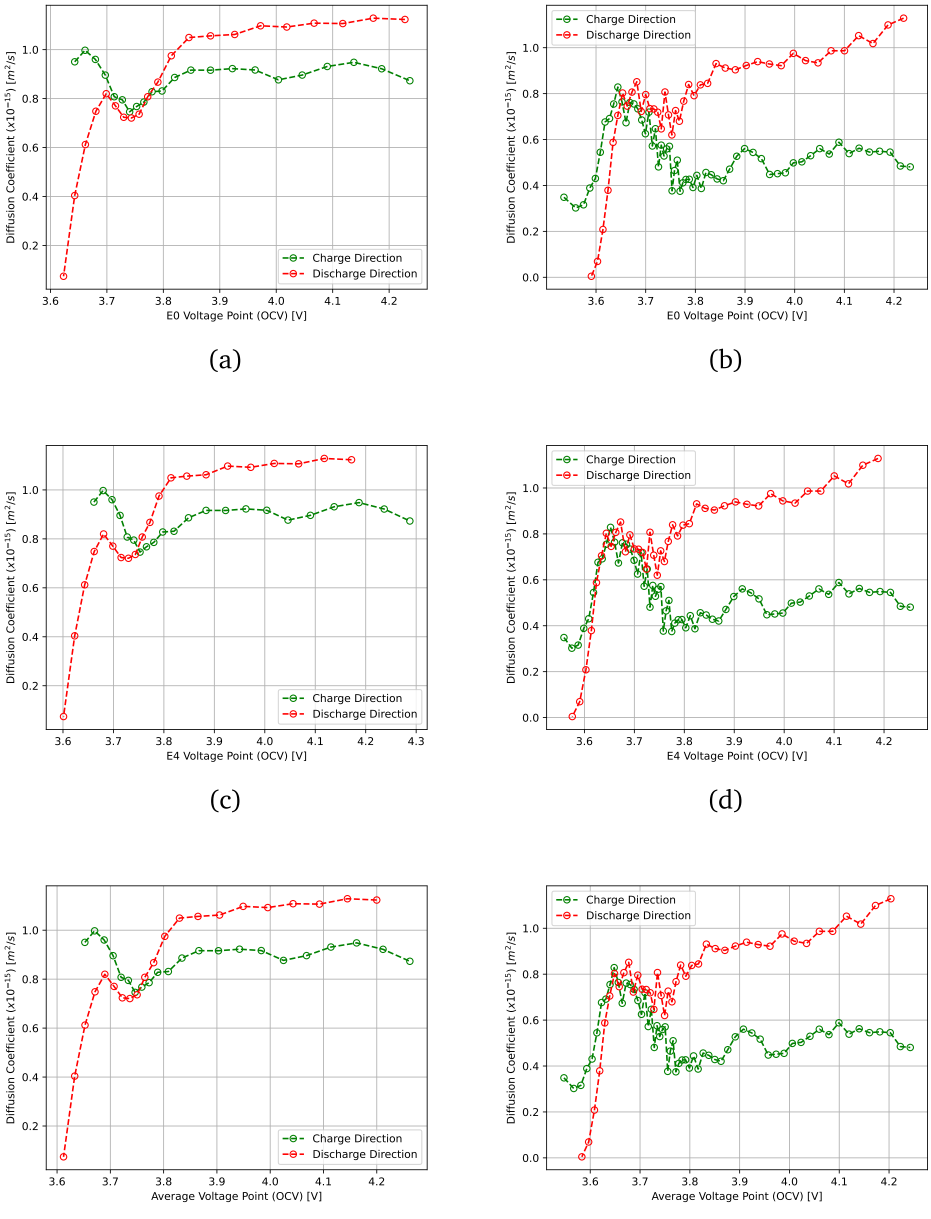

(a) (b)

(c) (d)

(e) (f)

Figure A.6: NMC622 diffusion coefficients using equation 1 in charge (green curve) and discharge (red curve) direction. Diffusion coefficients plotted against (a) E0 voltage points at C/10, (b) E0 voltage points at C/20, (c) E4 voltage points at C/10, (d) E4 voltage points at C/20, (e) Average of E0 and E4 voltage points at C/10, (f) Average of E0 and E4 voltage points at C/20

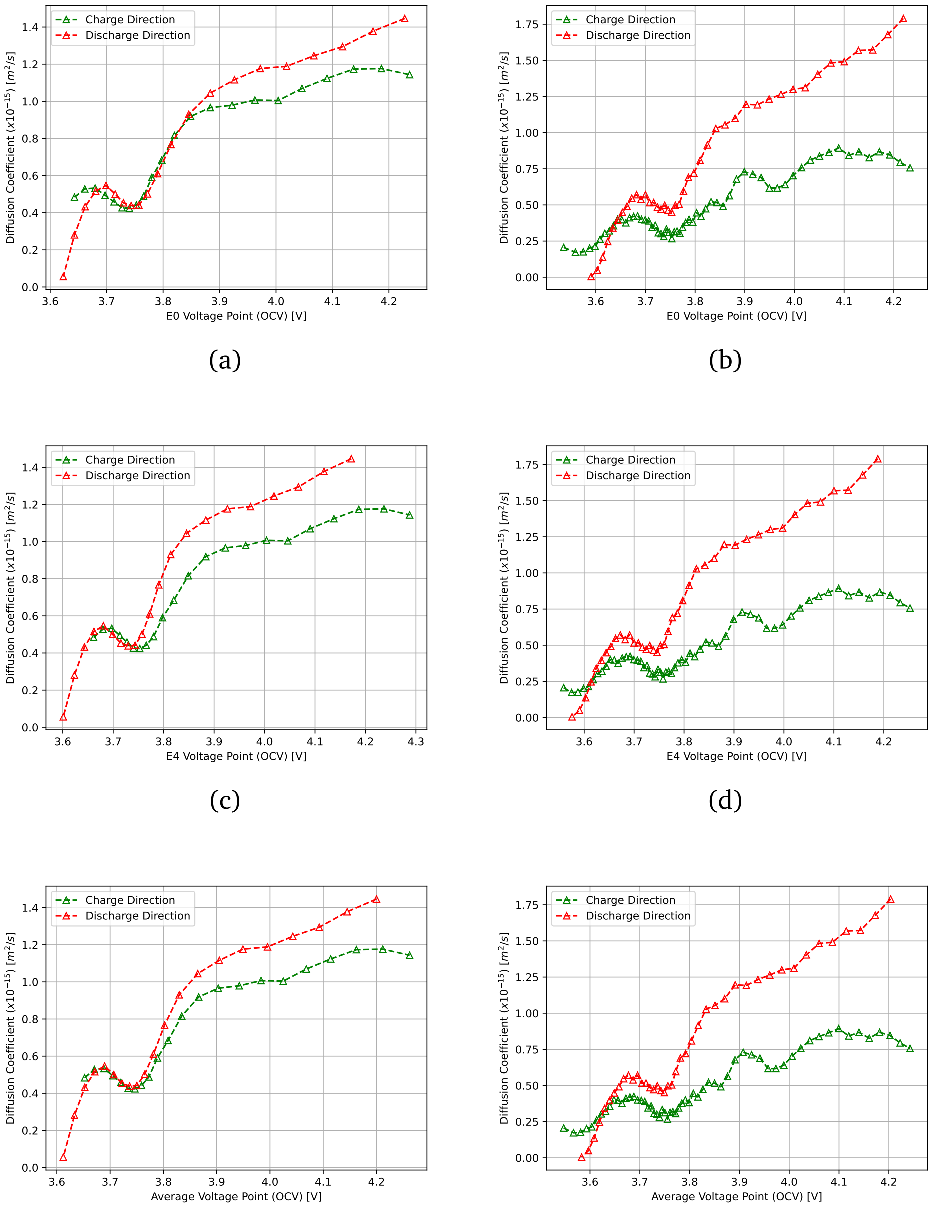

(a) (b)

(c) (d)

(e) (f)

Figure A.7: NMC622 diffusion coefficients using equation 2 in charge (green curve) and discharge (red curve) direction. Diffusion coefficients plotted against (a) E0 voltage points at C/10, (b) E0 voltage points at C/20, (c) E4 voltage points at C/10, (d) E4 voltage points at C/20, (e) Average of E0 and E4 voltage points at C/10, (f) Average of E0 and E4 voltage points at C/20

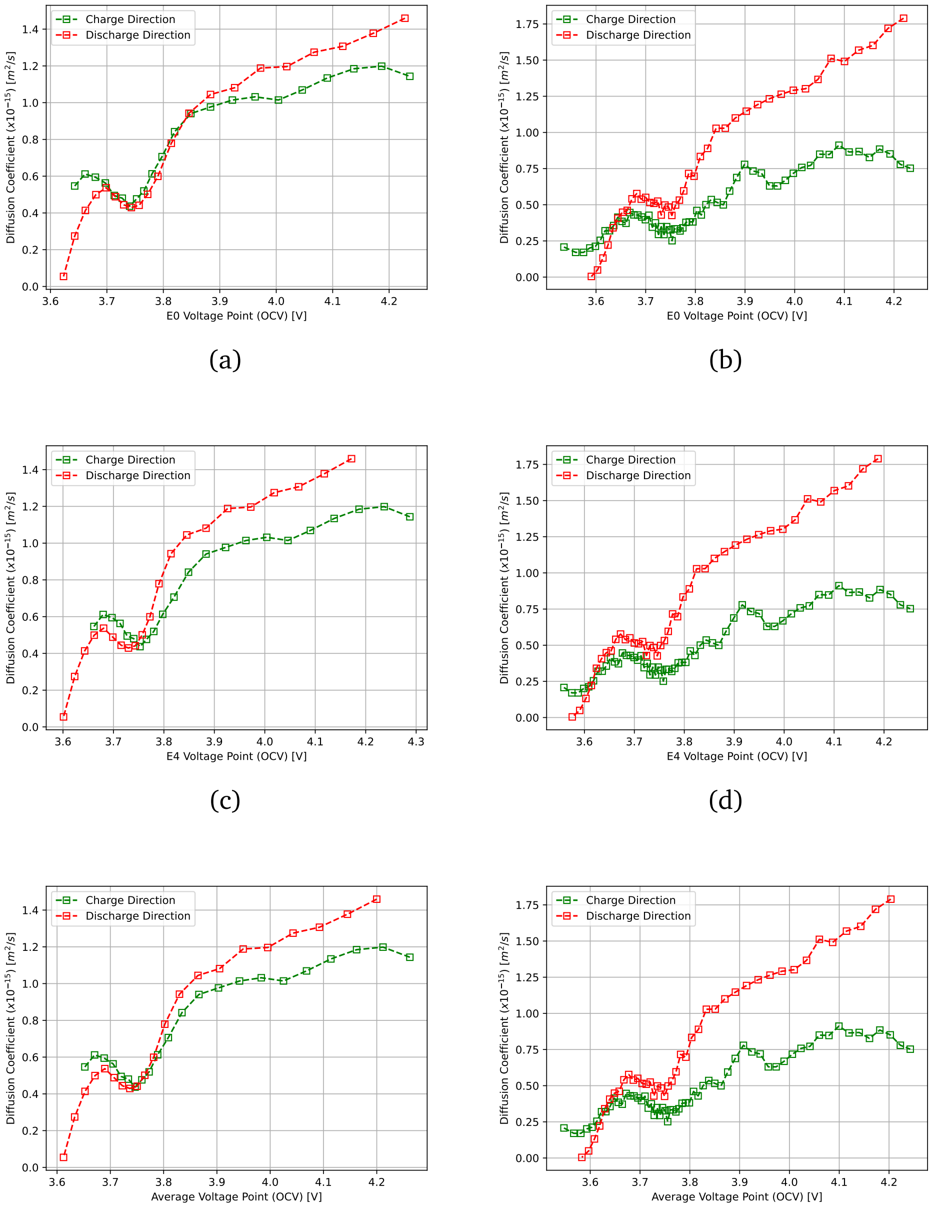

(a) (b)

(c) (d)

(e) (f)

Figure A.8: NMC622 diffusion coefficients using equation 3 in charge (green curve) and discharge (red curve) direction. Diffusion coefficients plotted against (a) E0 voltage points at C/10, (b) E0 voltage points at C/20, (c) E4 voltage points at C/10, (d) E4 voltage points at C/20, (e) Average of E0 and E4 voltage points at C/10, (f) Average of E0 and E4 voltage points at C/20

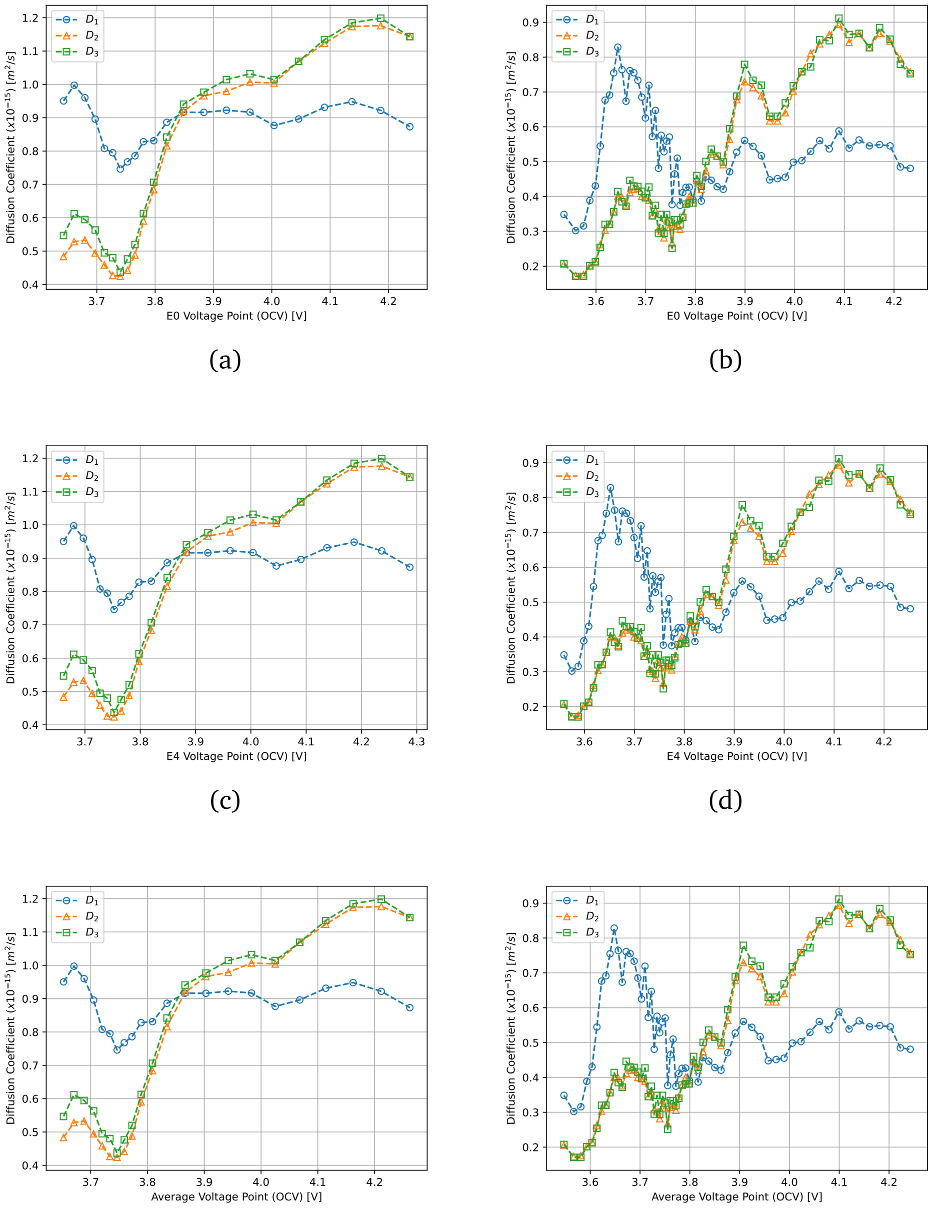

(a) (b)

(c) (d)

(e) (f)

Figure A.9: NMC622 diffusion coefficient comparison between three different equations in charge direction. Diffusion coefficients from equation 1, 2 and 3 are shown in blue (circle marker), orange (triangle marker) and green (square marker) colour curve respectively. Diffusion coefficients plotted against (a) E0 voltage points at C/10, (b) E0 voltage points at C/20, (c) E4 voltage points at C/10, (d) E4 voltage points at C/20, (e) Average of E0 and E4 voltage points at C/10, (f) Average of E0 and E4 voltage points at C/20

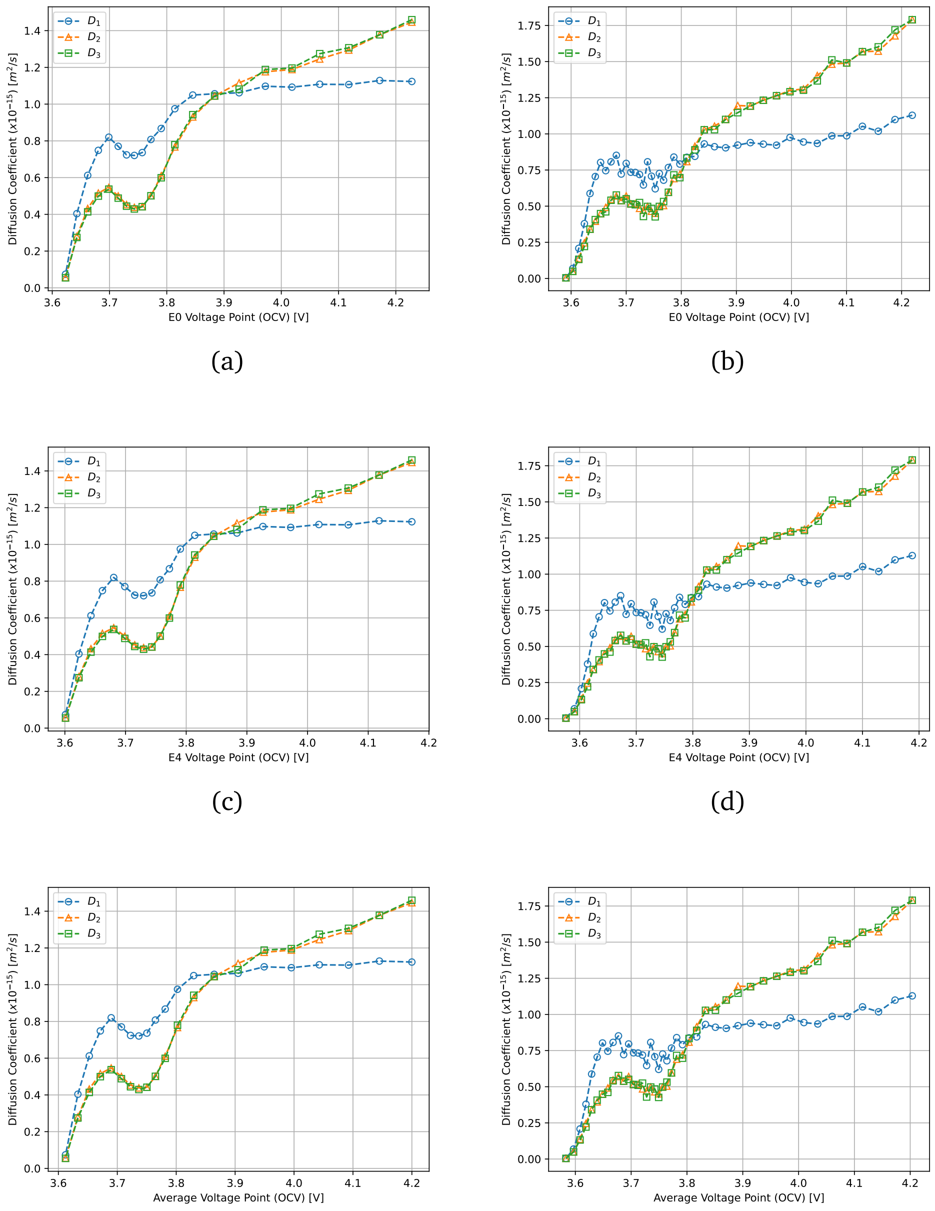

(a) (b)

(c) (d)

(e) (f)

Figure A.10: NMC622 diffusion coefficient comparison between three different equations in discharge direction. Diffusion coefficients from equation 1, 2 and 3 are shown in blue (circle marker), orange (triangle marker) and green (square marker) colour curve respectively. Diffusion coefficients plotted against (a) E0 voltage points at C/10, (b) E0 voltage points at C/20, (c) E4 voltage points at C/10, (d) E4 voltage points at C/20, (e) Average of E0 and E4 voltage points at C/10, (f) Average of E0 and E4 voltage points at C/20

A.3 NMC811 vs Li GITT data

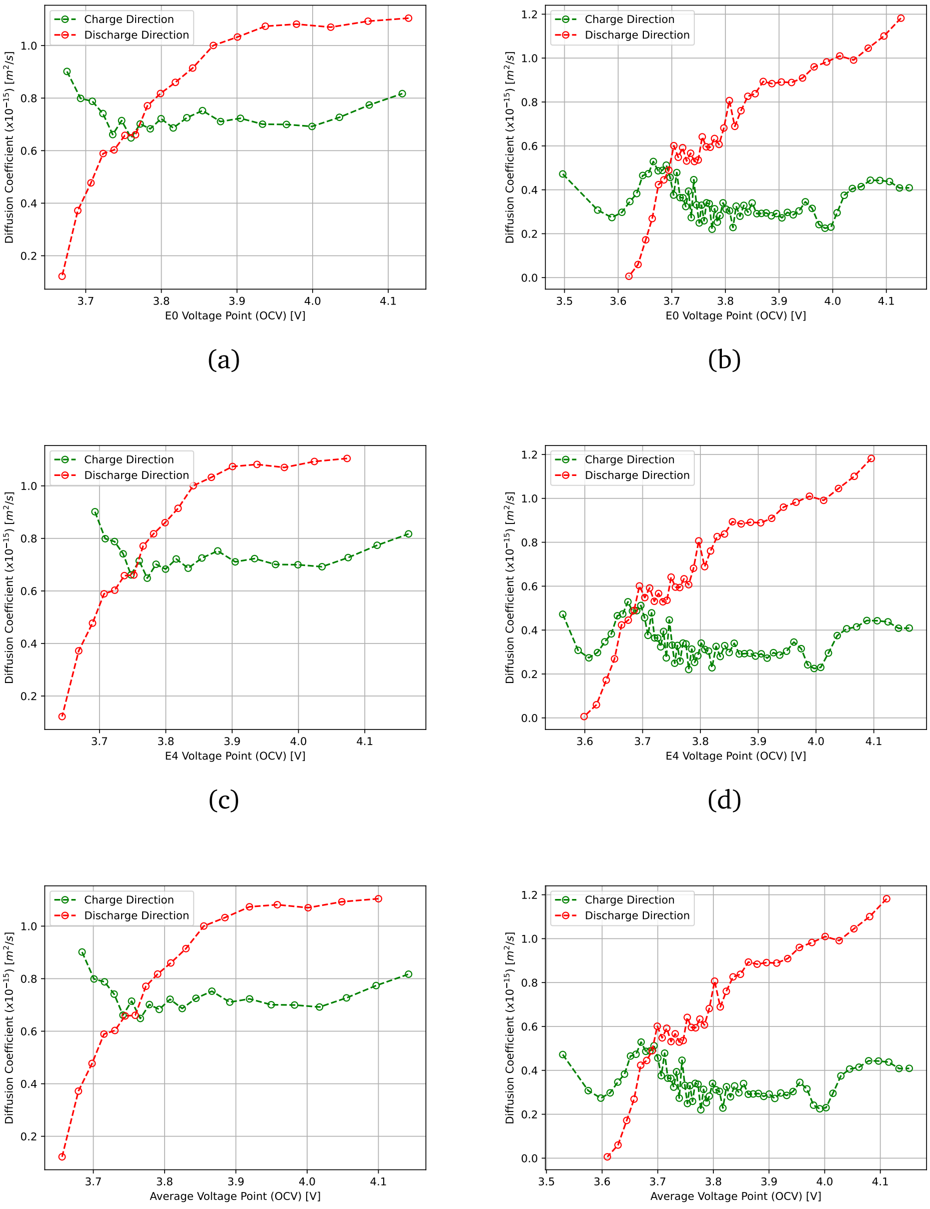

(a) (b)

(c) (d)

(e) (f)

Figure A.11: NMC811 diffusion coefficients using equation 1 in charge (green curve) and discharge (red curve) direction. Diffusion coefficients plotted against (a) E0 voltage points at C/10, (b) E0 voltage points at C/20, (c) E4 voltage points at C/10, (d) E4 voltage points at C/20, (e) Average of E0 and E4 voltage points at C/10, (f) Average of E0 and E4 voltage points at C/20

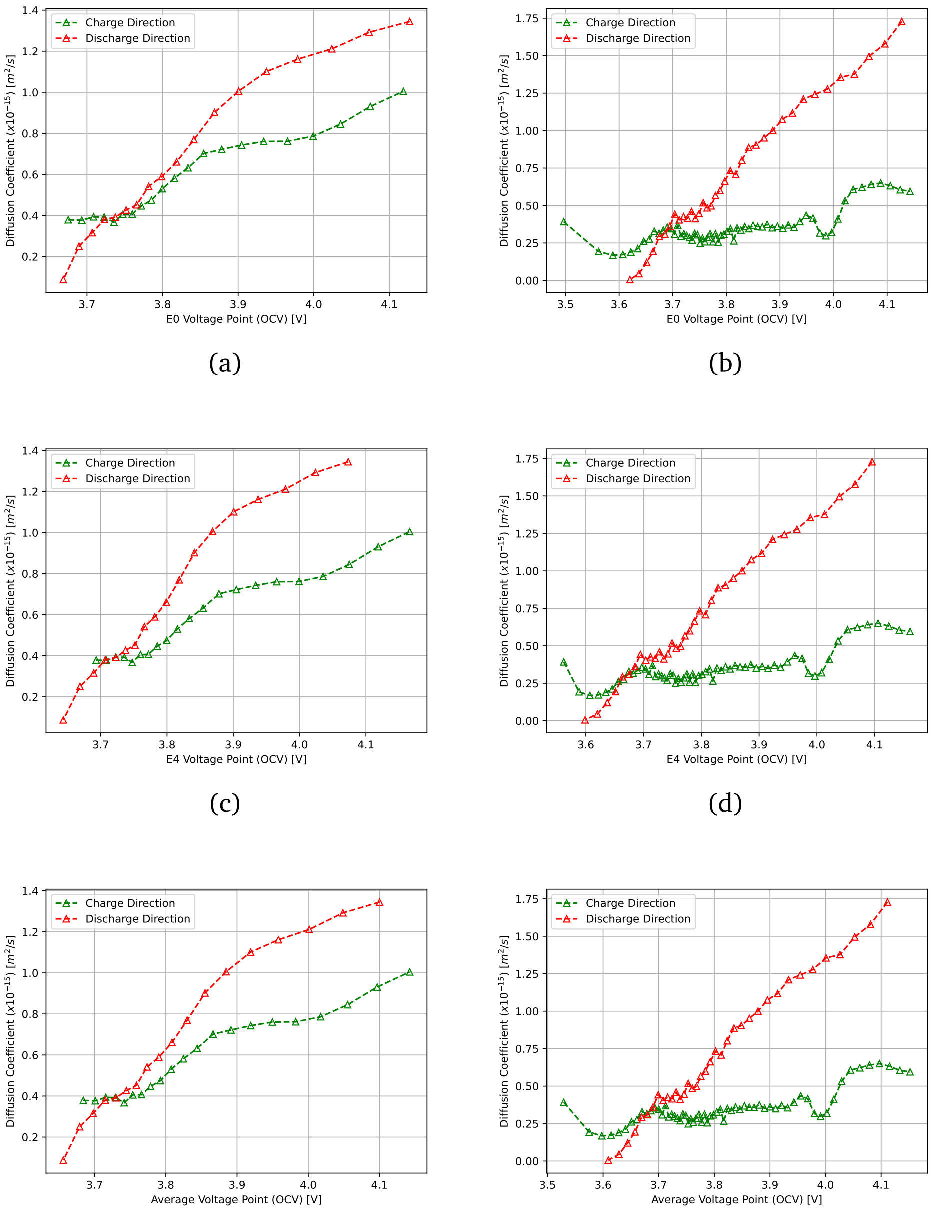

(a) (b)

(c) (d)

(e) (f)

Figure A.12: NMC811 diffusion coefficients using equation 2 in charge (green curve) and discharge (red curve) direction. Diffusion coefficients plotted against (a) E0 voltage points at C/10, (b) E0 voltage points at C/20, (c) E4 voltage points at C/10, (d) E4 voltage points at C/20, (e) Average of E0 and E4 voltage points at C/10, (f) Average of E0 and E4 voltage points at C/20

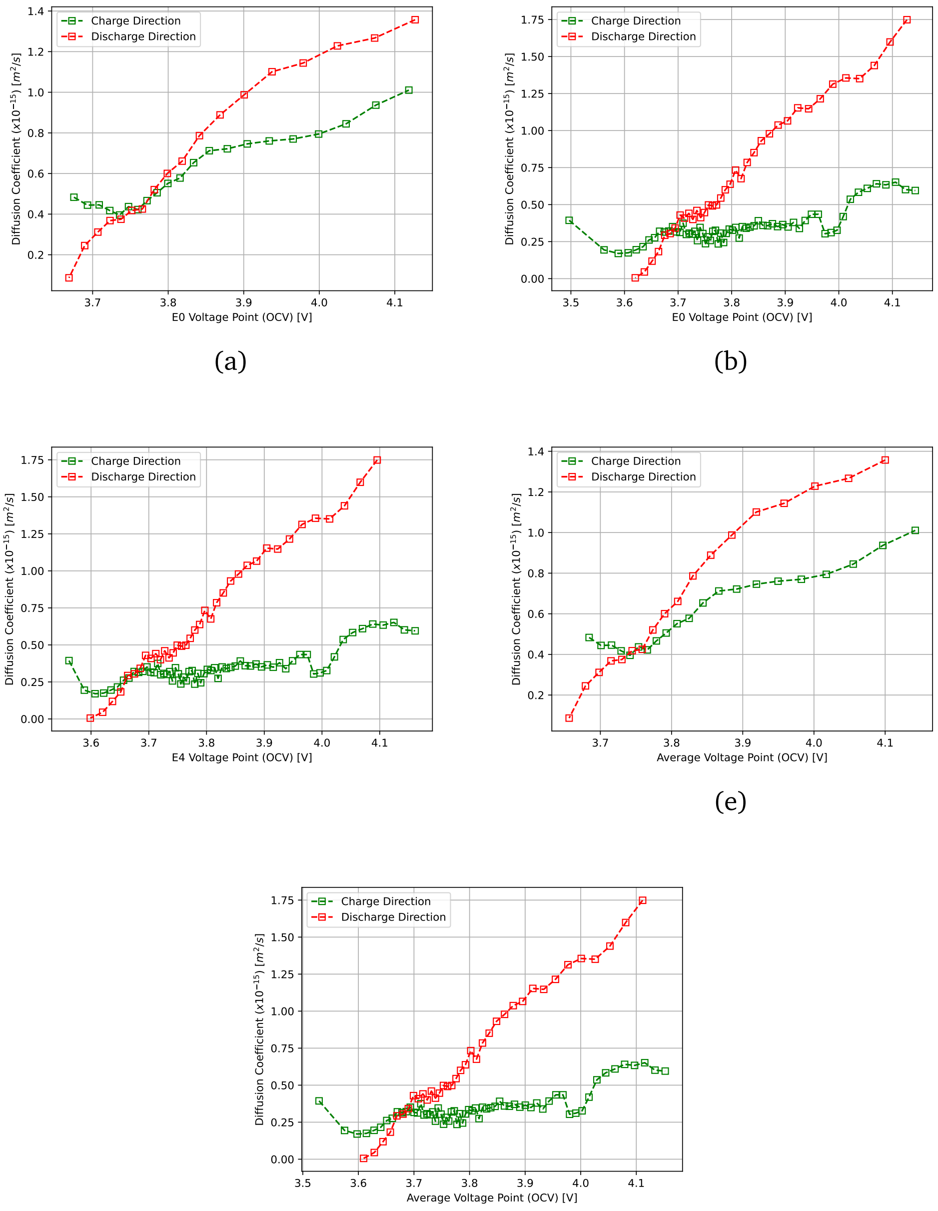

(a)

(b)

(e)

(f)

Figure A.13: NMC811 diffusion coefficients using equation 3 in charge (green curve) and discharge (red curve) direction. Diffusion coefficients plotted against (a) E0 voltage points at C/10, (b) E0 voltage points at C/20, (c) E4 voltage points at C/10, (d) E4 voltage points at C/20, (e) Average of E0 and E4 voltage points at C/10, (f) Average of E0 and E4 voltage points at C/20
fig:NMC811DCEq3

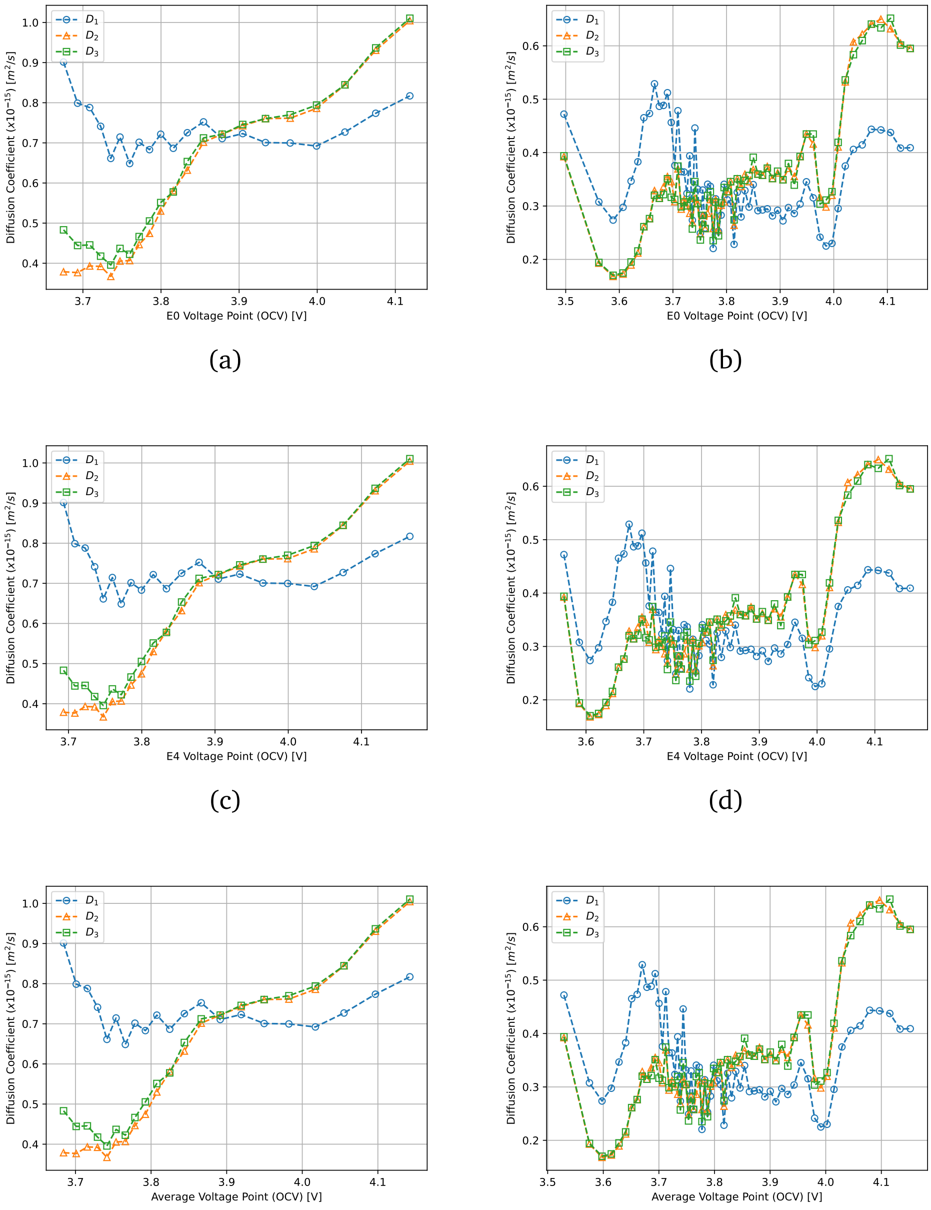

(a) (b)

(c) (d)

(e) (f)

Figure A.14: NMC811 diffusion coefficient comparison between three different equations in charge direction. Diffusion coefficients from equation 1, 2 and 3 are shown in blue (circle marker), orange (triangle marker) and green (square marker) colour curve respectively. Diffusion coefficients plotted against (a) E0 voltage points at C/10, (b) E0 voltage points at C/20, (c) E4 voltage points at C/10, (d) E4 voltage points at C/20, (e) Average of E0 and E4 voltage points at C/10, (f) Average of E0 and E4 voltage points at C/20

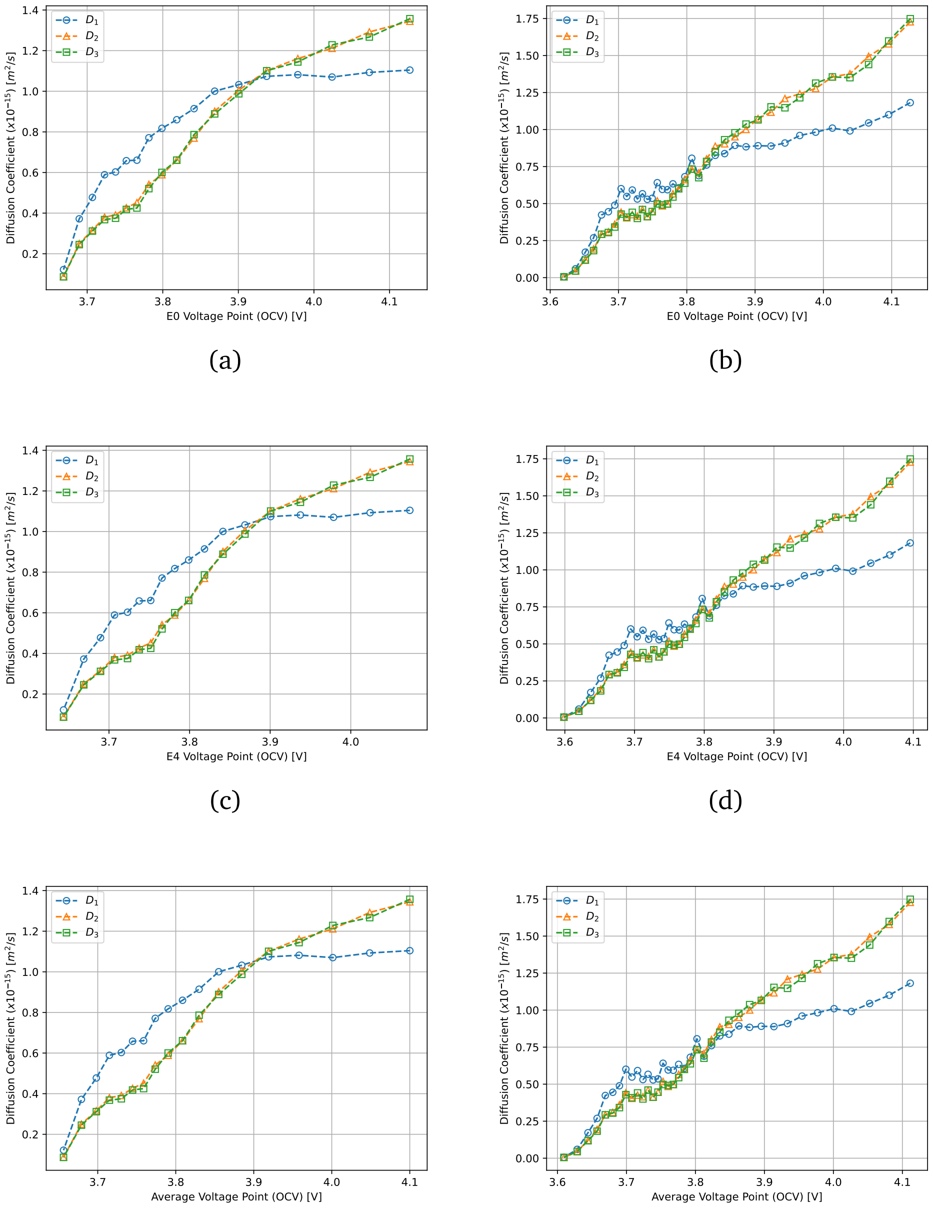

(a) (b)

(c) (d)

(e) (f)

Figure A.15: NMC811 diffusion coefficient comparison between three different equations in discharge direction. Diffusion coefficients from equation 1, 2 and 3 are shown in blue (circle marker), orange (triangle marker) and green (square marker) colour curve respectively. Diffusion coefficients plotted against (a) E0 voltage points at C/10, (b) E0 voltage points at C/20, (c) E4 voltage points at C/10, (d) E4 voltage points at C/20, (e) Average of E0 and E4 voltage points at C/10, (f) Average of E0 and E4 voltage points at C/20

B

Appendix 2: Electrochemical Impedance Spectroscopy (EIS)

B.1 NMC111 vs GSi half cell EIS fit data

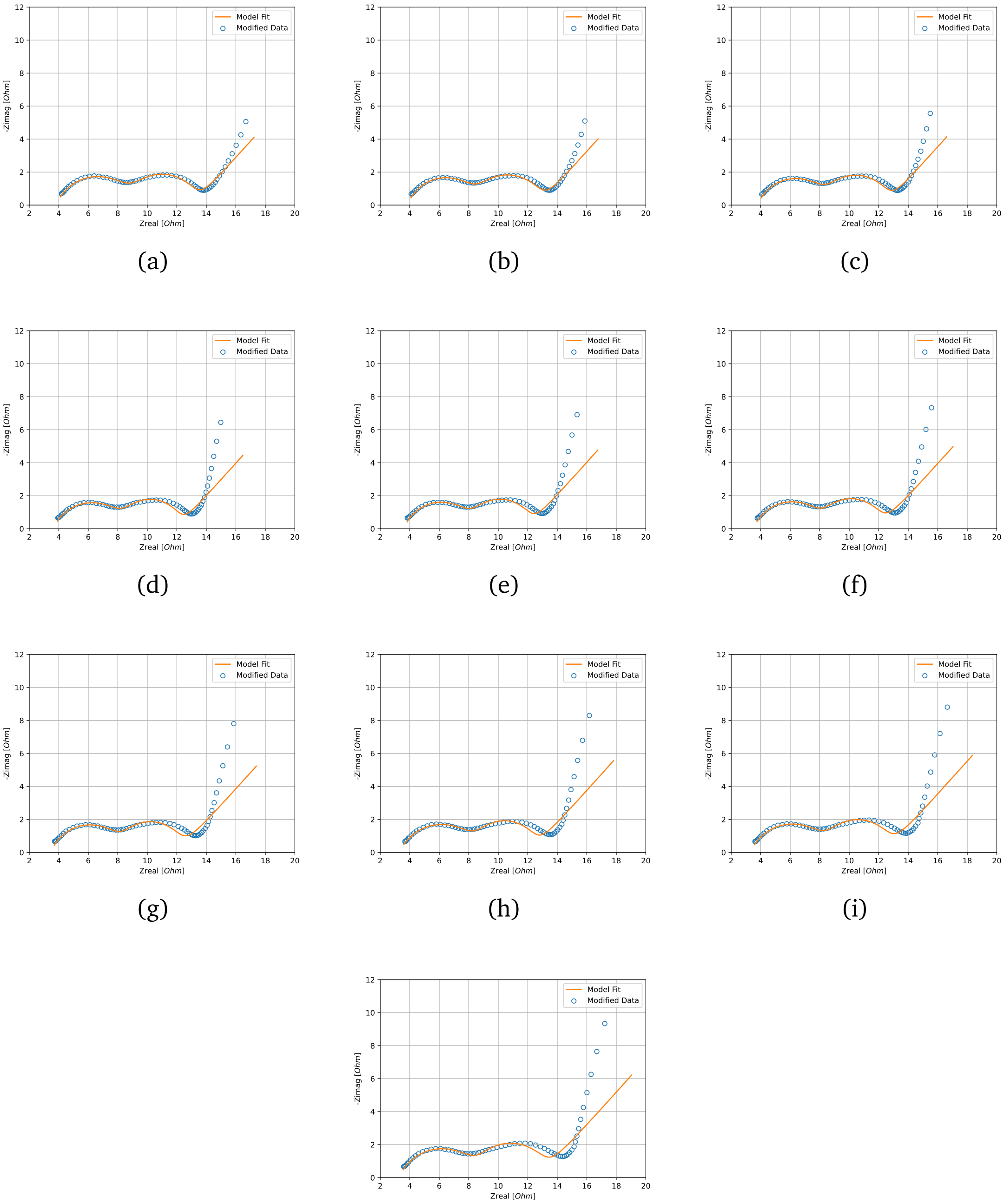

(a) (b) (c)

(d) (e) (f)

(g) (h) (i)

(j)

Figure B.1: NMC111vsGSi half cell EIS fits at (a) 4.159V, (b) 4.084V, (c) 4.029V, (d) 3.973V, (e) 3.938V, (f) 3.901V, (g) 3.866V, (h) 3.836V, (i) 3.811V, (j) 3.789V mean voltages

Table B.1: NMC111 vs GSi half cell EIS fit data

Vmean	R0	ER0	R1	ER1	Y1	EY1	a1	Ea1	R2	ER2	sigma	Esigma	Y2	EY2	a2	Ea2	GoF
4.159	3.8	0	4.153	0.4211	0.008072	0.001837	0.8245	0.07403	5.195	0.3354	0.6885	0.04178	0.0003804	1.067e-05	0.7127	0.02822	2.44e-4
4.084	3.85	0	4.212	0.4058	0.007911	0.001758	0.8117	0.07121	4.712	0.3198	0.7048	0.04229	0.0003182	9.414e-05	0.7417	0.03011	4.13e-4
4.029	3.8	0	3.994	0.3905	0.007619	0.001737	0.8325	0.07245	4.694	0.3114	0.6855	0.03894	0.0003609	0.0001067	0.7295	0.02993	6.11e-4
3.973	3.6	0	3.527	0.3684	0.007049	0.001727	0.8817	0.0773	4.915	0.3024	0.6359	0.03219	0.0004757	0.00013336	0.6982	0.02813	1.12e-3
3.938	3.6	0	3.723	0.3593	0.007024	0.001658	0.8604	0.0731	4.667	0.287	0.5935	0.02865	3.547e-04	9.987e-05	0.7349	0.02854	1.16e-3
3.901	3.5	0	3.733	0.3856	0.00578	0.001474	0.8916	0.07728	4.887	0.2952	0.5695	0.0267	0.000392	0.0001064	0.7222	0.02736	1.3e-3
3.886	3.45	0	3.804	0.3864	0.005771	0.001455	0.8926	0.07645	4.975	0.2929	0.5417	0.02463	0.0003844	0.0001011	0.7242	0.02663	1.47e-3
3.836	3.3	0	3.663	0.3637	0.007364	0.001729	0.8895	0.07483	5.31	0.2921	0.5085	0.02218	0.0004816	0.0001193	0.6945	0.02485	1.52e-3
3.811	3.3	0	3.928	0.3665	0.007637	0.001701	0.873	0.07135	5.266	0.2871	0.4807	0.02057	0.0004318	0.0001058	0.7076	0.02472	1.62e-3
3.789	3.25	0	4.165	0.3721	0.00808	0.001706	0.8689	0.0689	5.432	0.286	0.455	0.01925	0.0004506	0.0001065	0.7015	0.023855	1.75e-3

B.2 NMC622 vs GSi half cell EIS fit data

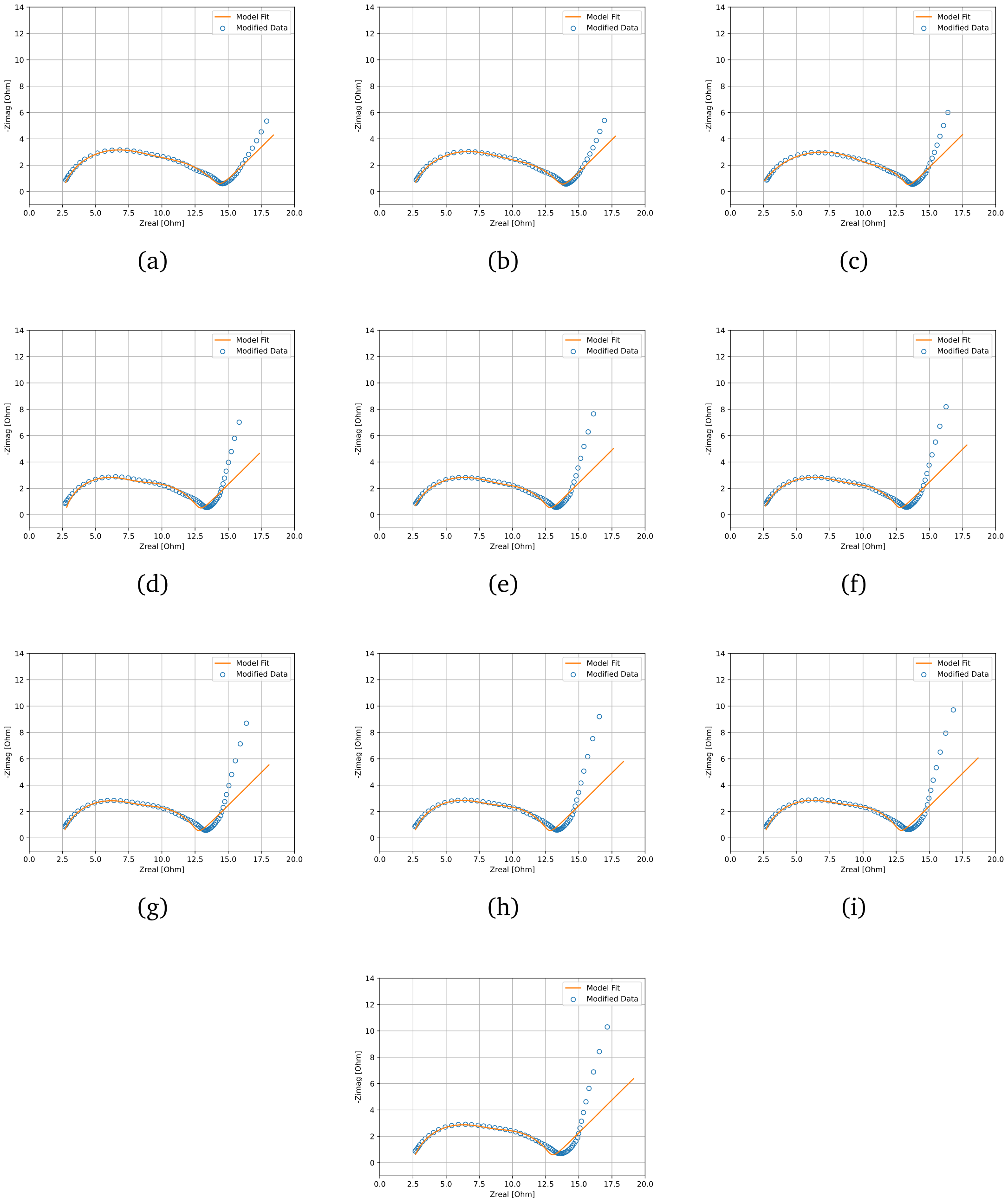

(a) (b) (c)

(d) (e) (f)

(g) (h) (i)

(j)

Figure B.2: NMC622vsGSi half cell EIS fits at (a) 4.157V, (b) 4.084V, (c) 4.029V, (d) 3.971V, (e) 3.930V, (f) 3.884V, (g) 3.843V, (h) 3.808V, (i) 3.782V, (j) 3.761V mean voltages

Table B.2: NMC622 vs GSi half cell EIS fit data

Vmean	R0	ER0	R1	ER1	Y1	EY1	a1	Ea1	R2	ER2	sigma	Esigma	Y2	EY2	a2	Ea2	GoF
4.157	2.5	0	6.249	1.675	6.52e-05	2.143e-05	0.8585	0.04667	5.381	1.76	0.6586	0.03911	0.001996	0.0006059	0.71117	0.1035	3.47e-4
4.084	2.4	0	6.734	1.336	8.884e-05	2.247e-05	0.8213	0.03179	4.434	1.408	0.6728	0.03859	0.002166	0.0007284	0.7438	0.1109	4.09e-4
4.029	2.1	0	9.075	0.6941	0.0002107	3.81e-05	0.7198	0.01764	2.013	0.735	0.6531	0.03421	0.003183	0.00196	0.9092	0.1786	7.16e-4
3.971	2.7	0	5.149	1.089	0.0009831	0.0002655	0.787	0.08413	4.858	1.03	0.6069	0.02896	3.365e-05	1.135e-05	0.9369	0.04297	1.85e-3
3.930	2.4	0	6.549	0.898	8.947e-05	2.08e-05	0.8209	0.02518	3.65	0.9482	0.5622	0.02512	0.001475	0.0005483	0.829	0.1077	1.44e-3
3.884	2.4	0	6.267	0.9119	7.69e-05	1.835e-05	0.8393	0.02637	3.871	0.9622	0.533	0.0227	0.001277	0.0004515	0.8294	0.1022	1.68e-3
3.843	2.5	0	5.647	0.946	5.787e-05	1.533e-05	0.873	0.03058	4.39	0.9979	0.5094	0.0209	0.001026	0.0003256	0.822	0.09218	2.02e-3
3.808	2.5	0	5.713	0.924	5.686e-05	1.477e-05	0.8745	0.02971	4.356	0.9753	0.4873	0.01931	0.0009665	0.0003108	0.8315	0.09203	2.23e-3
3.782	2.5	0	5.776	0.9225	5.817e-05	1.496e-05	0.8717	0.02922	4.331	0.9731	0.4654	0.01784	0.0009437	0.0003066	0.8363	0.09245	2.42e-3
3.761	2.5	0	5.844	0.9232	5.974e-05	1.526e-05	0.8683	0.02896	4.411	0.9753	0.4426	0.01651	0.0009682	0.0003112	0.8337	0.09169	2.62e-3

B.3 NMC811 vs GSi half cell EIS fit data

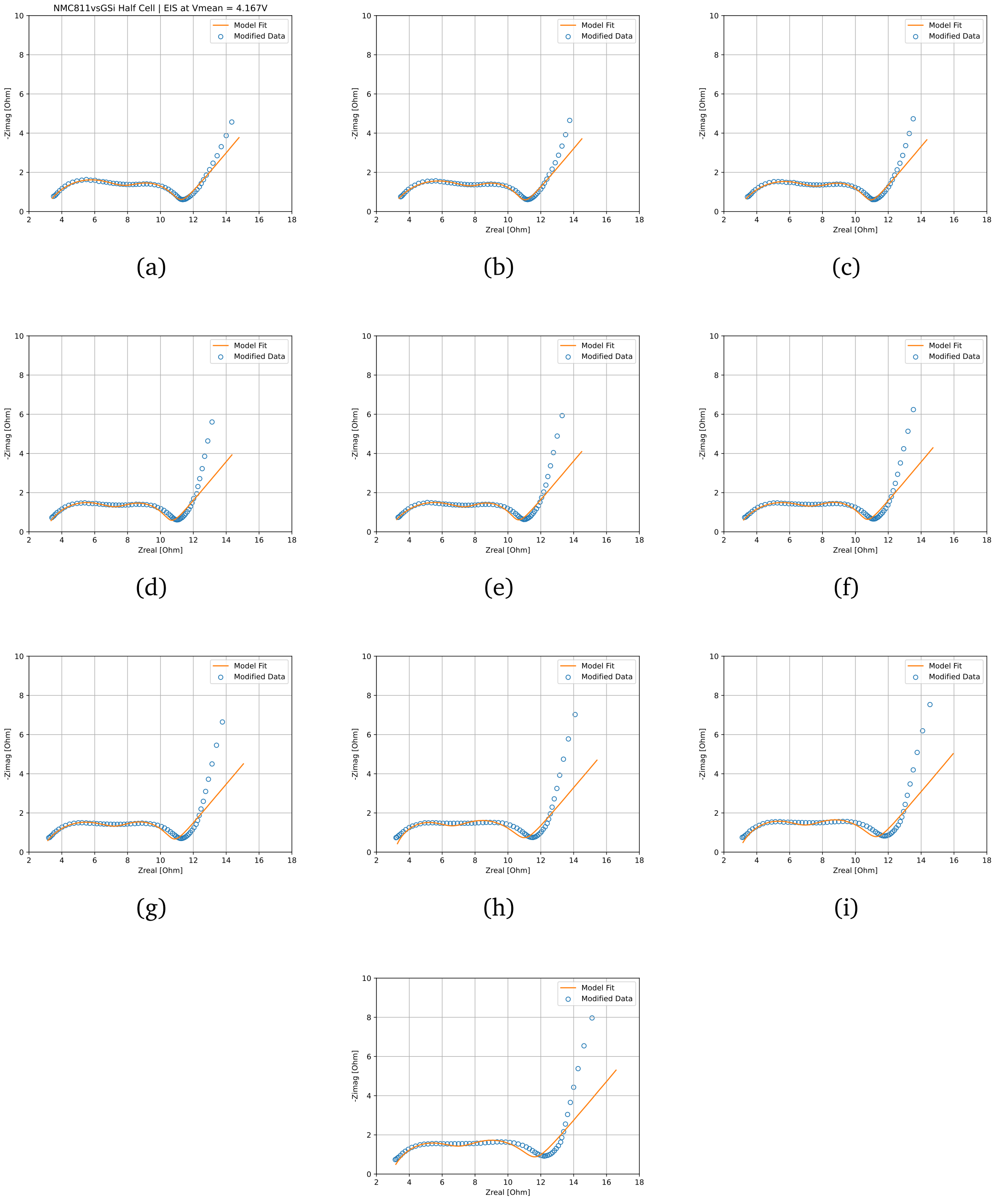

(a) (b) (c)

(d) (e) (f)

(g) (h) (i)

(j)

Figure B.3: NMC811vsGSi half cell EIS fits at (a) 4.167V, (b) 4.094V, (c) 4.073V, (d) 3.980V, (e) 3.941V, (f) 3.905V, (g) 3.870V, (h) 3.841V, (i) 3.816V, (j) 3.794V mean voltages

Table B.3: NMC811 vs GSi half cell EIS fit data

Vmean	R0	ER0	R1	ER1	Y1	EY1	a1	Ea1	R2	ER2	sigma	Esigma	Y2	EY2	a2	Ea2	GoF
4.167	2.9	0	5.252	0.4592	0.0004315	0.0001327	0.6668	0.02913	2.895	0.5236	0.7498	0.04024	0.004834	0.0017	0.8388	0.1047	1.92e-4
4.094	2.8	0	5.446	0.4585	0.0006029	0.0001825	0.6339	0.02835	2.577	0.5132	0.7622	0.04012	0.004689	0.001763	0.881	0.113	3.14e-4
4.073	2.8	0	5.299	0.4464	0.0005952	0.0001818	0.6377	0.02865	2.621	0.501	0.7724	0.04069	0.004655	0.0017	0.8792	0.1093	4.04e-4
3.980	2.94	0	4.606	0.4096	0.0004087	0.0001319	0.689	0.03095	2.885	0.4547	0.7192	0.03473	0.004549	0.001435	0.845	0.09186	9.69e-4
3.941	2.7	0	5.236	0.4178	0.0006405	0.0001906	0.6352	0.0287	2.484	0.4666	0.6904	0.03198	0.003966	0.001481	0.9175	0.109	1.01e-3
3.905	2.7	0	5.097	0.4352	0.0006379	0.0001925	0.6398	0.02844	2.655	0.4731	0.6585	0.0297	0.004868	0.001605	0.8758	0.09977	1.07e-3
3.870	2.7	0	4.929	0.4094	0.0004985	0.00014766	0.6666	0.02821	2.925	0.4546	0.6265	0.02758	0.004825	0.001475	0.8548	0.09089	1.23e-3
3.841	3.1	0	4.302	0.4826	0.004304	0.001001	0.736	0.06807	3.333	0.413	0.6021	0.02676	0.0001318	5.048e-05	0.8303	0.03998	1.84e-3
3.816	2.9	0	3.966	0.4728	0.004855	0.001189	0.7692	0.07282	4.077	0.4058	0.5623	0.02407	0.0002286	7.329e-05	0.763	0.03224	1.75e-3
3.794	2.9	0	4.221	0.5017	0.00532	0.001234	0.7587	0.07144	4.179	0.4283	0.533	0.02273	0.0002741	8.733e-05	0.7545	0.03204	1.79e-3

DEPARTMENT OF SOME SUBJECT OR TECHNOLOGY
CHALMERS UNIVERSITY OF TECHNOLOGY
Gothenburg, Sweden
www.chalmers.se

CHALMERS
UNIVERSITY OF TECHNOLOGY